REPORT DOCUMENTATION PAGE

Form Approved
OMB No. 0704-0188

1. AGENCY USE ONLY (Leave blank)	2. REPORT DATE	3. REPORT TYPE AND DATES COVERED
	30 Sept. 1995	Final Tech. 01 Apr. 93-30 Sep. 95

4. TITLE AND SUBTITLE
Generalized Linear Elastic Fracture Model for Advanced Materials

5. FUNDING NUMBERS
F49620-93-1-0256

6. AUTHOR(S)
James G. Goree (Principal Investigator)
Alex. S. Selvarathinam (Ph.D. Student)

AFOSR-TR-96
0152

7. PERFORMING ORGANIZATION NAME(S) AND ADDRESS(ES)
Department of Mechanical Engineering
209 Fluor Daniel EIB
Box 340921
Clemson University
Clemson, SC 29634-0921

9. SPONSORING/MONITORING AGENCY NAME(S) AND ADDRESS(ES)
Department of the Air Force
Air Force Office of Scientific Research (AFMC)
110 Duncan Avenue, Suite B115
Bolling Air Force Base, DC 20332-0001
Dr. Walter F. Jones, Monitor

NA
2302 DS

10. SPONSORING/MONITORING AGENCY REPORT NUMBER

11. SUPPLEMENTARY NOTES

12a. DISTRIBUTION/AVAILABILITY STATEMENT
Approved for public release, distribution unlimited

19960404 043

13. ABSTRACT (Maximum 200 words)

The branched crack problem for both an isotropic and anisotropic material is solved using the method of dislocations, and the stress intensity factors and T-stress in front of the branched crack are evaluated numerically. The T-stress based fracture criteria, developed by Cotterell and Rice for a flat crack, is modified by incorporating an experimentally determined critical T-stress value (T_{crit}). Based on this T_{crit}, a modified T-stress based fracture criteria is proposed. This criteria is applied to the branched crack and the direction of growth of the branched crack is discussed by comparing the theoretically evaluated T-stress values with some available experimentally determined T_{crit} values. The T-stress for the isotropic case is obtained in terms of applied load, kink length and kink angle. For the anisotropic case the T-stress also depends on the relative stiffness properties. For a uniaxial loading case it is demonstrated that a short kink length will turn from its initial direction and realign with the main crack. If the loading is biaxial, kink growth direction depends strongly on applied transverse stress s_{xx}^{∞} For a longer kink length, kink growth direction depends on the kink angle, loading and relative stiffness.

14. SUBJECT TERMS	15. NUMBER OF PAGES
Fracture, Branched Crack, T-Stress	143
	16. PRICE CODE

17. SECURITY CLASSIFICATION OF REPORT	18. SECURITY CLASSIFICATION OF THIS PAGE	19. SECURITY CLASSIFICATION OF ABSTRACT	20. LIMITATION OF ABSTRACT

Mechanical Engineering Department
College of Engineering
Clemson University
Clemson, South Carolina

DISCLAIMER NOTICE

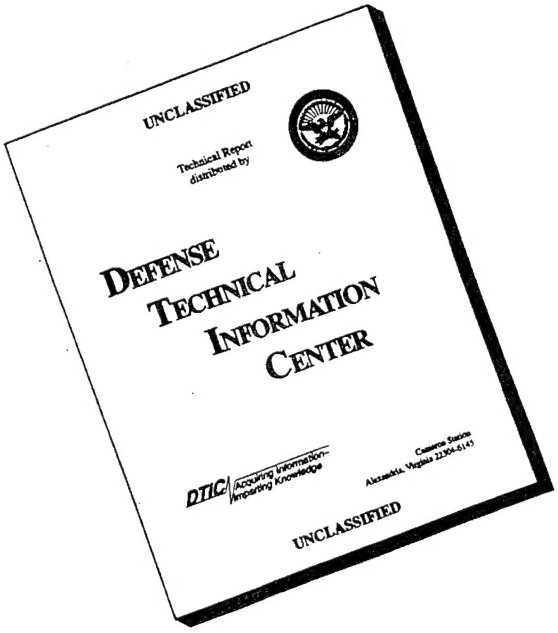

THIS DOCUMENT IS BEST QUALITY AVAILABLE. THE COPY FURNISHED TO DTIC CONTAINED A SIGNIFICANT NUMBER OF PAGES WHICH DO NOT REPRODUCE LEGIBLY.

GENERALIZED LINEAR ELASTIC FRACTURE MODEL FOR ADVANCED MATERIALS

Grant No. F49620–93–1–0256
Effective Date 01, April 1993
Duration 30 Months

Final Technical Report
(01 Apr 93–30 Sep 95)

Department Of The Air Force
Air Force Office Of Scientific Research (AFMC)
110 Duncan Avenue, Suite B115
Bolling Air Force Base, DC 20332–0001
Dr. Walter F. Jones, Monitor

Principal Investigator

James G. Goree
Centennial Professor and Professor of
Mechanical Engineering and Engineering Mechanics

Graduate Student

Alex S. Selvarathinam
Ph.D Candidate In Engineering Mechanics

Department of Mechanical Engineering
209 Fluor Daniel E.I.B
Box 340921
Clemson University
Clemson, SC 29634–0921

ABSTRACT

The branched crack problem for both an isotropic and anisotropic material is solved using the method of dislocations, and the stress intensity factors and T–stress in front of the branched crack are evaluated numerically . The T–stress based fracture criteria, developed by Cotterell and Rice for a flat crack, is modified by incorporating an experimentally determined critical T–stress value (T_{crit}). Based on this T_{crit}, a modified T–stress based fracture criteria is proposed. This criteria is applied to the branched crack and the direction of growth of the branched crack is discussed by comparing the theoretically evaluated T–stress values with some available experimentally determined T_{crit} values.

The solution for the branched crack problem is obtained in terms of a singular integral equation which is solved using three different numerical schemes, the merits of which are discussed. The nature of the stress singularity at the reentrant wedge corner of the branched crack is analyzed and is verified for the isotropic case. It is shown that the T–stress and the stress intensity factors are insensitive to the order of the singularity assumed at the reentrant wedge corner of the branched crack in either an isotropic or anisotropic material. The T–stress for the isotropic case is obtained in terms of applied load, kink length and kink angle. For the anisotropic case the T–stress also depends on the relative stiffness properties of the fibre and matrix. For a uniaxial loading case, by applying the modified T–stress based criteria to the branched crack, it is demonstrated that for a short kink length the kink will turn from its initial direction and realign with the main crack. If the loading is biaxial then the kink growth direction depends strongly on applied transverse stress σ_{xx}^{∞}. For a longer initial kink length the kink growth direction depends on the kink angle, loading and relative stiffness of the fibre and matrix.

TABLE OF CONTENTS

Table of Contents (Continued)

Table of Contents (Continued)

LIST OF TABLES

LIST OF FIGURES

List of Figures (Continued)

List of Figures (Continued)

CHAPTER I

INTRODUCTION

Background

Linear Elastic Fracture Mechanics (LEFM) proposes that for brittle materials a single parameter, the stress intensity factor (K_{IC}), is sufficient for predicting fracture. It is also implied that the K_{1C} is a property of the material similar to Young's modulus and the ultimate strength. Over the years LEFM has been applied to a wide range of materials with reasonably good success. But it has been observed by a number of researchers [1–4] that for some materials both K_{IC} and crack growth direction can depend on the coupon geometry. Albritton and Goree [5] demonstrated, through a number of experiments, a significant influence of geometry on K_{IC} for silicon carbide reinforced aluminum coupons. Three types of coupons were tested, namely compact–tension (CT), center–crack–tension (CCT) and single–edge–notch tension (SENT). It was observed that crack turning occurred for CT coupons while it did not occur for SENT and CCT coupons with the same configuration. These results led to further investigation of the problem by Richardson and Goree [6]. They proposed an empirical two–parameter (the parameters are K_{IC} and T–stress) fracture criterion which accounted for the geometry of the coupon. The validity of the model was demonstrated for Polymethyl methacrylate (PMMA) [6]. This model however did not account for turned cracks.

In the present study the crack turning behavior in isotropic and anisotropic materials is analyzed and the T–stress evaluated in front of a branched crack (or kink). The geometry of the branched crack problem with the relevant labels is shown in Figure 1. An infinite body (isotropic or anisotropic) with a main crack of length 2c and a kink (or branched crack) of length l is shown. The branched crack makes an angle θ with the X axis. Bi–axial loads σ and $k\sigma$ are applied remotely along the Y and X axis respectively. The T–stress is defined

as the constant term in the asymptotic stress expansion in front of the kink or the stress component which acts parallel to and along the kink. Cotterell and Rice [7] evaluated the T–stress in front of an unbranched or flat crack and proposed a criterion which determines the direction of crack growth. This T–stress based criterion is modified, and the modified criterion is extended in the present study to the case of the branched crack. A detailed description of the development of this T–stress based model is given in Chapter V.

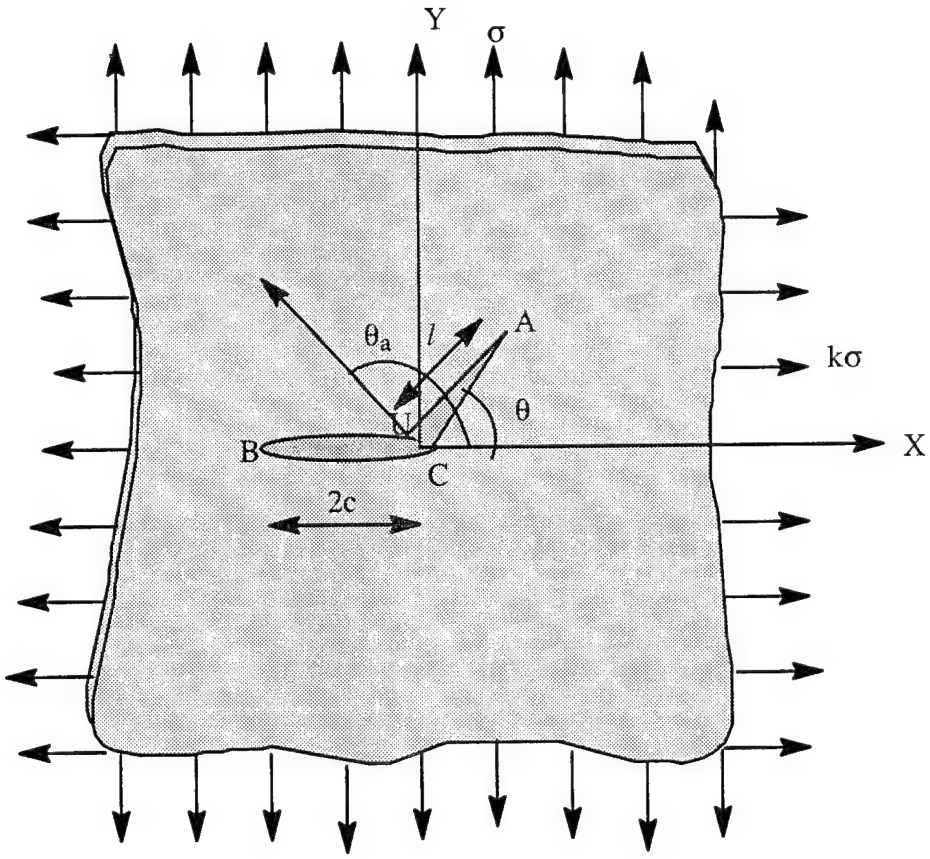

Figure 1. Geometry of the Branched Crack Problem

In order to study the influence of the T–stress on the branched crack it is necessary to solve the branched crack problem in an infinite panel for both isotropic and anisotropic materials. In the remainder of this chapter a review of the literature on the branched crack problem

is presented. A brief survey of related fracture models for predicting crack growth and stability which are available in the open literature is also given.

Literature Review On the Branched Crack Problem–Isotropic Materials

A large volume of literature is available on the subject of the branched crack in an isotropic material. It is interesting to note that crack branching was first studied for the dynamic crack growth problem before the focus shifted to crack branching during quasi–static crack growth. The term quasi–static (or static) is used to describe the condition when the crack–tip velocity is small, and there is no sudden change in velocity and the dynamic effect that it produces can be neglected.

Yoffee [8] was one of the earliest to study crack branching during dynamic crack growth in a brittle material like glass. She was the first to propose that fracture will take place in a direction normal to the maximum tensile stress in a dynamic crack growth situation. Based on this assumption, a critical velocity of crack growth was determined, above which crack branching occurred. Schardin [9], Clark and Irwin [10] and Congleton and Petch [11] studied similar problems both analytically and experimentally. Mostovy, et al., [4] and Carter [12] studied crack branching due to stress corrosion in high strength steel.

The analytical study of static crack branching can generally be grouped, based on the methodology used, into (1) conformal mapping techniques, (2) dislocation techniques, (3) Mellin transforms and (4) perturbation techniques.

Using conformal mapping, the geometry of the branched crack is first mapped on to an equivalent circle and then the mapped problem is solved. This method is used to calculate the stress intensity factors and the energy release rates at the branched or kinked crack tip. The disadvantage of this method is that its accuracy decreases as the kink length becomes infinitesimally small.

In the dislocation technique the kink is modeled as an edge dislocation. With this method it is possible to calculate the fracture parameters for infinitesimally small branched

cracks also. The dislocation technique is used in the formulation of the problem in the present study since a range of kink lengths, from infinitesimally small to very large can easily be modelled.

Mellin transform and perturbation techniques can also be used to solve infinitesimally small kink length problems. Perturbation techniques can be used to obtain solutions for finite kink lengths if more relevant terms are included in the series solution. Sometimes a combination of the above methods are used to solve the branched crack problem.

In the next few paragraphs a review of the literature on branched crack is given, which traces the development of studying branched crack problems in an isotropic and anisotropic material.

Conformal Mapping Techniques

Andersson [13,14] was the first to calculate the stress intensity factors at the tips of a star shaped contour in an infinite tensile sheet, with remote loading, using conformal mapping and Muskhelishvili [15] complex variable methods. Dudukalenko and Romalis [16] used conformal mapping techniques to map a finite crack with a branch onto a circle. They used maximum energy release criteria to determine the crack turning direction. Palaniswamy and Knauss [17] used conformal mapping techniques to study the branched crack problem. They compared the stress and energy based fracture criteria for mixed–mode fracture problems and concluded that the energy based criteria was conservative when compared to the maximum stress criteria. They also performed experiments relating to mixed–mode fracture and discussed the results in light of their analytical solution. Chatterjee [18] solved the branched crack problem by using conformal mapping method. He calculated the stress intensity factors in front of the kink and the main crack for small kink length of the order of 1/1000 th the main crack length. For smaller kink angles it was reported that the numerical scheme became unstable. Chatterjee also was the first to show that the stress singularity at the kink corner was indeed the Williams [19] singularity. It should be kept in mind that the

methodology used by Chatterjee for solving the problem was conformal mapping. A similar proof for verifying that the singularity at the kink corner is that given by the Williams [19] singularity for the branched crack problem (solved by dislocation techniques) will be discussed in this study. Hussain, et al., [20] used the conformal mapping technique to study the branched crack problem in an infinite plane and calculated the crack growth path based on Griffith's energy release criteria when the branched crack was very small compared to the main crack length. Kitagawa, et al., [21] and Kitagawa and Yuuki [22] also analyzed the problem of the branched crack using conformal mapping. They examined bent, curved, branched and zig–zag crack geometries. The influence of biaxial loading on the stability of crack growth was also addressed by them. They used the Erdogan and Sih [23] maximum hoop stress criteria to determine the angle of growth of a kinked crack. With their model they were able to analyze only finite kink geometry.

Dislocation Technique

Lo [24] was the first to solve the branched crack problem using the dislocation method and he obtained the stress intensity factors for the entire range of kink length varying from infinitesimally small to large kink length. The results obtained by Lo [24] agreed with the results of Chatterjee [18], Kitagawa, et al., [21] for finite kink lengths but disagreed with those of Dudukalenko, et al. [16], and Hussain, et al., [20] for infinitesimally small kink lengths. Karihaloo, et al., [25] used the dislocation method to reexamine the problem addressed by Cotterell and Rice [7] (who had obtained first order solutions) and constructed a second–order solution for the branched crack. For an infinitesimally small kink they were able to express the stress intensity factors in front of the kink in terms of the stress intensity factors in front of the main crack in a manner similar to Cotterell and Rice [7]. They were also able to obtain the correction terms for large kink angles by means of which the results obtained by Cotterell and Rice [7] could be extended for kink angles more than 40 degrees. It should be noted that Table. 1 in their paper (Karihaloo, et al. [25]) contains some numerical

errors but can be corrected if the formula they give earlier in the paper is used to calculate the quantities in the table. Hayashi and Nemat–Nasser [26], using dislocations, expressed the stress intensities and the energy release rate of the kink in terms of the stress intensities existing in front of the main crack and some coefficients whose numerical values were given in a tabular form. Datsyshin and Savruk [27] analyzed the problem of multiple arbitrarily oriented cracks using a method similar to the dislocation method. They obtained the solution in terms of singular integral equations where the unknown was the slope of the crack opening displacement just as in the dislocation method. They, however, did not study the case when the cracks touch each other. Theocaris and Ioakimidis [28] analyzed the symmetrically branched crack in an infinite body using a method similar to that used by Datsyshin and Savruk [27]. They also found that their results for stress intensity factors compared well with the experimental results of symmetrically branched cracks which was determined using the method of caustics [29]. Later Theocaris [30] also analyzed the problem of asymmetrically branched crack and found good agreement with the stress intensity factors obtained experimentally using the method of caustics [29]. The disadvantage of using the method used by Theocaris to solve branched crack problem is that instead of obtaining one complex singular integral equation as in the case of dislocation method, two complex singular integral equations are obtained.

Mellin Transform

Khrapkov [31], using Mellin transforms, obtained the solution for a branched crack emanating from a semi–infinite notch. Bilby and Cardew [32] obtained the stress intensity factors in front of the kink tip in terms of the stress intensity factors of the main crack for infinitesimally short kink lengths. The stress intensity factors for the in–plane and anti–plane problem were calculated using the methodology developed by Khrapkov [31]. They included the constant stress term (T–stress) parallel to the main crack in the analysis and made use of the maximum energy release criterion to predict the initial angle of crack kink-

ing. Later Bilby, et al., [33] solved the problem of forked cracks using the same methodology as discussed in [31]. They compared their results for a single branched crack with Chatterjee [18] and Kitagawa, et al., [21]. Their results for a branched crack agreed with Chatterjee [18] but disagreed with Kitagawa, et al. [21]. Melin [34] used the Mellin transform technique to obtain the stress intensity factors accurately in front of an infinitesimally small branched crack.

Perturbation Technique

Banichuk [35], using perturbation techniques and Muskhelishvili complex stress functions [15], obtained the solution for a weakly curved, infinitesimally small crack, in a brittle material using the local symmetry of the stress state (i.e., $K_{II}=0$) and the Griffith energy criterion. Gol'dstein and Salganik [36] used perturbation methods to calculate the stress intensity factors in front of an infinitesimally short kink. They used the criterion of local symmetry (i.e., $K_{II}=0$) to determine the growth direction of the kink. Cotterell and Rice [7] used methods similar to the ones used by Banichuk [35] and Gol'dstein, et al. [36], to solve the infinitesimally small branched crack with a small deviation from the main crack direction. They also incorporated the constant stress acting parallel to the main crack (T–stress) in their formulation and determined a stability criterion for crack branching using the T–stress. For an infinitesimally small kink Cotterell and Rice [7] compared their calculated stress intensity factors with those obtained by Bilby, et al., [33] and found good agreement even for larger (up to 40 degrees) angles of kink. For finite kinks their results matched well with those of Kitagawa, et al., [21]. They also expressed the stress intensity factors in front of the kink in terms of the stress intensity factor of the main crack and coefficients which are functions of the the kink angle. These coefficients are the terms containing the angular variation in the Irwin–Williams asymptotic stress expansion in front of the crack tip. The stress intensity factors obtained by Cotterell and Rice [7] were of first order approximation. Sumi, et al., [37] using perturbation methods and an alternating scheme developed a solution to de-

termine crack growth path in a finite geometry. They assumed a shape for the crack extension and by using the principle of local symmetry determined the crack growth path in a finite geometry. They also noted that for a first order approximation, the far field stresses in a finite body were not affected by the shape of the crack extension. Karihaloo, et al., [38] made use of the perturbation technique to obtain the curvature of the infinitesimally small growing kink. They reported that the curvature depended not only on the T–stress term but also on the derivatives of the stress intensities of the main crack with respect to the main crack length. Leblond [39] and Amestoy and Leblond [40] obtained a more exact expression for the stress intensity factors in front of the kink by using more terms in their asymptotic expansion. By making use of the principle of local symmetry and maximum energy release rate criterion they proposed a method to trace the path of a growing mixed–mode crack.

Literature Review On the Branched Crack Problem–Anisotropic Material

Branched cracks in an anisotropic body have been studied considerably less than the isotropic case. Eshelby [41] was the first to give expressions for the elastic displacement and energy due to a dislocation in an anisotropic body. This work was followed by Frank [42] who laid down the foundations of crystal dislocation theory. Eshelby, et al., [43] derived the general solution of the elasticity equations for an arbitrary homogeneous solid where the elastic state is independent of one of the three Cartesian coordinates. Following this earlier work Stroh [44] developed the expressions for the stresses in an general anisotropic body (where the field is independent of one of the three Cartesian coordinates) due to a dislocation, a pile of parallel dislocations and a crack. Atkinson [45] investigated the behavior of a moving semi–infinite plane crack in an anisotropic material where the direction of propagation lies in the plane of material symmetry. Atkinson [46] followed this work with a study of the interaction between a crack and a dislocation in an infinite anisotropic body where again the field is independent of one of the coordinate axis.

A general anisotropic elasticity theory was also developed independently by Lekhnits-

kii [47], Green and Zerna [48] and Savin [49]. The foundations of fracture mechanics as applied to cracks in anisotropic bodies was first introduced by Sih, et al., [50] and Wu [51]. Steen Krenk [52] developed the general solution for a finite number of collinear cracks in an anisotropic infinite body using the Muskhelishvili complex variable formulation. From the analysis he concluded that if the loads on the crack surface were self equilibrating then the normal and shear stresses on the lines of the crack were independent of the elastic constants. He also developed expressions for stress intensity factors in front of the crack tip. Tan and Bigelow [53] used the boundary force method to analyze an edge crack and an inclined single edge crack in a finite anisotropic body.

Obata, et al., [54] solved the branched crack problem using dislocation techniques. Their method was similar to that developed by Lo [32] for an isotropic case. Their analysis was valid only for infinitesimally small branched crack. They calculated the stress intensity factors and energy release rate in front of the kink and from the analysis concluded that the behavior of the stress intensity factor was similar to that of the isotropic case whereas the behavior of the energy release rate was different. Their conclusion was based on analyzing the problem in which the stiffer material axis was always perpendicular to or inclined at a small angle to the main crack. Obata, et al., [54] did not consider anisotropy in the fracture toughness of the material.

Chiang [55] gave an approximate solution for determining the stress intensity factors at the kink tip in terms of the stress intensity factors of the main crack for the case where the kink is infinitesimally small. The asymptotic stress field around the kink tip was derived for the degenerate case when the anisotropy becomes isotropic. Chiang [55] also notes that the maximum stress intensity necessarily does not occur when the kink angle is zero.

Gao and Chiu [56] used Stroh's [44] formulation to solve the infinitesimally small branched crack problem in an anisotropic body. With their model they were able to analyze wavy, jogged and kinked cracks. They provided first and second order perturbation solutions for stress intensity factors at the tip of the kink in terms of the stress intensity factors of the

main or macro crack. They also included the T–stress acting parallel to the macro crack in their formulation. It was observed that the stress intensity based fracture criteria leads to physically unreasonable branching angles whereas the strain energy based fracture criteria gave physically reasonable results for crack branching angles. Based on the energy criterion they were able to show that the T–stress can be used in the same way as in the isotropic case to determine the stability of crack propagation. They also did not include a variation in strength in their formulation.

Xu and Keer [57] used a perturbation technique in a manner similar to Cotterell and Rice [33] and Sumi, et al., [35] to express the stress intensity factors in front of the kink in terms of the stress intensity factors of the main crack. They incorporated anisotropy in strength in their model. By using the normal stress ratio criterion developed by Buczek and Herakovich [58] and Gregory and Herakovich [59] they were able to show that the T–stress may not behave the same way as in the isotropic case. For example, they showed that for some stiffness ratio and material orientation a negative T–stress caused unstable crack growth which is contrary to what is observed in isotropic materials.

Since the present study involves development of a fracture criteria to determine the behavior of a kinked crack, a brief survey of the development of several fracture criteria is given below.

Review of Salient Fracture Criteria–Isotropic Material

In the next few paragraphs some of the important fracture criteria are outlined for an isotropic material. The fracture criteria can be generally classified as either stress based or energy based. All the criteria discussed below are only for plane problems.

Griffith [60,61] was the first to develop the energy based fracture criteria. He postulated that the crack in a material grew if the rate of change of elastic energy of a material with respect to the crack length exceeded a critical energy rate. He determined that every material had a specific critical energy rate, called the critical energy release rate, which if exceeded

caused the crack to grow.

Irwin [62] used the stress intensity factors to determine when the crack grew and showed the equivalence between the energy release rate criteria and the stress intensity factors. All the work for some time was related to mode one fracture.

Erdogan and Sih [29] and Panasyuk, et al., [63] were the first to study the mixed mode static crack problem. Erdogan and Sih [29] argued that the crack travels in a direction perpendicular to the maximum hoop stress which also corresponds to zero shear stress. Based on experiments they performed, they observed that their model predicted experimental results reasonably well even though some discrepancy existed. Williams and Ewing [64] studied this problem further and showed that by including the non–singular stress term, namely the T–stress, the experimental results obtained by Erdogan and Sih [29] could be matched much better with their analytical results. Since the T–stress was included, the hoop stress had to be calculated at a certain distance from the crack tip. This distance was considered to be a material parameter which varied with materials but was fixed for a particular material. Finnie and Saith [65] pointed out an error in the Williams and Ewing [64] calculation which substantially improved the correlation between experiment and theory. Sih [66–67] introduced a fracture criterion based on strain energy density called the S–criterion. He proposed that fracture occurs along the direction in which the strain energy density attains a minimum value at a specific distance from the crack tip. This distance is a material parameter. A sample of the literature dealing with the energy or the stress based fracture criteria is listed in reference [68–72].

Review of Fracture Criteria–Anisotropic Materials

The fracture criteria for anisotropic bodies are much less developed than those for isotropic bodies. In fact, it has been only recently that a number of task groups have been established by ASTM to determine if isotropic fracture criterion could be extended to orthotropic bodies. Albritton and Goree [5] carried out experiments on silicon carbide reinforced alumi-

num and determined that the ASTM standards used for isotropic material cannot be applied to an orthotropic material like silicon carbide reinforced aluminum.

Sih, et al., [50] developed the equations for the near–crack–tip asymptotic stress fields for both in–plane and anti–plane problems. They also developed methods for determining stress intensity factors at the crack tip in an anisotropic body. The stress intensities were defined in such a manner that the form of the stress intensity factor was similar to the isotropic case but the actual magnitudes of the stresses were different since they depended on the material parameters. Based on this, Sih, et al., [50] concluded that same fracture criteria developed for isotropic materials could be extended to the anisotropic materials. They did not consider the variation in strength for the anisotropic material.

Maiti [73] used the stress intensities for an infinitesimal small kink to derive the energy release rate for an infinitesimal small kink and studied the variation of the energy release rate with the kink angle.

Saouma, et al., [74] studied the inclined crack problem (mixed–mode) in an anisotropic body. They maximized the ratio of the circumferential stress to the critical tensile strength of the material and observed that the material anisostropy significantly affected crack extension when compared to the predictions made by a similar isotropic model.

Zhang [75] studied the problem of relating the fracture toughness, parallel and perpendicular to the fiber of an orthotropic material. He proposed including the shear stress term for deriving the stress state in front of a crack perpendicular to a fiber. By including the shear stress term, the theoretical prediction matched closely to the experimental results.

Sarkar and Maiti [76] provided a formula for relating the critical fracture toughness of an orthotropic material due to a crack parallel to the fibers, to the critical fracture toughness when the crack is inclined at an angle to the fibers.

Zhang, et al., [77] proposed a new energy based fracture criterion to predict mixed mode crack initiation and propagation called the Z–criterion. This criterion suggests that mode I crack initiation is controlled by dilational strain energy, mode II crack initiation is

controlled by distortional strain energy and mixed mode crack initiation and propagation by the damage energy density factor called the Z–criterion. Zhang, et al., [78] extended Tsai–Hill and Norris criteria to predict crack turning in orthotropic materials.

Obata, et al., [54] solved the problem of an infinitesimally small kinked crack in an orthotropic material. They base their formulation on Lekhnitskii's [47] approach. Based on their results, they concluded that the behavior of the stress intensity factors for an orthotropic material is similar in nature to isotropic materials. But they note that the variation in energy is different from the isotropic case.

Chiang [55] solved the problem of a semi–infinite crack with a kink in an orthotropic material. He expressed the stress intensity factors in front of the kink in terms of the the stress intensity of the main crack and also derived the asymptotic stress field around the crack tip when the material becomes isotropic.

Ellyin and El Kadi [79] proposed a critical strain energy density criterion that predicts crack growth direction closer to experimental results. They also compare their results with the normal stress ratio criterion and minimum strain energy density and find that their model predicts crack turning angle better than the above mentioned models.

Gao and Chiu [56] use Stroh's formulation to solve the kinked crack problem in an anisotropic body. They point out to some erroneous conclusions by Obata, et al [54] which are described below. Gao and Chiu [56] observe that when the main crack is parallel to the fiber direction the local maximum for K_1 does not occur when the kink angle is zero which is contrary to what was reported by Obata, et al., [54]. They show that using stress intensity factors to predict crack turning angles leads to some physically impossible conclusions which are contrary to the isotropic case. The energy based criteria is shown to be a much better way of calculating the kink angles. This point was missed by Obata, et al., [54] since the formula they used to calculate the energy release rate was incorrect. Gao, et al., [56] also show that, based on energy criteria, the Cotterell and Rice [7] T–stress criteria to predict crack growth direction in isotropic material can be also extended to orthotropic materials. This conclusion

should be treated with caution since they did not include a variation in fracture toughness in their model.

Xu and Keer [57] used a perturbation technique to obtain the solution of an infinitesimally small kinked crack in an orthotropic material. They use the normal stress ratio criterion to predict crack growth direction and show that, for some stiffness ratios, negative T–stress leads to unstable crack growth which is contrary to the isotropic case.

This brief survey of existing literature suggests that much works needs to be done in the area of fracture mechanics as related to orthotropic materials.

How is the Present Study Different from Other T–stress Based Studies?

In the review of literature so far discussed, for isotropic and anisotropic materials, it should be noted that the T–stress calculated in front of the main crack tip has been used only to determine the stability of the crack growth. In other words the constant term in the asymptotic stress expansion in front of a flat crack has been used to determine the stability of the crack once it branches or kinks. What this study attempts to do differently is to first calculate the local T–stress in front of the branched crack or kink rather than calculate the T–stress when the kink is flat (or coincides with the main crack). By doing this, the stability of the branched or kinked crack itself can be discussed in terms of the local T–stress, which is a function of the length and angle of the kink and the remote loads. Also Cotterell and Rice's [7] T–stress criteria is modified to include an experimentally determined T_{crit} value and the modified criteria is applied to the branched crack, and the behavior of the branched crack is discussed in light of the modified T–stress criteria.

An Overview of this Study

This thesis is divided into two major subdivisions: (1) The Isotropic Case and (2) The Anisotropic Case.

The Isotropic Case: First a description of the problem is given followed by the for-

mulation of the analytical solution, which is similar to the one derived by Lo [24]. The difference between this formulation and Lo [24] is that a remote biaxial loading is included in the model. The analytical solution is obtained in terms of a singular integral equation in which the slope of the kink–opening–displacement is the unknown. This is followed by a proof showing that the singularity at the internal corner is given by the roots of the Williams' characteristic equation [19]. Then the singular integral equation is solved for the unknown slopes of the crack opening displacement using three different numerical schemes. The advantages and disadvantages of each numerical scheme is discussed in detail based on computational time, numerical stability and rate of convergence. Next, the method used to calculate the stress intensity factors and the local T–stress in front of the kink tip is outlined. This is followed by the description of the T–stress based fracture criteria to predict how an already kinked crack behaves. The influence of biaxial load on the local T–stress is also studied.

The Anisotropic Case: The details in this subdivision are very similar to that outlined in the isotropic Case. A brief description of the problem is followed by a general analytical solution to a branched crack problem in an orthotropic body. This is an extension of the methodology established by Obata, et al., [54]. The Obata, et al., [54] solution can be used only for infinitesimal small kink lengths where as the present formulation is capable of handling any kink length. The solution is obtained in terms of a singular integral equation where the slope of the crack opening displacement is the unknown. The singular integral equation is solved using three different numerical schemes. Again the effectiveness of each numerical scheme is discussed in the light of computational time, numerical stability and rate of convergence. The methods for calculating the stress intensity factors and the T–stress are established. The influence of anisotropy on the T–stress and stress intensity factors are discussed and a T–stress based fracture criteria is proposed which helps in the better understanding of crack turning in an anisotropic material.

CHAPTER II

ISOTROPIC MATERIAL

Analytical Formulation

The formulation of the branched crack problem in an isotropic material follows the procedure first developed by Lo [24]. Lo's formulation is extended to include bi–axial loads. Given below are the necessary equations in the final form. For more details on the derivation of the equations, the reader is referred to Appendix A.

The geometry of the problem with the relevant labels is shown in Figure 1 (page 2). Throughout the development of the analytical solution for the above branched crack problem, Muskhelishvili's [15] complex variable approach is used. Dislocations are used to model the kinked crack. A brief description of the dislocation function is given next.

Description of Dislocation Function

Physically, on an atomic level, dislocations occurs because of some vacant spaces in an atomic structure. In other words the continuity in the matter is lost. A line dislocation can be defined as a boundary between a perfect (unslipped) and imperfect (slipped) region in a crystal. The direction and magnitude of the slip is given by the Burgers vector $\vec{b}$. This line dislocation is classified into two types, namely the edge dislocation and the screw dislocation, depending on the direction of the Burgers vector. If the Burgers vector is perpendicular to the dislocation line (AD) it is known as an edge dislocation (Figure 2) and if the Burgers vector is parallel to the dislocation it is known as a screw dislocation (Figure 3).

Mathematically an edge dislocation is used to represent inplane shear (Figure 4) and normal stress (Figure 5) acting on a crack surface, while the screw dislocation is used to represent antiplane shear (Figure 6).

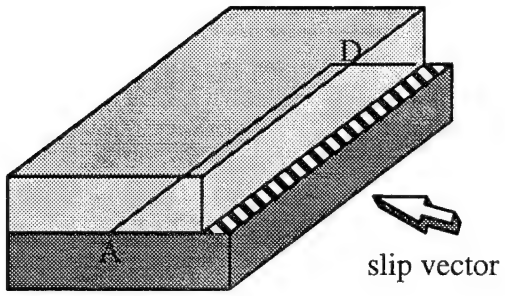

Figure 2. Edge Dislocation

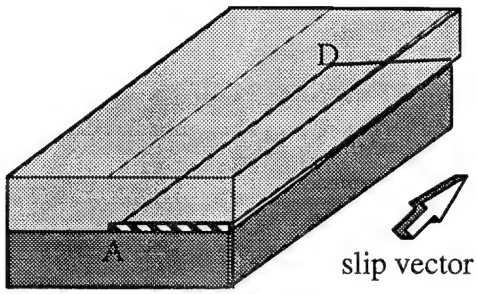

Figure 3. Screw Dislocation

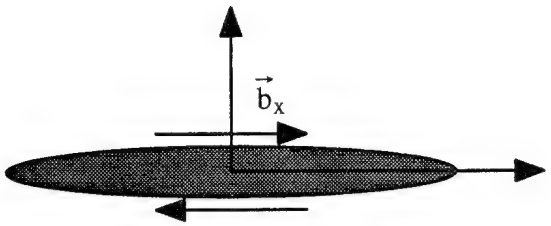

Figure 4. In Plane Shear

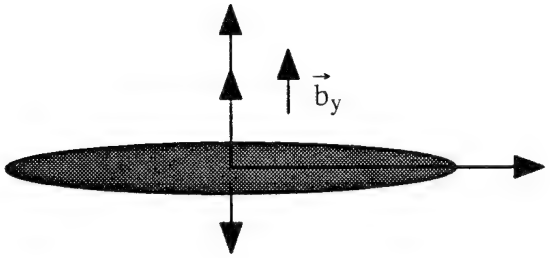

Figure 5. Normal Stress

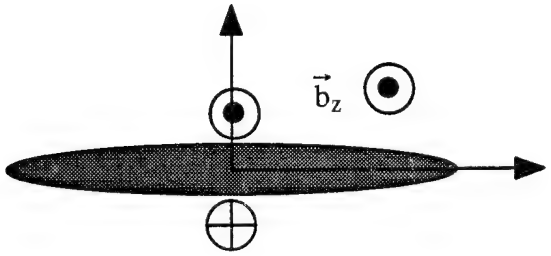

Figure 6. Anti Plane Shear

From a macroscopic view point a crack can be assumed to be made up of a series of these dislocations. Therefore, the stress fields due to a single dislocation can be viewed mathematically as a Green's function for a point discontinuity; and to obtain the stress field for a crack of finite length *l*, the Green's function is integrated over the length *l*.

Method of Superposition Explained

Superposition is used to solve the branched crack problem (Figure 7). First the stress functions ($\Phi_D(z),\psi_D(z)$) due to a single edge dislocation in an infinite isotropic body is formulated, this is step 1 in Figure 7. The stresses due to this line dislocation on the main crack which is of length 2c is obtained. The negative of this stress is applied on the main crack which is step 2 in Figure 7. The stress potentials ($\Phi_M(z),\psi_M(z)$) due to this loading conditions are next developed. By summing up step 1 and 2, the stress free main crack in the presence of a single dislocation is obtained. To obtain the stress functions for a kink the sum of the stress functions obtained in step 1 and 2 are integrated over the length of the kink. Next the stress fields ($\Phi_L(z),\psi_L(z)$) due to the main crack alone with loads at infinity are obtained as step 3 in Figure 7. The stress potentials for the kinked crack problem is given by the addition of the above three solutions. Finally a singular integral equation, in terms of the dislocation density function $\Theta(t_o)$, is obtained by satisfying the stress free boundary condition on the kink. The unknown $\Theta(t_o)$ is solved for by using a suitable numerical scheme.

Formulation of the Problem

Step 1

The stress functions due to a single dislocation in an infinite plane can be written as (see equations A.1–A.16).

$$\phi_D(z) = \Theta(t_o)\ln(z - z_o) \tag{1}$$

$$\psi_D(z) = \overline{\Theta(t_o)}\ln(z - z_o) - \Theta(t_o)\bar{z}_o/(z - z_o), \tag{2}$$

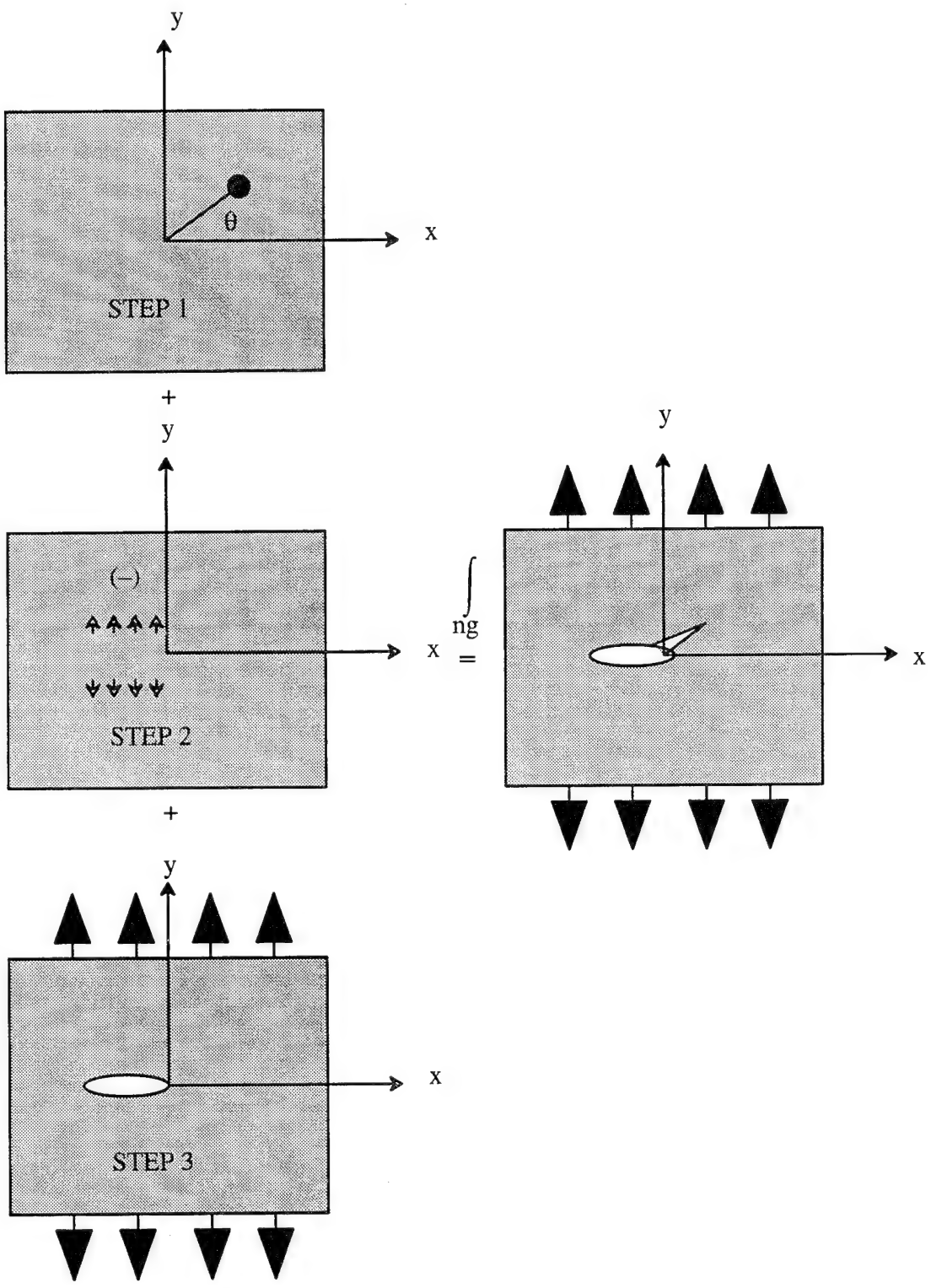

Figure 7. Superposition Steps in Solving the Kinked Crack Problem

where z defines the position of a point in the infinite plane and z_o defines the position of a dislocation. $\Theta(t_o)$ is the unknown function which is given by the jumps in displacements across the crack surfaces.

$$\Theta(t_o) = Eb(t_o)e^{i\theta}/\{\pi i(\varkappa + 1)\} \quad . \tag{3}$$

$$\vec{b}(t_o) = [u_r^+ - u_r^-] + i[u_\theta^+ - u_\theta^-], \tag{4}$$

where, $z=te^{i\theta a}$, $z_o=t_oe^{i\theta}$, E=Youngs Modulus, $\vec{b}(t_o)$ is the Burgers' vector, θ is the kink angle and κ is a constant whose value depends on the plane stress or plane strain assumption. The components of the Burgers' vector $\vec{b}(t_o)$ is shown in Figure 8 and Figure 9.

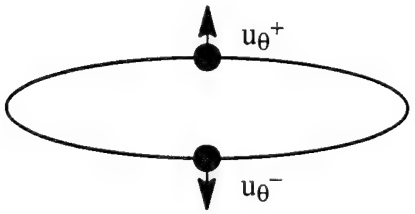

Figure 8. Tangential Jump

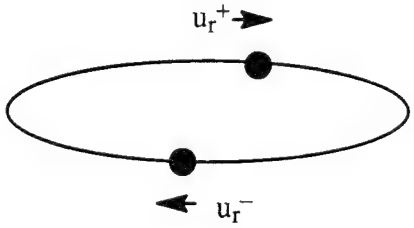

Figure 9. Radial Jump

The stresses are related to the differentials of the above functions (ϕ_D, ψ_D) and the differentials can be written as,

$$\phi'_D(z) = \Phi_D(z) = \Theta(t_o)/(z - z_o), \tag{5}$$

$$\psi'_D(z) = \Psi_D(z) = \overline{\Theta(t_o)}/(z - z_o) + \Theta(t_o)\bar{z}_o/(z - z_o)^2. \tag{6}$$

Step 2

The stresses acting on the main crack due to this dislocation is next evaluated and the negative of these stresses are applied on the main crack as shown in Figure 7. The corresponding stress functions are given as (see A.20–A.72),

$$\Phi_M(z) = -[\alpha(t_o)F(z,z_o) + \alpha(t_o)F(z,\ \bar{z}_o) + \overline{\alpha(t_o)}(z_o - \bar{z}_o)G(z,\ \bar{z}_o)], \tag{7}$$

$$\Psi_M(z) = \bar{\Phi}_M(z) - \Phi_M(z) - z\Phi'_M(z), \tag{8}$$

where,

$$F(z,z_o) = \frac{1}{2}\left[1 - \frac{X(z_o)}{X(z)}\right]/(z - z_o),$$

$$G(z,z_o) = \frac{\partial}{\partial z_o}F(z,z_o).$$

Step 3

The stress functions for step 3, i.e. the main crack with remote infinite loading in both the X and Y directions can be written down as (see A.73–A.85),

$$\Phi_L(z) = \frac{\sigma_{yy}^{\infty}}{2}\left[\frac{z+c}{X(z)} + \frac{k-1}{2}\right], \tag{9}$$

$$\Psi_L(z) = \frac{\sigma_{yy}^{\infty}}{2}\left[\frac{zc^2}{(X(z))^3} + (1-k)\right], \tag{10}$$

where,

$$X(z) = \sqrt{z(z+2c)},\ k = \frac{\sigma_{xx}^{\infty}}{\sigma_{yy}^{\infty}} \tag{11}$$

In the above equations, c is the half length of the main crack, and k is the biaxial stress ratio. By the principle of superposition the stress functions developed in steps 1,2 and 3 can be added to obtain the complete solution of the problem, as given below.

$$\Phi(z) = \Phi_D(z) + \Phi_M(z) + \Phi_L(z). \tag{12}$$

$$\Psi(z) = \Psi_D(z) + \Psi_M(z) + \Psi_L(z). \tag{13}$$

Once the stress functions are known, the stresses at any point in the infinite plane can be written in terms of the stress functions in polar co–ordinates as follows.

$$\sigma_{\theta\theta}(z) + i\sigma_{r\theta}(z) = \Phi(z) + \overline{\Phi(z)} + e^{2i\theta}[\bar{z}\Phi'(z) + \Psi(z)]. \tag{14}$$

$$\sigma_{rr}(z) - i\sigma_{r\theta}(z) = \Phi(z) + \overline{\Phi(z)} - e^{2i\theta}[\bar{z}\Phi'(z) + \Psi(z)]. \tag{15}$$

On the kink surface both the normal stress ($\sigma_{\theta\theta}$) and the shear stress ($\sigma_{r\theta}$) vanish. Imposing this condition and using Plemelj formula [15] the following singular integral equation is obtained (see A.86–A.90).

$$\sigma_{\theta\theta}(t) + i\sigma_{r\theta}(t) = 2\int_0^l \frac{\overline{\Theta(t_o)}e^{i\theta}dt_o}{t - t_o} + \int_0^l M(t, t_o; \Theta(t_o))dt_o + \sigma^{\infty}_{\theta\theta}(z) + i\sigma^{\infty}_{r\theta}(z) = 0, \tag{16}$$

where,

$$M(t, t_o, \alpha(t_o)) = \Phi_M(z) + \overline{\Phi_M(z)} + e^{2i\theta}[(\bar{z} - z)\Phi_M'(z) - \Phi_M(z) + \overline{\Phi_M}(z)]. \tag{17}$$

The above singular integral equation is in terms of the unknown $\Theta(t_o)$ whose behavior at the end points 0 and l has to be determined. From the geometry of the crack problem (Figure 1, page 2) it can be observed that the tip of the kink (A) has the well known square root singularity. At the other end of the kink (i.e. at the origin), the upper side of the kink, indicated by the letter U, is an external corner of a wedge and according to Williams [19], does not give rise to any stress singularity. The lower side of the kink, represented by C, is an internal corner of a wedge and (following Williams [19]) one would expect it to give rise to singular stresses. It has been shown by Chatterjee [18], by using conformal mapping techniques, that the lower side of the kink represented by C indeed gives rise to singular stresses. A similar exercise using the dislocation technique is lacking in the literature. It has been customary for researchers working the branched crack problem with the dislocation technique to recognize that the Williams' singularity exists at the wedge internal corner without proof.

In the section below, a complete proof verifying the existence of the Williams' singularity at the internal corner is given.

Verification of Existence of Williams' Singularity at the Internal Wedge Corner

Extension of Theorems for Singular Integrals to Bounded Integrals

For developing the proofs to verify the Williams' singularity at the lower side of the kink, it is necessary to extend theorems developed for singular integrals to bounded integrals. The bounded integral near the integration limits tends to a bounded (finite non–zero) part and a part which vanishes. It is essential to know how the vanishing term of the bounded integral goes to zero.

Following Muskhelishvili [83], consider the behavior of a Cauchy integral of the form,

$$F(z) = \int_0^l \frac{\alpha(t_o)}{t_o - z} dt_o, \tag{18}$$

near the limits of integration. The function $\alpha(t_o)$ is bounded every where in the region of integration $(0 - l)$ (i.e. it satisfies Holders condition in the range $0 - l$) except near the end points 0 and l. Near the end points $\alpha(t_o)$ can be assumed to be of the form

$$\alpha(t_o) = \frac{\lambda(t_o)}{t_o^{\alpha}(l - t_o)^{\beta}}, \tag{19}$$

where $\lambda(t_o)$ is bounded in the entire range of integration. α and β are assumed to be always between 0 and 1 in order to have bounded integrals. If the above conditions are satisfied, then, near the end of integration limit (say 0), F(z) can be written as follows (Muskhelishvili [83], see eq. 29.5, pg 74).

$$\lim_{z\to 0} F(z) = \lim_{z\to 0} \int_0^l \frac{\lambda(t_o)}{t_o^{\alpha}(1-t_o)^{\beta}} \frac{dt_o}{t_o - z} = \frac{\pi\lambda(0)e^{\pi i\alpha}}{\sin(\pi\alpha)} \lim_{z\to 0} \frac{1}{z^{\alpha}} + bf, \qquad (20)$$

where bf is a bounded function. A similar relation can be written for the behavior of the function at the other end l. If the restriction that $\alpha > 0$ is removed for the lower end (i.e. $\alpha < 1$ only) then α can have negative values and hence in the limit the integral has a part that vanishes and a bounded part. It should be noted that the same proof used to get the above relationship (20) can be used even when α is less than 0. Hence any asymptotic value for a Cauchy integral can be extended for the range $-\infty \leqq \alpha < 1$. It should be noted that when $\alpha = 0$ logarithmic singularities occur and equation (20) is no longer valid.

Proof For Verification of Williams Singularity

In order to verify the singularity at the wedge corner it is sufficient to examine the sum of the hoop and radial stresses. This simplifies the expression used for the asymptotic analysis. Using the stress functions the sum of the radial and hoop stresses can be written as,

$$\sigma_{rr}(z) + \sigma_{\theta\theta}(z) = 4\mathrm{Re}[\Phi(z)]. \qquad (21)$$

Since all the stresses vanish at the external corner of the wedge the sum of the radial and hoop stresses must also vanish at the external corner. Therefore using (5), (7), (9) and (12) in (21) the following expression is obtained.

$$\mathrm{Re}\{\Phi(z)\} = \mathrm{Re}\left[I_1(z) + I_2(z) + I_3(z) + I_4(z) + I_5(z) + I_6(z) + I_7(z) + C_1\right] = 0 \qquad (22)$$

where,

$$I_1(z) = \frac{1}{2}\int_0^l \frac{\Theta(t_o)}{z - z_o} dt_o,$$

$$I_2(z) = -\frac{1}{2}\int_0^l \frac{\Theta(t_o)}{z - \bar{z}_o} dt_o,$$

$$I_3(z) = \frac{1}{2}\int_0^l \frac{\Theta(t_o)X(z_o)}{X(z)(z - z_o)}dt_o,$$

$$I_4(z) = \frac{1}{2}\int_0^l \frac{\Theta(t_o)\overline{X(z_o)}}{X(z)(z - \overline{z}_o)}dt_o,$$

$$I_5(z) = -\frac{1}{2}\int_0^l \frac{\overline{\Theta(t_o)}(z_o - \overline{z}_o)}{(z - \overline{z}_o)^2}dt_o,$$

$$I_6(z) = -\frac{1}{2}\int_0^l \frac{\overline{\Theta(t_o)}(z_o - \overline{z}_o)\overline{X(z_o)}}{X(z)\ (z - \overline{z}_o)^2}dt_o,$$

$$I_7(z) = \frac{1}{2}\int_0^l \frac{\overline{\Theta(t_o)}(z_o - \overline{z}_o)(\overline{z}_o + c)}{X(z)X(\overline{z}_o)\ (z - \overline{z}_o)^2}dt_o,$$

$$C_1 = -\frac{1}{4} + \frac{(z + c)}{2X(z)},$$

where, X(z) is given by (11).

Using the limiting value of each integral near the end point, i.e. z = 0, the asymptotic values of each can be written down. Integrals with X(z) in their denominator require special attention. It is these integrals which have to be evaluated using the behavior for bounded integrals as discussed earlier. For example, consider integral I_3 which can be written as,

$$I_3(z) = \frac{1}{2}\int_0^l \frac{\Theta(t_o)X(z_o)}{X(z)(z - z_o)}dt_o,$$

$$= \frac{1}{2X(z)}\int_0^l \frac{\Theta(t_o)X(z_o)}{(z - z_o)}dt_o.$$

Now (see B.5, B.6),

$$\int_0^l \frac{\Theta(t_o)X(z_o)}{(z - z_o)}dt_o = -\frac{\sqrt{2c}\,\pi\beta(0)ie^{-i\theta_a}e^{-i[\alpha(\theta_a-\pi)]}e^{-i[\theta(1-\alpha)]}}{\cos(\pi\alpha)}\frac{1}{t^{\alpha-\frac{1}{2}}} + bf_3, \tag{23}$$

therefore,

$$\lim_{t\to 0} I_3(z) = \lim_{t\to 0}\frac{1}{2}\int_0^l \frac{\Theta(t_o)X(z_o)}{X(z)(z - z_o)}dt_o$$

$$= -\frac{\pi\beta(0)ie^{-i[\alpha(\theta_a-\pi)]}e^{-i[\theta(1-\alpha)]}}{2\cos(\pi\alpha)}\lim_{t\to 0}\frac{1}{t^{\alpha}} + \frac{bf_3}{\sqrt{t}}. \tag{24}$$

where bf_3 is a bounded function. If α is assumed to be less than 1/2 then the first term in equation (23) vanishes. If the vanishing term is neglected this would leave only the bounded part which from equation (24) results in only the $bf_3/t^{1/2}$ term. But if the vanishing term is retained and it is multiplied by X(z) then the first term in equation (24) results, plus the term containing bf_3. The other integrals can be evaluated in a similar manner. Refer to Appendix B for more details.

$$\lim_{t\to 0} I_1(z) = \lim_{t\to 0}\frac{1}{2}\int_0^l \frac{\Theta(t_o)}{z - z_o}dt_o = -\frac{\pi\beta(0)e^{-i[\alpha(\theta_a-\pi)]}e^{-i[\theta(1-\alpha)]}}{2\sin(\pi\alpha)}\lim_{t\to 0}\frac{1}{t^{\alpha}} + bf_1. \tag{25}$$

$$\lim_{t\to 0} I_2(z) = \lim_{t\to 0}\frac{1}{2}\int_0^l \frac{\Theta(t_o)}{z - \overline{z}_o}dt_o = -\frac{\pi\beta(0)e^{-i[\alpha(\theta_a-\pi)]}e^{-i[\theta(\alpha-1)]}}{2\sin(\pi\alpha)}\lim_{t\to 0}\frac{1}{t^{\alpha}} + bf_2. \tag{26}$$

$$\lim_{t\to 0} I_4(z) = \lim_{t\to 0}\frac{1}{2}\int_0^l \frac{\Theta(t_o)\overline{X(z_o)}}{X(z)(z - \overline{z}_o)}dt_o$$

$$= -\frac{\pi\beta(0)ie^{-i[\alpha(\theta_a-\pi)]}e^{-i[\theta(\alpha-1)]}}{2\cos(\pi\alpha)}\lim_{t\to 0}\frac{1}{t^{\alpha}} + \frac{bf_4}{\sqrt{t}}. \tag{27}$$

$$\lim_{t\to 0} I_5(z) = -\lim_{t\to 0}\frac{1}{2}\int_0^l \frac{\overline{\Theta(t_o)}(z_o - \overline{z}_o)}{(z - \overline{z}_o)^2}dt_o$$

$$= -\frac{\pi\overline{\beta(0)}i(1-\alpha)e^{-i[\alpha(\theta_a-\pi)]}e^{-i[\theta(\alpha-2)]}}{\sin(\pi\alpha)}\lim_{t\to 0}\frac{1}{t^{\alpha}} + bf_5 \tag{28}$$

$$\lim_{t\to 0} I_6(z) = -\lim_{t\to 0}\frac{1}{2}\int_0^{l}\frac{\overline{\Theta(t_o)}(z_o-\overline{z}_o)\overline{X(z_o)}}{X(z)\ (z-\overline{z}_o)^2}dt_o$$

$$= -\frac{\pi\overline{\beta(0)}(2\alpha-3)\sin(\theta)e^{-i[\alpha(\theta_a-\pi)]}e^{-i[\theta(\alpha-2)]}}{2\cos(\pi\alpha)}\lim_{t\to 0}\frac{1}{t^{\alpha}} + \frac{bf_6}{\sqrt{t}}. \tag{29}$$

$$\lim_{t\to 0} I_7(z) = \lim_{t\to 0}\frac{1}{2}\int_0^{l}\frac{\overline{\Theta(t_o)}(z_o-\overline{z}_o)(\overline{z}_o+c)}{X(z)\ (z-\overline{z}_o)^2}dt_o$$

$$= \frac{\pi\overline{\beta(0)}e^{-i[\alpha(\theta_a-\pi)]}e^{-i[\theta(\alpha-2)]}}{2\cos(\pi\alpha)}\lim_{t\to 0}\frac{1}{t^{\alpha}} + \frac{bf_7}{\sqrt{t}}. \tag{30}$$

$$C = -\frac{1}{4} + \frac{bf_c}{\sqrt{t}}, \tag{31}$$

where bf_i, i = 1..7 and bf_c are bounded functions. Substituting equations (24) to (31) in equation (22) and then using (22) in equation (21) and simplifying, the following equation is obtained.

$$\mathrm{Re}\Bigg[\Bigg\{\frac{-\beta(0)e^{-i[\alpha(\theta_a-\pi)-\frac{\pi}{2}]}\sin[\theta(\alpha-1)+\pi\alpha]}{\sin(2\pi\alpha)}$$

$$-\frac{\overline{\beta(0)}e^{-i[\alpha(\theta_a-\pi)-\frac{\pi}{2}]}e^{-i(\theta(\alpha-2))}\sin(\theta)(1-\alpha)e^{-i\pi\alpha}}{\sin(2\pi\alpha)} + (Bf)t^{\alpha}\Bigg\}\frac{1}{t^{\alpha}}$$

$$+\{A_1 + iA_2\}\frac{1}{\sqrt{t}}\Bigg] = 0 \tag{32}$$

where, $Bf=\{bf_1+bf_2+bf_5-1/4\}$, $A_1 = \mathrm{Re}\{bf_3+bf_4+bf_6+bf_7+bf_c\}$ and $A_2=\mathrm{Im}\{bf_3+bf_4+bf_6+bf_7+bf_c\}$.

As t tends to zero the coefficient of the $1/t^{1/2}$ term and the coefficient of $1/t^{\alpha}$ term should vanish. Considering the coefficient of the $1/t^{\alpha}$ term it can be written as,

$$\mathrm{Re}\Big[\beta(0)e^{-i[\alpha(\theta_a-\pi)-\frac{\pi}{2}]}\sin[\theta(\alpha-1)+\pi\alpha]$$

$$+ \overline{\beta(0)} \sin(\theta) e^{-i[\alpha(\theta_a - \pi) - \frac{\pi}{2}]} (1 - \alpha) e^{-i[\theta(\alpha - 2) + \pi\alpha]} \Big] = 0. \tag{33}$$

Since if the real part of a complex function is zero the real part of the complex conjugate should also be zero. Therefore,

$$\mathrm{Re}\Big[\overline{\beta(0)} e^{i[\alpha(\theta_a - \pi) - \frac{\pi}{2}]} \sin[\theta(\alpha - 1) + \pi\alpha]$$

$$+ \beta(0) \sin(\theta) e^{i[\alpha(\theta_a - \pi) - \frac{\pi}{2}]} (1 - \alpha) e^{i[\theta(\alpha - 2) + \pi\alpha]} \Big] = 0. \tag{34}$$

The above equation (34) can be written in matrix form as follows,

$$\mathrm{Re}\begin{bmatrix} \sin[\theta(\alpha - 1) + \pi\alpha] e^{i[\alpha(\theta_a - \pi) - \frac{\pi}{2}]} & e^{-i(\theta(\alpha - 2))} \sin(\theta)(1 - \alpha) e^{-i\pi\alpha} e^{i[\alpha(\theta_a - \pi) - \frac{\pi}{2}]} \\ e^{i(\theta(\alpha - 2))} \sin(\theta)(1 - \alpha) e^{i[\alpha(\theta_a - \pi) - \frac{\pi}{2}]} e^{i\pi\alpha} & \sin[\theta(\alpha - 1) + \pi\alpha] e^{-i[\alpha(\theta_a - \pi) - \frac{\pi}{2}]} \end{bmatrix}$$

$$\begin{bmatrix} \beta(0) \\ \overline{\beta(0)} \end{bmatrix} = \begin{bmatrix} 0 \\ 0 \end{bmatrix}. \tag{35}$$

If $\beta(0)$ and $\overline{\beta(0)}$ do not vanish, then the determinant of the above equation should vanish (i.e. at least one non–trivial solution exists). Therefore,

$$\sin[\theta(\alpha - 1) + \pi\alpha] + (1 - \alpha) \sin\theta = 0 \tag{36}$$

$$\sin[\theta(\alpha - 1) + \pi\alpha] - (1 - \alpha) \sin\theta = 0 \tag{37}$$

If equations (36) or (37) or both are satisfied by choosing α suitably, then the coefficient of $1/t^{\alpha}$ term vanishes. Considering the $1/t^{1/2}$ terms, an equation of the form,

$$A_1 = 0, \tag{38}$$

is obtained as t tends to zero.

Now let z approach the internal corner (C in Figure 1) of the wedge. X(z) is the only function which changes sign as the internal corner is approached. Performing an asymptotic analysis as before, the following relationship is obtained.

$$\sigma_{rr}(z) + \sigma_{\theta\theta}(z) = 4\mathrm{Re}\Bigg[\Bigg\{\frac{-\beta(0) e^{-i[\alpha(\theta_a - \pi) - \frac{\pi}{2}]} \sin[\theta(1 - \alpha) + \pi\alpha]}{\sin(2\pi\alpha)}$$

$$- \frac{\overline{\beta(0)} e^{-i[\alpha(\theta_a - \pi) - \frac{\pi}{2}]} e^{-i(\theta(\alpha - 2))} \sin(\theta)(1 - \alpha) e^{-i\pi\alpha}}{\sin(2\pi\alpha)} + (Bf) t^{\alpha} \Bigg\} \frac{1}{t^{\alpha}}$$

$$- \{A_1 + iA_2\}\frac{1}{\sqrt{t}}\Bigg] \tag{39}$$

The coefficient of the $1/t^{\alpha}$ terms in the above equation is not satisfied if equations (36) or (37) is satisfied. From equation (38) the coefficient of the $t^{1/2}$ term vanishes. Therefore as the reentrant corner is approached the stresses are $1/t^{\alpha}$ singular.

Consider equations (36) and (37) which are the same expression obtained for an isotropic wedge by Timoshenko[84]. According to Timoshenko [84] the Williams characteristic equations for a wedge can be written as,

$$\lambda \sin 2\alpha + \sin 2\lambda\alpha = 0, \tag{40}$$

$$\lambda \sin 2\alpha - \sin 2\lambda\alpha = 0. \tag{41}$$

The geometry of the wedge is given below in Figure 10.

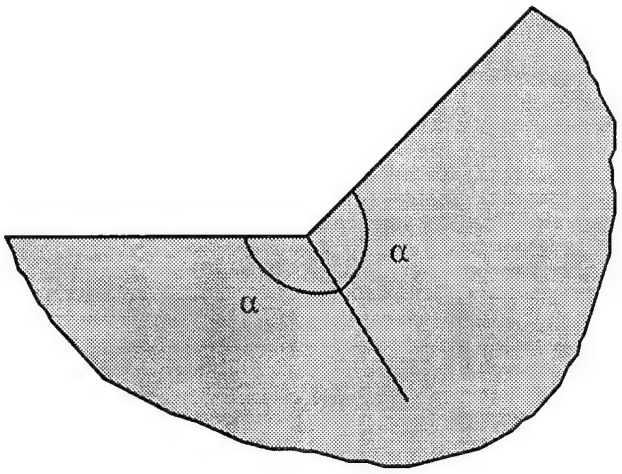

Figure 10. Geometry of the Wedge as Defined in Timoshenko, et al., [84]

Using the following change of variables,

$$\lambda = 1 - \alpha, \tag{42}$$

$$\alpha = \frac{\pi + \theta}{2}, \tag{43}$$

and substituting them (equations (42) and (43)) in equations (40) and (41), equations (36) and (37) can be recovered.

It has been conclusively shown that, in order for the stresses to vanish at the external corner of the wedge, the Williams' characteristic equations for the interior isotropic wedge has to be satisfied. Since the order of the stress singularity at the kink corner (C and U in Figure 1, page 2) is determined, the singular integral equation (16) can now be solved by using a suitable numerical scheme.

CHAPTER III

ANISOTROPIC MATERIAL

Analytical Formulation

The formulation of the branched crack problem in an anisotropic material follows the procedure developed by Krenk[52] and Lo [24]. This problem was also solved by Obata, et al., [54] using a different procedure, but the solution they developed was restricted to the infinitesimally small kink. In contrast, the solution developed below can be used for any kink length. The necessary equations in the final form are given below. For more details on the derivation of the equations the reader is referred to Appendix C.

The geometry of the problem with the relevant labels is shown in Figure 11. An infinite anisotropic body with a main crack of length 2c and a kink (or branched crack) of length l is shown. The branched crack makes an angle θ with the X axis. Bi–axial loads σ and $k\sigma$ are applied remotely along the Y and X axis respectively.

Throughout the development of the analytical solution for the above branched crack problem, Muskhelishvili's [14] complex variable approach is used. The problem is solved using the method of superposition in the same manner as for the isotropic case (Chapter II).

Development of Dislocation Function

The dislocation stress functions are given as (see C.40–C.55),

$$\Phi_D(z_1) = \phi'_D(z_1) = \frac{s_1 B_x - B_y}{(s_1 - s_2)(s_1 - s_3)(s_1 - s_4)c_{11}} \frac{1}{(z_1 - z_{01})}. \tag{44}$$

$$\Psi_D(z_2) = \psi'_D(z_2) = \frac{s_2 B_x - B_y}{(s_2 - s_1)(s_2 - s_3)(s_2 - s_4)c_{11}} \frac{1}{(z_2 - z_{02})} \tag{45}$$

where B_x and B_y are the components of the Burgers' vector.

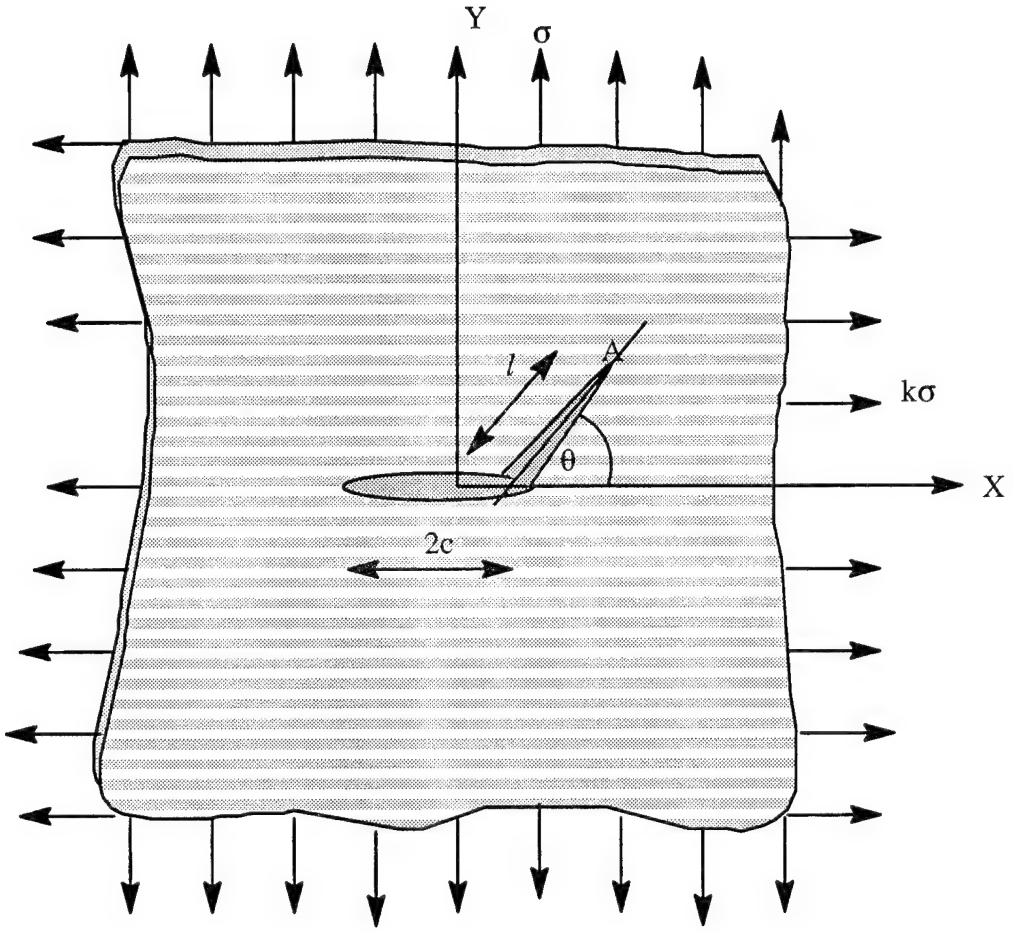

Figure 11. Geometry Of Anisotropic Branched Crack Problem

$$z_i = x + s_i y,\ z_{oi} = x_o + s_i y_o. \tag{46}$$

where, i = 1, 4. x_o and y_o indicates the position of the dislocation in the infinite plane.

Formulation of Stress Functions for the Main Crack Which Opens Up Due to the Presence of a Dislocation

The stress fields on the main crack due to a single dislocation are next evaluated by using the dislocation stress functions. Then the negative of these stresses are applied on the main crack and the stress functions are developed, following the formulation of Krenk [52]. After satisfying the condition for single valuedness of displacement, the following expressions are obtained (see C.56–C.117).

$$\Phi_M(z) = \frac{1}{c_{11}}\frac{1}{4\pi i}\frac{1}{(s_2 - s_1)}\left\{\frac{s_1 B_x - B_y}{(s_1 - s_3)(s_1 - s_4)}\frac{1}{z - z_{01}}\left(1 - \frac{X(z_{o1})}{X(z)}\right)\right.$$

$$- \frac{s_3 B_x - B_y}{(s_3 - s_4)(s_3 - s_1)}\frac{1}{z - z_{03}}\left(1 - \frac{X(z_{o3})}{X(z)}\right)$$

$$\left. - \frac{s_4 B_x - B_y}{(s_4 - s_3)(s_4 - s_1)}\frac{1}{z - z_{04}}\left(1 - \frac{X(z_{o4})}{X(z)}\right)\right\}.$$

$$\Psi_M(z) = \frac{1}{c_{11}}\frac{1}{4\pi i}\frac{1}{(s_1 - s_2)}\left\{\frac{s_2 B_x - B_y}{(s_2 - s_3)(s_2 - s_4)}\frac{1}{z - z_{02}}\left(1 - \frac{X(z_{o2})}{X(z)}\right)\right.$$

$$- \frac{s_3 B_x - B_y}{(s_3 - s_4)(s_3 - s_2)}\frac{1}{z - z_{03}}\left(1 - \frac{X(z_{o3})}{X(z)}\right)$$

$$\left. - \frac{s_4 B_x - B_y}{(s_4 - s_3)(s_4 - s_2)}\frac{1}{z - z_{04}}\left(1 - \frac{X(z_{o4})}{X(z)}\right)\right\}.$$

Formulation of Stress Functions for the Main Crack Which Opens Up Due to Loads at Infinity

The stress functions for the problem of the main crack with remote loadings can be obtained using the same general approach as discussed for the isotropic case and are given below (see C.118–C.133).

$$\Phi_L(z) = 2\,\mathrm{Re}\left(\frac{s_2\sigma_{yy}^{\infty}}{2(s_2 - s_1)}\frac{z}{X(z)} + i\frac{\sigma_{xx}^{\infty} + (\alpha_1\alpha_2 - \beta_1\beta_2)\sigma_{yy}^{\infty}}{2(s_2 - s_1)(\beta_1 + \beta_2)}\right). \tag{47}$$

$$\Psi_L(z) = 2\,\mathrm{Re}\left(\frac{s_1\sigma_{yy}^{\infty}}{2(s_1 - s_2)}\frac{z}{X(z)} + i\frac{\sigma_{xx}^{\infty} + (\alpha_1\alpha_2 - \beta_1\beta_2)\sigma_{yy}^{\infty}}{2(s_1 - s_2)(\beta_1 + \beta_2)}\right). \tag{48}$$

Formulation of the Singular Integral Equation

By satisfying the stress–free condition on the branched crack, the following expressions are obtained.

$$\begin{aligned}\sigma_{\theta\theta} =& \int_0^l \frac{M_{11}B_x(t_o) + M_{12}B_y(t_o)}{t - t_o}dt_o \\ &+ \int_0^l 2\,\mathrm{Re}\Big[(s_1\sin\theta + \cos\theta)^2\Phi_M(z_1) + (s_2\sin\theta + \cos\theta)^2\Psi_M(z_2)\Big]dt_o \\ &+ 2\,\mathrm{Re}\Big[(s_1\sin\theta + \cos\theta)^2\Phi_L(z_1) + (s_2\sin\theta + \cos\theta)^2\Psi_L(z_2)\Big] = 0\end{aligned} \tag{49}$$

$$\begin{aligned}\sigma_{r\theta} =& \int_0^l \frac{M_{21}B_x(t_o) + M_{22}B_y(t_o)}{t - t_o}dt_o \\ &+ \int_0^l 2\,\mathrm{Re}\Big[\Big(\big(1 - s_1^2\big)\sin\theta\cos\theta - s_1\cos 2\theta\Big)\Phi_M(z_1) \\ &+ \Big(\big(1 - s_2^2\big)\sin\theta\cos\theta - s_2\cos 2\theta\Big)\Psi_M(z_2)\Big]dt_o \\ &+ 2\,\mathrm{Re}\Big[\Big(\big(1 - s_1^2\big)\sin\theta\cos\theta - s_1\cos 2\theta\Big)\Phi_L(z_1) \\ &+ \Big(\big(1 - s_2^2\big)\sin\theta\cos\theta - s_2\cos 2\theta\Big)\Psi_L(z_2)\Big] = 0\end{aligned} \tag{50}$$

where,

$$z_i = a + t(\cos\theta + s_i\sin\theta),$$

$$z_{oi} = a + t_o(\cos\theta + s_i \sin\theta),$$

and i = 1, 2. M_{11}, M_{12}, M_{21} and M_{22} are given in the Appendix C (C.136–C.139).

CHAPTER IV

EVALUATION OF STRESS INTENSITY FACTORS AND T–STRESS

Isotropic Material

The mode I and mode II stress intensity factors are evaluated by extracting the singular parts of the stresses at the tip of the kink. Only the singular parts of the dislocation function contribute to the stress singularity at the kink tip. So only the stress functions associated with the dislocation functions are examined. The stress intensity factors at the kink tip are defined in terms of hoop and shear stresses in front of the kink as follows,

$$K_I + iK_{II} = \sqrt{2\pi}(r - l)^{\frac{1}{2}}\left[\sigma_{\theta\theta} + i\sigma_{r\theta}\right] \tag{51}$$

where r and θ are defined in Figure 12. The above stresses have already been normalized with respect to the applied uniaxial load σ_{yy}^{∞}.

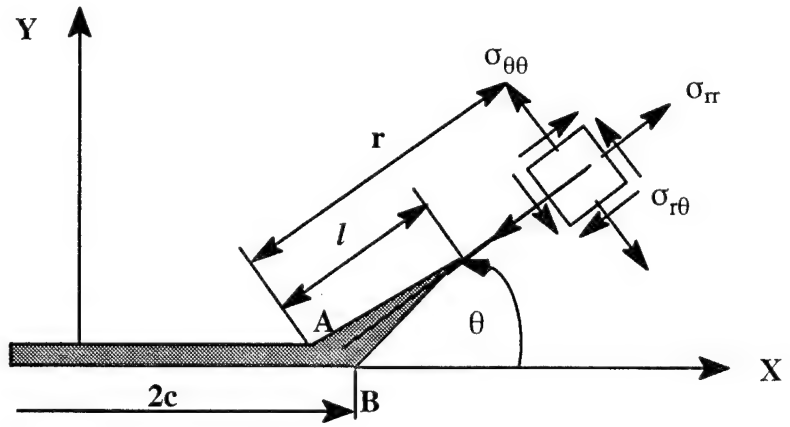

Figure 12. Configuration Describing Near–Kink–Tip Stresses for Evaluating Stress Intensity Factors

Using the stress functions, the stresses are written as,

$$\sigma_{\theta\theta} + i\sigma_{r\theta} = \Phi_D(z) + \overline{\Phi_D(z)} + e^{2i\theta}[\bar{z}\Phi_D'(z) + \Psi_D(z)], \tag{52}$$

where,

$$z = re^{i\theta}, \quad z_o = t_o e^{i\theta} \ (0 < t_o < l). \tag{53}$$

Substituting for the stress functions using equations (5) and (6) and simplifying, the following equation is obtained.

$$\sigma_{\theta\theta} + i\sigma_{r\theta} = 2\int_0^l \frac{\overline{\Theta(t_o)}e^{i\theta}}{r - t_o}dt_o, \text{ where} \tag{54}$$

$$\Theta(t_o) = \frac{\beta(t_o)}{l^{\alpha}(l - t_o)^{\beta}}, \text{ and} \tag{55}$$

α and β are the stress singularities at the kink corner and the kink tip respectively. The above equation is non–dimensionalized using the following transformation equations.

$$t_o = \frac{l}{2}(\xi_o + 1), \ r = \frac{l}{2}(\xi + 1), \ dt_o = \frac{l}{2}d\xi_o. \tag{56}$$

After substituting the transformation equations in equation (54) and simplifying, the following equation is obtained,

$$\sigma_{\theta\theta} + i\sigma_{r\theta} = 2\left(\frac{2}{l}\right)^{\alpha+\beta}\int_{-1}^{1} \frac{\overline{\beta(\xi_o)}e^{i\theta}}{(1 + \xi_o)^{\alpha}(1 - \xi_o)^{\beta}}\frac{d\xi_o}{\xi - \xi_o} \tag{57}$$

The limiting value of the above integral as ξ approaches 1 is evaluated using techniques in Muskhelishvili [83] for singular integrals.

$$\lim_{\xi\to 1}\int_{-1}^{1} \frac{\overline{\beta(\xi_o)}e^{i\theta}}{(1 + \xi_o)^{\alpha}(1 - \xi_o)^{\beta}}\frac{d\xi_o}{\xi - \xi_o} = \lim_{\xi\to 1}\frac{\pi\overline{\beta(1)}e^{i\theta}}{2^{\alpha}\sin\pi\beta}\frac{1}{(\xi - 1)^{\beta}}. \tag{58}$$

Using the above equation in equation (57) and then substituting into equation (51) and simplifying, the following is obtained where $\beta = 1/2$.

$$K_I + iK_{II} = \frac{4\pi^{3/2}\overline{\beta(1)}e^{i\theta}}{l^{\alpha+1/2}}. \tag{59}$$

In a similar manner, using the method developed by Sih, et al., [50] the stress intensity factors for the main crack can also be evaluated. Only the stress functions due to the main crack with loads at infinity and the stress functions due to the interaction between the main crack and a dislocation contribute to the singular stresses. Therefore

$$K_{MI} - iK_{MII} = -2i\sqrt{2\pi}\lim_{z\to z_1}(z - z_1)^{1/2}[\Phi_M(z) + \Phi_L(z)] \tag{60}$$

where K_{MI} and K_{MII} are mode I and mode II stress intensity factors for the main crack respectively. In this case $z_1 = -2c$ and $c \neq 0$. Substituting for the stress functions using equations (7), and (9) and simplifying, the following equation is obtained.

$$K_{MI} - iK_{MII} = -2i\sqrt{2\pi}\left\{\frac{i}{2\sqrt{2c}}\int_0^l \frac{\Theta(t_o)X(z_o)}{2c + z_o}dt_o + \frac{i}{2\sqrt{2c}}\int_0^l \frac{\Theta(t_o)X(\bar{z}_o)}{2c + \bar{z}_o}dt_o\right.$$

$$\left. - \frac{i}{2\sqrt{2c}}\int_0^l \frac{\overline{\Theta(t_o)}(z_o - \bar{z}_o)X(\bar{z}_o)}{(2c + \bar{z}_o)^2}dt_o + \frac{i}{2\sqrt{2c}}\int_0^l \frac{\overline{\Theta(t_o)}(z_o - \bar{z}_o)(\bar{z}_o + c)}{X(z_o)(2c + \bar{z}_o)}dt_o + \frac{i\sqrt{c}}{2\sqrt{2}}\right\} \tag{61}$$

All the integrals in the above equation are bounded and can be evaluated numerically once the unknown $\Theta(t_o)$ is calculated. If the kink vanishes then $\Theta(t_o) = 0$, therefore

$$K_{MI} - iK_{MII} = \sqrt{\pi c}$$

which is the stress intensity of the main crack alone under uniaxial tensile load. When the kink becomes flat i.e. $\theta = 0$ then the mode I stress intensity factor K_{IM} at the tip of the main crack becomes equal to the mode I stress intensity factor at the kink tip (K_I), i.e.

$$K_{MI} = \frac{2\sqrt{\pi}}{\sqrt{c}}\int_0^l \frac{\Theta(t_o)X(t_o)}{2c + t_o}dt_o + \sqrt{\pi c} = K_I. \tag{62}$$

Evaluation of the T–Stress for Isotropic Material

The T–stress is defined as the constant, 'ρ' independent term in the asymptotic expansion of the stress field around the tip of the crack (see equations 63 – 65). In the case of the branched crack problem two types of T–stress can be defined. One is the T–stress associated

with the main crack alone, i.e. without the branched crack and the other is the local T–stress defined at the tip of the branched crack. For a coordinate system as shown in Figure 13, the asymptotic stress expansion is given up to the constant term in the following equations.

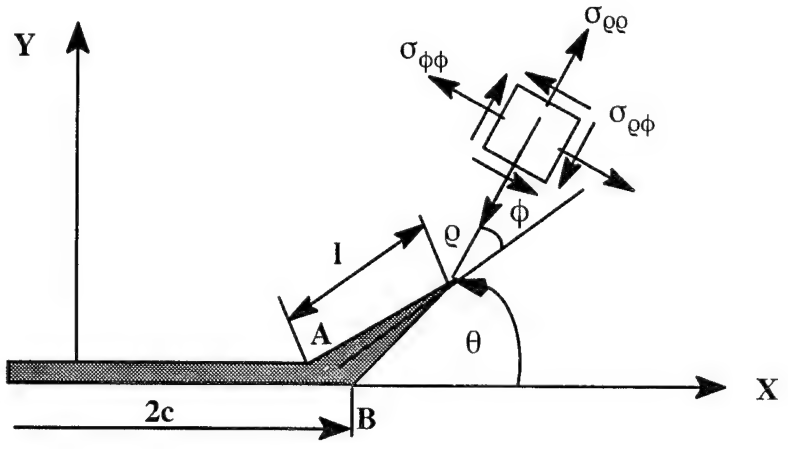

Figure 13. Near Crack–Tip Stresses for the Branched Crack.

$$\sigma_{\varrho\varrho} = \frac{K_I}{\sqrt{2\pi\varrho}}\left[\frac{5}{4}\cos\frac{\phi}{2} - \frac{1}{4}\cos 3\frac{\phi}{2}\right] + \frac{K_{II}}{\sqrt{2\pi\varrho}}\left[-\frac{5}{4}\sin\frac{\phi}{2} + \frac{3}{4}\sin 3\frac{\phi}{2}\right] + T\cos^2\phi, \tag{63}$$

$$\sigma_{\phi\phi} = \frac{K_I}{\sqrt{2\pi\varrho}}\left[\frac{3}{4}\cos\frac{\phi}{2} + \frac{1}{4}\cos 3\frac{\phi}{2}\right] + \frac{K_{II}}{\sqrt{2\pi\varrho}}\left[-\frac{3}{4}\sin\frac{\phi}{2} - \frac{3}{4}\sin 3\frac{\phi}{2}\right] + T\sin^2\phi, \tag{64}$$

$$\sigma_{\varrho\phi} = \frac{K_I}{\sqrt{2\pi\varrho}}\left[\frac{1}{4}\sin\frac{\phi}{2} + \frac{1}{4}\sin 3\frac{\phi}{2}\right] + \frac{K_{II}}{\sqrt{2\pi\varrho}}\left[\frac{1}{4}\cos\frac{\phi}{2} + \frac{3}{4}\cos 3\frac{\phi}{2}\right] - T\sin\phi\cos\phi. \tag{65}$$

If $\phi = 0$ and $\rho = 0$, then

$$\sigma_{\phi\phi} - \sigma_{\varrho\varrho} = -T. \tag{66}$$

i.e. the T–stress is given by the difference in the hoop stress and radial stress evaluated at the kink tip.

From Muskhelishvili [15],

$$\sigma_{\phi\phi} - \sigma_{\varrho\varrho} = 2\mathrm{Re}\left\{[\bar{z}\Phi'(z) + \Psi(z)]e^{2i\theta}\right\}, \tag{67}$$

where,

$$\Phi = \Phi_D + \Phi_M + \Phi_L$$

$$\Psi = \Psi_D + \Psi_M + \Psi_L$$

Consider the contribution from the dislocation function only, which can be written as

$$2\mathrm{Re}\left\{\left[\bar{z}\Phi_D'(z) + \Psi_D(z)\right]e^{2i\theta}\right\} = 2\,\mathrm{Re}\left\{\int_0^l \frac{e^{i\theta}\overline{\Theta(t_o)} - e^{-i\theta}\Theta(t_o)}{r - t_o}dt_o\right\}, \tag{68}$$

where $z = re^{i\theta}$. The integrand is a pure imaginary number and therefore there is no contribution to the T–stress from the dislocation function. Next, consider the contribution from Φ_M and Ψ_M.

$$2\mathrm{Re}\left\{\left[\bar{z}\Phi_M'(z) + \Psi_M(z)\right]e^{2i\theta}\right\} = 2\,\mathrm{Re}\left\{\overline{\Phi_M}(z) - \Phi_M(z) + (\bar{z} - z)\Phi_M'(z)\right\}. \tag{69}$$

After substituting for the above stress functions, by observation, the following singular integrals are isolated as 'r' approaches 'l'. The remaining integrals in the above equation (69) are bounded and converge to a finite limit which contributes to the T–stress.

$$\Phi_M(z) = -\frac{1}{2}\int_0^l \frac{\Theta(t_o)}{z - z_o}dt_o + \frac{1}{2}\int_0^l \frac{\Theta(t_o)X(z_o)}{X(z)}\frac{dt_o}{z - z_o} \tag{70}$$

$$\Phi'_M(z) = \frac{1}{2}\int_0^l \frac{\Theta(t_o)}{(z - z_o)^2}dt_o - \frac{1}{2}\int_0^l \frac{\Theta(t_o)X(z_o)(z + c)}{X(z)^3}\frac{dt_o}{z - z_o}$$

$$-\frac{1}{2}\int_0^l \frac{\Theta(t_o)X(z_o)}{X(z)}\frac{dt_o}{(z - z_o)^2} \tag{71}$$

$$\overline{\Phi}_M(z) = -\frac{1}{2}\int_0^l \frac{\overline{\Theta(t_o)}}{z - z_o}dt_o + \frac{1}{2}\int_0^l \frac{\overline{\Theta(t_o)}X(z_o)}{X(z)}\frac{dt_o}{z - z_o}$$

$$-\frac{1}{2}\int_0^l \frac{\Theta(t_o)(\bar{z}_o - z_o)}{(z - z_o)^2}dt_o + \frac{1}{2}\int_0^l \frac{\Theta(t_o)(\bar{z}_o - z_o)X(z_o)}{X(z)}\frac{dt_o}{(z - z_o)^2}$$

$$+\frac{1}{2}\int_0^l \frac{\Theta(t_o)(\bar{z}_o - z_o)(z + c)}{X(z)X(z_o)}\frac{dt_o}{z - z_o} \tag{72}$$

Therefore, substituting the above stress functions in equation (69) and simplifying, the following expression is obtained.

$$2\,\mathrm{Re}\left[\overline{\Phi_M}(z) - \Phi_M(z) + (\bar{z} - z)\Phi_M'(z)\right] =$$

$$2\,\mathrm{Re}\Bigg\{ -\frac{1}{2}\int_0^l \frac{\overline{\Theta(t_o)}}{z - z_o}dt_o + \frac{1}{2}\int_0^l \frac{\overline{\Theta(t_o)}X(z_o)}{X(z)}\frac{dt_o}{z - z_o}$$

$$+\frac{1}{2}\int_0^l \frac{\Theta(t_o)}{z - z_o}dt_o - \frac{1}{2}\int_0^l \frac{\Theta(t_o)X(z_o)}{X(z)}\frac{dt_o}{z - z_o}$$

$$-\frac{1}{2}\int_0^l \frac{\Theta(t_o)(\bar{z}_o - z_o)}{(z - z_o)^2}dt_o + \frac{1}{2}\int_0^l \frac{\Theta(t_o)(\bar{z}_o - z_o)X(z_o)}{X(z)}\frac{dt_o}{(z - z_o)^2}$$

$$+\frac{1}{2}\int_0^l \frac{\Theta(t_o)(\bar{z}_o - z_o)(z + c)}{X(z)X(z_o)}\frac{dt_o}{z - z_o} - \frac{1}{2}\int_0^l \frac{\Theta(t_o)X(z_o)(z + c)}{X(z)^3}\frac{dt_o}{z - z_o}$$

$$+\frac{1}{2}\int_0^l \frac{\Theta(t_o)}{(z - z_o)^2}dt_o - \frac{1}{2}\int_0^l \frac{\Theta(t_o)X(z_o)}{X(z)}\frac{dt_o}{(z - z_o)^2}\Bigg\} \tag{73}$$

In the limit as z tends to l the singular part of each pair of integrals given above cancel each other. Therefore, the contribution to the T–stress from Φ_M and Ψ_M is only a constant. Hence, if the real part of equation (69) is calculated at the crack tip it will be a constant which contributes to the T–stress. Consider the contribution from Φ_L and Ψ_L to the T–stress which is given by equation (74) for a biaxial loading condition.

$$2\mathrm{Re}\left\{\left[\bar{z}\Phi_L'(z) + \Psi_L(z)\right]e^{2i\theta}\right\} = 2\,\mathrm{Re}\left\{\left(\frac{c^2(z - \bar{z})}{2X(z)^3} - \frac{(k - 1)}{2}\right)e^{2i\theta}\right\}\sigma_{yy}^{\infty}, \tag{74}$$

where k is the biaxial stress ratio. The above equation can also be evaluated at the kink tip (i.e. $z=le^{i\theta}$). Therefore, by adding equations (74) and (69), the local T–stress can be evaluated at the kink tip. Some simplifications to the above expression for the T–stress can be made if an infinitesimally small kink length is assumed. Under this assumption the contribution to the T–stress from Φ_M and Ψ_M becomes small. Consider the contribution from Φ_L and Ψ_L only which, for infinitesimally small kink length can be expressed as,

$$2\mathrm{Re}\left\{\left[\bar{z}\Phi_L'(z) + \Psi_L(z)\right]e^{2i\theta}\right\} = \left\{\left[- \sqrt{\frac{c}{l}}\frac{\sin\theta \sin\frac{\theta}{2}}{\sqrt{2}} - (k - 1)\cos 2\theta \right]\right\}\sigma_{yy}^{\infty}. \tag{75}$$

Therefore,

$$T = \left\{\left[\sqrt{\frac{c}{l}}\frac{\sin\theta \sin\frac{\theta}{2}}{\sqrt{2}} - (k - 1)\cos 2\theta \right]\right\}\sigma_{yy}^{\infty} + \delta\ (\Phi_M, \Psi_M), \tag{76}$$

where $\delta(\Phi_M,\Psi_M)$ represents a small but finite contribution to the T–stress from Φ_M and Ψ_M. Using further manipulations the local T–stress in front of the incipient kink can be expressed in terms of the main crack mode I stress intensity factor K_{MI} (i.e. K_{MI} is calculated in front of the main crack as if the kink did not exist) as follows.

$$T = \frac{K_{MI}}{2\sqrt{2\pi l}}\left[\cos\left(\frac{\theta}{2}\right) - \cos\left(\frac{3\theta}{2}\right)\right] - \cos 2\theta\sigma_{yy}^{\infty}(k - 1) + \delta(\Phi_M, \Psi_M). \tag{77}$$

From the above equation, for a uniaxial load (i.e. k = 0), it can be seen that when θ = 0, from equation (69), $\delta(\Phi_M,\Psi_M) = 0$ and $T = -\sigma_{yy}^{\infty}$. Which means that when the kink is flat i.e. when then the axis of the kink coincides with the axis of the main crack the T–stress is the negative of the applied remote stress. Now as θ is varied the T–stress becomes positive rapidly because l is very small. Note that the above expression for the T–stress can be used only for an infinitesimally small kink length. Equation 77 can also be expressed as follows,

$$T = \frac{K_{MI}}{2\sqrt{2\pi l}}\left[\cos\left(\frac{\theta}{2}\right) - \cos\left(\frac{3\theta}{2}\right)\right] - (\sigma_{\xi\xi}^{\infty} - \sigma_{\eta\eta}^{\infty}) + \delta(\Phi_M, \Psi_M). \tag{78}$$

where $\sigma_{\xi\xi}^{\infty}$ and $\sigma_{\eta\eta}^{\infty}$ are the components of the remote loads parallel to and perpendicular to the kink respectively as shown in Figure 14.

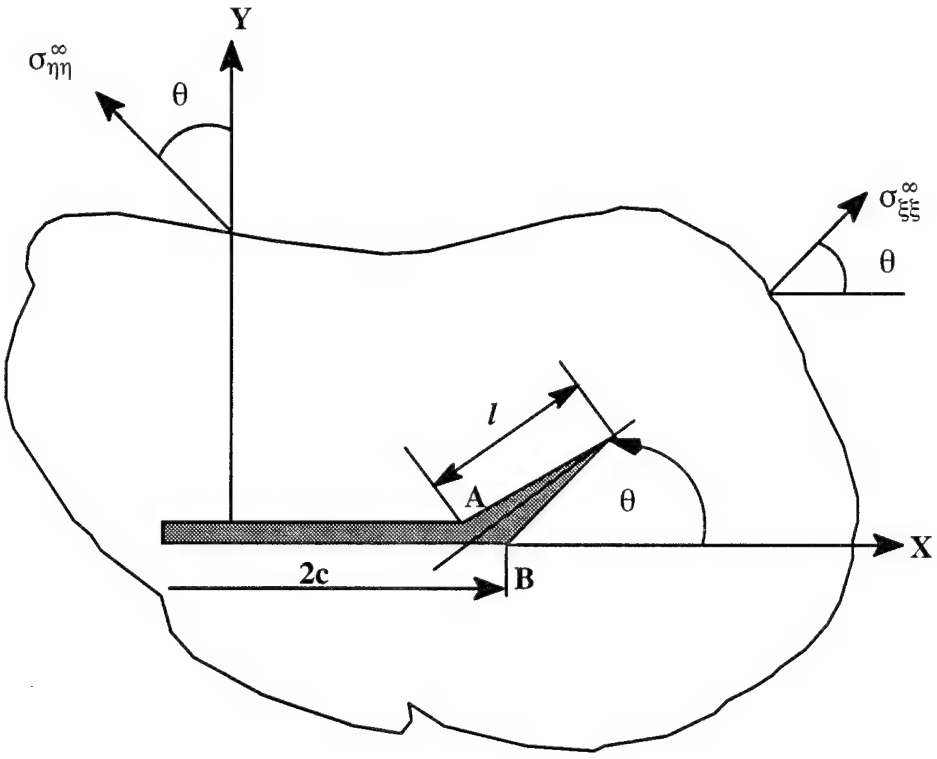

Figure 14. Components of Remote Loads Parallel to and Perpendicular to the Kink.

Anisotropic Material

The stress intensity factors at the kink tip for anisotropic material are evaluated the same way as the isotropic case. The mode I and mode II stress intensities are given as

$$K_I = \sqrt{2\pi}(r - l)^{\frac{1}{2}} \sigma_{\theta\theta} \tag{79}$$

$$K_{II} = \sqrt{2\pi}(r - l)^{\frac{1}{2}} \sigma_{r\theta} \tag{80}$$

where the stresses are evaluated along the kink axis. Using the stress functions,

$$\sigma_{\theta\theta} = \int_0^l \frac{M_{11}B_x(t_o) + M_{12}B_y(t_o)}{r - t_o} dt_o. \tag{81}$$

$$\sigma_{r\theta} = \int_0^l \frac{M_{21}B_x(t_o) + M_{22}B_y(t_o)}{r - t_o} dt_o. \tag{82}$$

Let,

$$B_x(t_o) = \frac{\beta_x(t_o)}{t_o^{\alpha}(l - t_o)^{\beta}}, \tag{83}$$

$$B_y(t_o) = \frac{\beta_y(t_o)}{t_o^{\alpha}(l - t_o)^{\beta}}. \tag{84}$$

Consider the integral associated with $\sigma_{\theta\theta}$. Using the following transformations, the integral equation can be normalized in the range from –1 to 1.

$$t_o = \frac{l}{2}(\xi_o + 1),\ r = \frac{l}{2}(\xi + 1),\ dt_o = \frac{l}{2}d\xi_o. \tag{85}$$

$$\sigma_{\theta\theta} = \left(\frac{2}{l}\right)^{\alpha+\beta} \int_{-1}^{1} \frac{M_{11}\beta_x(\xi_o) + M_{12}\beta_y(\xi_o)}{(1 + \xi_o)^{\alpha}(1 - \xi_o)^{\beta}(\xi - \xi_o)} d\xi_o. \tag{86}$$

As ξ tends to 1 the singular part is given as,

$$\sigma_{\theta\theta} = \frac{\pi 2^{\beta}}{l^{\alpha+\beta}} \frac{M_{11}\beta_x(1) + M_{12}\beta_y(1)}{(\xi - 1)^{\beta}} \tag{87}$$

Substituting the above equation in (79) and simplifying, after letting $\beta = 1/2$, the following is obtained.

$$K_I = 2\pi^{3/2} \frac{M_{11}\beta_x(1) + M_{12}\beta_y(1)}{l^{\alpha+1/2}}. \tag{88}$$

In a similar manner,

$$K_{II} = 2\pi^{3/2} \frac{M_{21}\beta_x(1) + M_{22}\beta_y(1)}{l^{\alpha+1/2}}. \tag{89}$$

Evaluating the T–stress for Anisotropic Material

Although the method of calculating the stress intensity factors are the same for the isotropic and anisotropic cases, the method of calculating the T–stress is different for anisotropic material since the equations do not lend themselves to simplifications as in the isotropic

case. The T–stress is calculated by evaluating the stresses on the flanks of the kink or branched crack. The only stress which is non–zero on the flank of the branched crack is the radial stress. The radial stress on the flank, near the kink tip, contains singular terms and a constant term which is the T–stress. By isolating the singular term the constant term can be calculated more accurately. The radial stress for any kink orientation θ is given as,

$$\sigma_{rr} = 2\,\mathrm{Re}\Big[\Phi(z_1)(s_1\cos\theta - \sin\theta)^2 + \Psi(z_2)(s_2\cos\theta - \sin\theta)^2\Big], \qquad (90)$$

where,

$$\Phi(z_1) = \Phi_D(z_1) + \Phi_M(z_1) + \Phi_L(z_1). \qquad (91)$$

$$\Psi(z_2) = \Psi_D(z_2) + \Psi_M(z_2) + \Psi_L(z_2). \qquad (92)$$

The subscript D indicates stress functions associated with the dislocation only, the subscript M indicates stress function associated with the interaction due to the main crack and dislocation and subscript L is associated with the main crack under remote loading. The radial stress σ_{rr} can thus be split up into three components,

$$\sigma_{rr} = \sigma_{rr}^D + \sigma_{rr}^M + \sigma_{rr}^L, \qquad (93)$$

where the superscripts have their usual meaning. Only the dislocation component of the stress (σ^D_{rr}) gives rise to singular stresses as the crack tip is approached along the kink. The remaining components are all bounded on the flank of the kink. The radial stress due to the dislocation is given as,

$$\sigma_{rr}^D = 2\,\mathrm{Re}\Big[\Phi_D(z_1)(s_1\cos\theta - \sin\theta)^2 + \Psi_D(z_2)(s_2\cos\theta - \sin\theta)^2\Big]. \qquad (94)$$

Substituting for the stress functions and simplifying,

$$\sigma_{rr}^D = \int_0^l \frac{M_{31}B_x(t_o) + M_{32}B_y(t_o)}{z_1 - z_{o1}}\,dt_o, \qquad (95)$$

where,

$$M_{31} = 2\,\mathrm{Re}\left[\frac{1}{2\pi i}\frac{1}{c_{11}}\left\{\frac{(s_1\cos\theta - \sin\theta)^2 s_1}{(s_1 - s_2)(s_1 - s_3)(s_1 - s_4)}\right.\right.$$

$$+\frac{(s_2\cos\theta-\sin\theta)^2 s_2}{(s_2-s_1)(s_2-s_3)(s_2-s_4)}\Bigg\}\Bigg],$$

$$M_{32} = -2\,\mathrm{Re}\Bigg[\frac{1}{2\pi i}\frac{1}{c_{11}}\Bigg\{\frac{(s_1\cos\theta-\sin\theta)^2}{(s_1-s_2)(s_1-s_3)(s_1-s_4)}$$

$$+\frac{(s_2\cos\theta-\sin\theta)^2}{(s_2-s_1)(s_2-s_3)(s_2-s_4)}\Bigg\}\Bigg]$$

and z_1 is any point on the infinite plane except on the kink or branched crack.

For calculating stresses on the flank, z_1 is allowed to be on the line of discontinuity (i.e. the branched crack). Therefore, using the Plemelj formulae,

$$\sigma^{\pm D}_{\pi} = \pm\,\pi i\left[M_{31}B_x(t) + M_{32}B_y(t)\right] + \int_0^{l}\frac{M_{31}B_x(t_o) + M_{32}B_y(t_o)}{t - t_o}dt_o. \qquad (96)$$

The above relation is valid at all points on the line of discontinuity $(0 - l)$ except at the end points. But the stresses we are interested in has to be evaluated at the end point. This is not a problem since accurate T–stresses can be obtained by removing the singular component and then evaluating the stresses very close to the end point but not at the end point itself. The singular component comes from the first terms in equation (96) and the second term is bounded for all values of t and t_o except at the end points. Therefore, by neglecting the first term in equation (96) and evaluating the sum of the terms in equation (93) accurate T–stresses can be calculated on the flank of the kink since the numerical evaluation is no longer obscured by terms which are very large.

CHAPTER V

RESULTS AND DISCUSSION–I

Isotropic Material

The singular integral equation (16) is solved using the three methods discussed in Appendix E. As discussed in Appendix E, in the first method (MI) a stronger singularity is assumed at the intersection of the kink corner and the main crack, i.e. a square root singularity is assumed at the kink corner while in reality the singularity there is less than square root. In the other two methods (MII and MIII) the correct singularity, which is given by the roots of the equations (36) and (37) is assumed at the kink corner. The numerical results for stress intensity factors (mode I and mode II) given by the three methods are compared with the solution obtained by Isida, et al., [86] for a range of kink to main crack length ratio (l/2c) and kink angles (θ). The boundary force method combined with perturbation techniques was used by Isida, et al., [86] to obtain the solution for the branched crack problem with various loading conditions. The loading configurations for which the comparisons are made are shown in Figure 15, Figure 16 and Figure 17. The reason for choosing Isida's [86] among the other available solutions in the literature is because numerical values can be obtained accurately from tables as opposed to obtaining numbers from a graph as in other cases. The numerical values compared are the mode I and II stress intensity factors (namely K_I and K_{II}) which are normalized with respect to the stress intensity factor of the main crack. One typical comparison using method I (MI) subjected to load case 1 for a kink to main crack length ratio of 0.005 is shown in Table 1. Numerical results using methods II (MII) and III (MIII) are compared in Table 2 and 3. From the numerical values given in these tables the following observations can be made. Method I, although it assumes a stronger (square root) singularity at the kink corner, still gives accurate results. Method II uses the correct singularity at the kink corner but it requires a large number of terms for convergence. This is due mainly to

the presence of other less dominant roots of the Williams characteristic equations (36) and (37) which results in the unboundedness of the slope of the bounded function. Once these roots are taken care of, as in Method III, the convergence rate is very fast (almost as fast as method I). The convergence is fast because not only the bounded function but also the singular nature of the slope of the bounded function is taken care of in the series representation of the unknown as discussed in the Appendix E. Table 4 shows the two roots of the Williams' characteristic equation used in the numerical method. The fourth column in the table gives the slope of the bounded function and the negative value is indicative of the fact that the derivatives are unbounded at the kink corner. It is due to this fact that the method II has a very slow convergence. Numerical results for load cases 2 and 3 shown in Figures 16 and 17 are compared with Isida, et al., [86] in Tables 5 and 6 for a kink to main crack length ratio of 0.005 using method I.

Tables 7 and 8 compares the mode I and mode II stress intensity factors obtained by using method I and III respectively with the solutions obtained by Isida et al., [86] and Mellin [34] when the kink becomes infinitesimally small. All the results given are for a unit loading at infinity, normal to the main crack. The difference in the stress intensity factors between the three methods is always less than 1%.

All the three methods give accurate values for mode I and II stress intensity factors. Method II (not shown) and III, where the correct singularity is assumed compare more favorably with the result obtained by Mellin [34] and Isida [86] for larger values of kink angles.

From the above comparison of mode I and II stress intensity factors it can be concluded that the nature of the stress singularity at the kink corner does not influence the stress intensity factors at the kink tip. A similar conclusion about the T–stress can be made from Table 9 where it can be observed that the difference in the T–stress values calculated by the three methods are negligible (< .5%). Though the particular case shown is for a kink to main crack length ratio of 0.005 the results hold true for all range of kink to main crack length ratios.

Table 1. Load Case 1 (No. of Quadrature Points = 121, Method I)

l/2c	θ	K_I[MI]	K_{II}[MI]	K_I[Isida]	K_{II}[Isida]	Diff% K_I	Diff% K_{II}
0.005	0	1.0025	0.0	1.0025	0.0	0	0
0.005	10	0.9911	0.0862	0.9912	0.0862	0.01	0.0
0.005	20	0.9579	0.1676	0.9580	0.1676	0.01	0.0
0.005	40	0.8344	0.2989	0.8344	0.2989	0.0	0.0
0.005	60	0.6594	0.3688	0.6592	0.3690	0.03	0.05
0.005	80	0.4677	0.3705	0.4672	0.3708	0.11	0.08
0.005	90	0.3759	0.3484	0.3752	0.3489	0.18	0.14

Table 2. Load Case 1 (No. of Terms in Polynomial, n = 40, Method II)

l/2c	θ	K_I[MII]	K_{II}[MII]	K_I[Isida]	K_{II}[Isida]	Diff% K_I	Diff% K_{II}
0.005	0	1.0027	0.0	1.0025	0.0	0.02	0.0
0.005	10	0.9912	0.0862	0.9912	0.0862	0.0	0.0
0.005	20	0.9579	0.1676	0.9580	0.1676	0.01	0.0
0.005	40	0.8345	0.2990	0.8344	0.2989	0.01	0.03
0.005	60	0.6593	0.3691	0.6592	0.3690	0.02	0.03
0.005	80	0.4673	0.3710	0.4672	0.3708	0.06	0.03
0.005	90	0.3753	0.3490	0.3752	0.3489	0.03	0.03

Table 3. Load Case 1 (No. of Terms in Polynomial, n_1= 6, n_2 =4, [see E.14] Method III)

l/2c	θ	K_I[MIII]	K_{II}[MIII]	K_I[Isida]	K_{II}[Isida]	Diff% K_I	Diff% K_{II}
0.005	10	0.9912	0.0862	0.9912	0.0862	0.0	0.0
0.005	20	0.9579	0.1676	0.9580	0.1676	0.01	0.0
0.005	40	0.8344	0.2990	0.8344	0.2989	0.0	0.03
0.005	60	0.6592	0.3691	0.6592	0.3690	0.0	0.03
0.005	80	0.4673	0.3710	0.4672	0.3708	0.06	0.03
0.005	90	0.3752	0.3490	0.3752	0.3489	0.0	0.03

Table 4. Two Roots of the Williams' Characteristic Equations (36) and (37) Used in Numerical Analysis

θ	α_1	α_2	$\alpha_1-\alpha_2-1$
10	0.0999	0.0	–0.9001
20	0.1813	0.0	–0.8187
40	0.3028	0.0	–0.6972
60	0.3842	0.0	–0.6158
80	0.4371	0.0195	–0.5824
90	0.4555	0.0914	–0.6359

Table 5. Load Case 2 (No. of Quadrature Points = 121)

l/2c	θ	K_I[MI]	K_{II}[MI]	K_I[Isida]	K_{II}[Isida]	Diff% K_I	Diff% K_{II}
0.005	0	0.0	0.0	0.0	0.0	0.0	0.0
0.005	10	–0.0027	0.0154	–0.0027	0.0154	0.	0.0
0.005	20	–0.0105	0.0291	–0.0105	0.0291	0.0	0.0
0.005	40	–0.0377	0.0460	–0.0376	0.0459	0.27	0.22
0.005	60	–0.0698	0.0438	–0.0698	0.0438	0.0	0.0
0.005	80	–0.0937	0.0246	–0.0936	0.0246	0.11	0.0
0.005	90	–0.0993	0.0113	–0.0993	0.0114	0.0	0.88

Table 6. Load Case 3 (No. of Quadrature Points = 121)

l/2c	θ	K_I[MI]	K_{II}[MI]	K_I[Isida]	K_{II}[Isida]	Diff% K_I	Diff% K_{II}
0.005	0	0.0	1.0025	0.0	1.0025	0.0	0.0
0.005	10	–0.2607	0.9785	–0.2607	0.9785	0.0	0.0
0.005	20	–0.5086	0.9085	–0.5086	0.9083	0.0	0.02
0.005	40	–0.9201	0.6524	–0.9199	0.6520	0.02	0.06
0.005	60	–1.1659	0.3035	–1.1655	0.3033	0.03	0.06
0.005	80	–1.2223	–0.0495	–1.2216	–0.0490	0.06	1.02
0.005	90	–1.1848	–0.2013	–1.1840	–0.2004	0.07	0.45

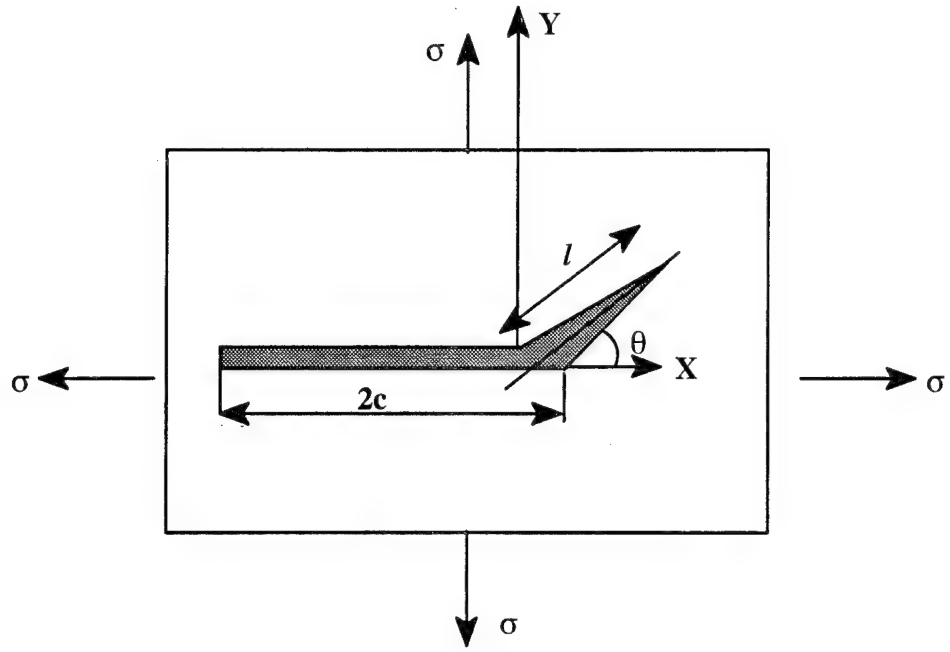

Figure 15. Loading Condition 1

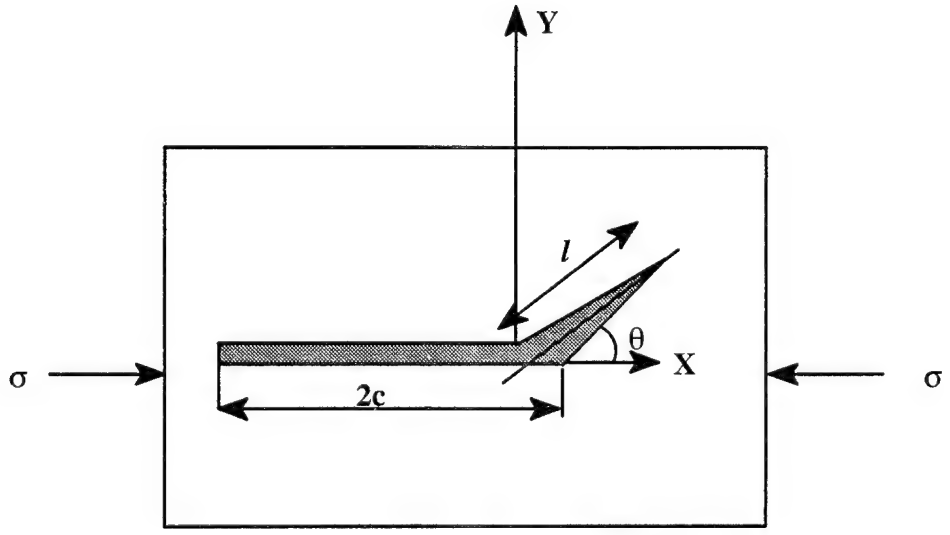

Figure 16. Loading Condition 2

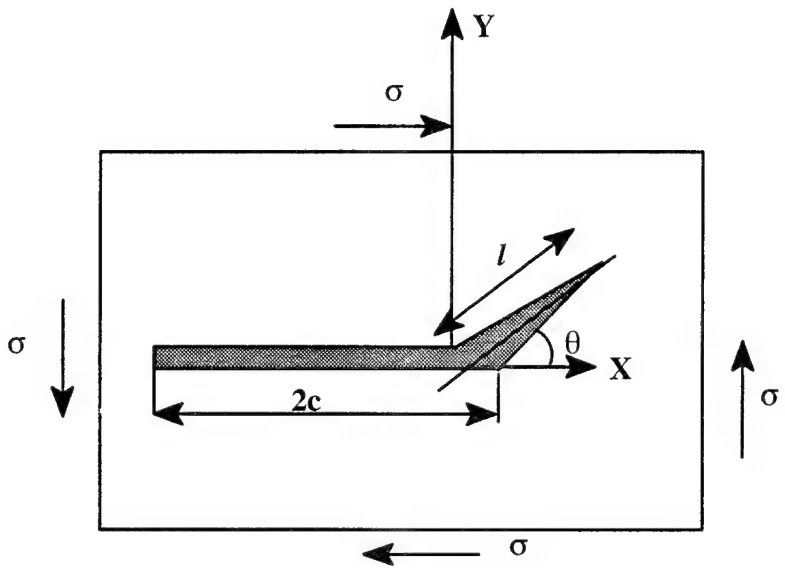

Figure 17. Loading Condition 3

Table 7. Comparison of Results with Mellin [34] and Isida [86] for $2c/l = \infty$ (Method I)

θ	K_I[MI]	K_{II}[MI]	K_I[Isida]	K_{II}[Isida]	K_I[Mellin]	K_{II}[Mellin]
0	1.0000	0.0	1.0000	0.0	1.0000	0.0
10	0.9886	0.0865	0.9887	0.0864	0.9886	0.0864
20	0.9552	0.1680	0.9553	0.168	0.9552	0.1680
40	0.8313	0.2994	0.8313	0.2994	0.8313	0.2994
60	0.6558	0.3690	0.6557	0.3691	0.6557	0.3693
80	0.4640	0.3700	0.4637	0.3703	0.4636	0.3705
90	0.3724	0.3476	0.3719	0.3480	0.3719	0.3481

Table 8. Comparison of Results with Mellin [34] and Isida [86] for $2c/l = \infty$ (Method III)

θ	K_I[MIII]	K_{II}[MIII]	K_I[Isida]	K_{II}[Isida]	K_I[Mellin]	K_{II}[Mellin]
0	1.0000	0.0	1.0000	0.0	1.0000	0.0
10	0.9886	0.0865	0.9887	0.0864	0.9886	0.0864
20	0.9553	0.1680	0.9553	0.1680	0.9552	0.1680
40	0.8314	0.2993	0.8313	0.2994	0.8313	0.2994
60	0.6554	0.3692	0.6557	0.3691	0.6557	0.3693
80	0.4636	0.3705	0.4637	0.3703	0.4636	0.3705
90	0.3717	0.3481	0.3719	0.3480	0.3719	0.3481

Table 9. Comparison of T–stress Obtained by the Three Methods for Unit Load at Infinity ($l/2c$=0.005)

θ	MI	MII	MIII
0	–1.0	–1.0	–1.0
10	0.1069	0.1069	0.1072
20	0.4185	0.4185	0.4197
40	1.5329	1.5327	1.5369
60	2.9709	2.9692	2.9769
80	4.2550	4.2497	4.2600
90	4.6975	4.6900	4.6992

Table 10 shows the comparison of T–stress values evaluated directly using equation (76), after neglecting $\delta(\Phi_M,\Psi_M)$, with the values obtained by solving the singular integral equation (16) and then using equation (67). The difference between these two values increases with the kink angle. This is due to the increase in $\delta(\Phi_M,\Psi_M)$ in equation (76) as the kink angle increases. $\delta(\Phi_M,\Psi_M)$, which can also be called a correction term, can be calculated for each kink angle by subtracting column 3 from column 2 in Table 10. The above method of expressing the T–stress for vanishingly small kink length is similar to the manner in which K_I and K_{II} are expressed in terms of sums of the main crack stress intensity factors and a correction term (for eg. Karihaloo, et al., [25]) which is given in a tabular form as a function of kink angles. From Table 10 it can be inferred that equation (76) is valid or infinitesimally small kink length and small angles. For larger angles the correction term has to be used.

Table 10. Comparison of Eq. (76) with Numerical T–stress Eq. (67) ($2c/l = \infty$).

θ	T (Numerical)	T (Eq.(76))	%Diff
0	–1.00	–1.00	0.0
10	76.53	74.73	2.4
20	301.06	296.12	1.66
40	1101.57	1099.06	0.23
60	2129.84	2165.56	1.65
80	3032.29	3166.05	4.22
90	3346.92	3536.53	5.36

Development of Fracture Model

A fracture model based on the T–stress which will predict qualitatively the behavior of a branched crack is discussed next. Recall from Chapter IV that the T–stress is a 'ρ' inde

pendent constant term which occurs in the asymptotic expansion of stresses near the kink tip. For a flat crack in an infinite panel subjected to an uniaxial normal load σ_{yy}^{∞} the T–stress is given as $-\sigma_{yy}^{\infty}$. This T–stress acts in a direction parallel to the flat crack. Similarly for a branched crack the T–stress at the kink tip can also be described as the stress which acts parallel to the kink direction. For a branched crack, the T–stress is a function of kink length, angle and the loading at infinity ($\sigma_{yy}^{\infty}, \sigma_{xx}^{\infty}$). This functional relationship can be seen from equation (77) which is for an infinitesimally small kink. The T–stress can either be tensile (positive T–stress) or compressive (negative T–stress).

At this stage it will be useful to state the Cotterell and Rice [7] T–stress based fracture stability criterion for a flat crack (unbranched crack) which will then be used to develop the fracture model for a branched crack. Cotterell and Rice [7] studied the influence of the sign of the T–stress evaluated in front of a flat crack on the behavior of the flat crack when it grows in its own plane. They showed that if the T–stress in front of the kink was negative (or compressive) then the crack tends to grow in the same direction it started growing, i.e. along the plane of the crack. This they called class I fracture. If the T–stress was positive then the crack deviates from its own plane, this fracture they termed as class II fracture.

The classification of the type of fracture based on the sign of the T–stress is based on an earlier work by Cotterell [93] in which some experimental verification was done regarding the influence of the sign of the T–stress on crack growth direction. Using photoelastic methods Cotterell [93] showed that in a plastic cleavage type specimen a flat crack ran straight when the T–stress in front of the crack was negative and the crack turned when the T–stress was positive.

Richardson [94] used the T–stress and the critical mode I stress intensity factor calculated in front of an edge crack in a finite geometry test coupon (isotropic, PMMA) to develop a relationship between the geometry of the coupon and critical mode I stress intensity factor K_{IC}. This resulted in an empirical curve called the Equivalent Ratio Biaxial Stress (ERBS) curve. The ERBS ratio B_e is evaluated by first finding an equivalent biaxial remote load for

an infinite coupon geometry with a crack which would give the same crack tip stress state as that of a finite coupon geometry with a crack and then finding the ratio of the biaxial remote loads. This is shown in Figure 18.

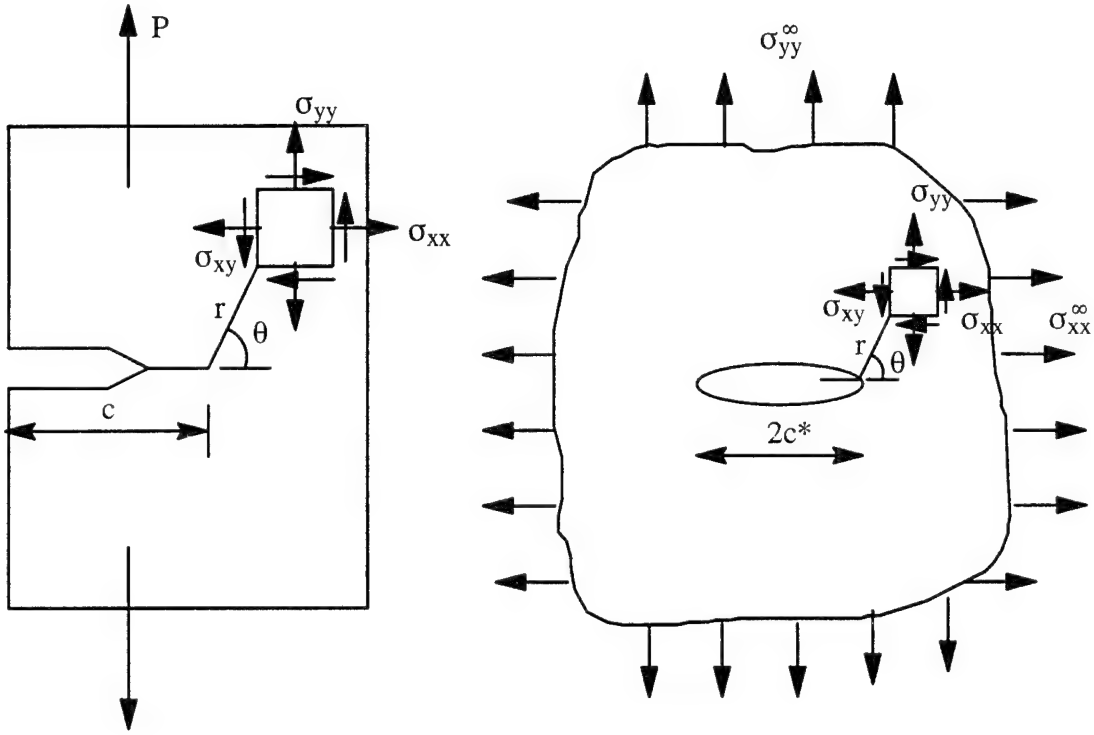

Figure 18. Comparison of an Arbitrary Cracked Coupon with an Infinite Center–Cracked Panel (Richardson [94])

The biaxial stress ratio B_e is defined as,

$$B_e = \frac{\sigma^{\infty}_{xx}}{\sigma^{\infty}_{yy}} \tag{97}$$

By equating the near crack tip stress state in front of the edge notched finite geometry coupon and the the crack in an infinite body Richardson [94] obtained the following equation for an isotropic body.

$$B_e = 1 + \frac{T\sqrt{\pi c^*}}{K_I} \tag{98}$$

The above equation (98) relates the T–stress and the mode I stress intensity factor, K_I evaluated in front of the edge notched finite geometry coupon to the biaxial stress ratio B_e related to the infinite panel. While performing experiments on PMMA test coupons of varying dimensions Richardson [94] observed that for large positive values of the ERBS ratio B_e crack turning occurred and the fracture mode was no longer purely mode I. Large values of B_e results when the T–stress is positive (see equation 98). Richardson [94] also observed that crack turning did not occur immediately after the T–stress became positive as stated by Cotterell and Rice [7], but at a considerably higher positive values of T–stress. For PMMA a critical T–stress (T_{crit}) above which crack turning occurs can be determined by using the ERBS curve given in Richardson [94] and is found to be 0.4489 ksi. For materials other than PMMA the critical T–stress (T_{crit}) must be determined experimentally. Therefore Richardson's [94] experiments shows a clear dependence of crack turning behavior on the T–stress evaluated in front of the crack in a finite geometry coupon.

The T–stress based fracture criterion developed for a flat crack can be extended to a branched crack. Consider the situation in which a kink is formed at an angle to the main crack as shown in Figure 1. If the local T–stress calculated in front of the kink tip is less than T_{crit} then the kink continues to run in the same direction as it started to kink. This type of crack growth is called class I fracture. On the other hand if the T–stress is greater than T_{crit} in front of the kink then the kink will not continue to run in the direction of initial kinking. This type of fracture in which the kink turns from its initial kinking direction is known as class II fracture. Hence, based on the calculated T–stress in front of the kink, the direction of kink growth can be qualitatively predicted. The types of fracture are illustrated in Figure 19.

In the present model, the local T–stress in front of the turned crack in an infinite coupon can be used to predict the most likely direction the turned crack or kink is going to grow. Based on this understanding of the behavior of the branched crack in an infinite plane the behavior of the turned crack in a finite coupon geometry can be predicted.

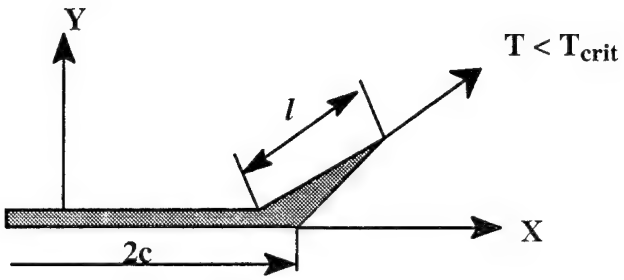

CLASS I

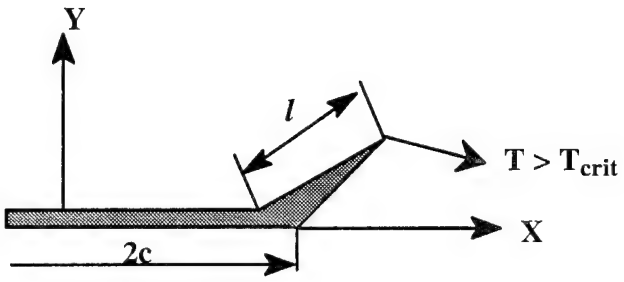

CLASS II

Figure 19. Definition of Class I and Class II Fracture.

The behavior of mode I and II stress intensity factors and the T–stress as a function of kink angle and length for both uniaxial and biaxial loading is discussed in the next few paragraphs.

Figures 20 and 21 shows the variation of the normalized mode I stress intensity factor with the normalized kink length for uniaxial and biaxial loading respectively. The biaxial stress ratio $\sigma^{\infty}_{xx}/\sigma^{\infty}_{yy}$ is represented by k. Similarly Figures 22 and 23 represent the variation in K_{II} and Figure 24 and Figure 25 the variation in T–stress.

Consider the uniaxial loading case first (i.e. k = 0, Figures 20, 22 and 24). From Figure 20 it can be seen that the mode I stress intensity factor is maximum and increases with the kink length when the kink angle is zero i.e. $\theta = 0$. For all other kink angles the stress intensity factor is lower than when $\theta = 0$, and initially drops with an increase in kink length before increasing again. Therefore it can be concluded that once the crack turns it requires more load to extend the crack again in the new direction. The variation of mode II stress intensity factor with kink length is shown in Figure 22. For all kink lengths, K_{II} is maximum when the kink angle is between 45 and 60 degrees. Also K_{II} is never zero for kink angles other than zero. The T–stress (Figure 24) behaves in an interesting manner. The T_{crit} value for a PMMA material is shown on the same figure. For very short kink lengths (less than 0.5% of the main crack length) and kink angles above zero the T–stress is greater than T_{crit} and as the kink grows the T–stress decreases. For kink angles less than 60 degrees and kink lengths more than 40% of the main crack length the T–stress is less than T_{crit}. Therefore, whenever a crack deviates from its path to form a kink such that the kink length is very small, since the T–stress in front of the kink is more than T_{crit}, it is likely that the kink will deviate again. If the kink length is long enough and the angle of deviation is also shallow, since the T–stress is less than T_{crit}, the kink can continue to run in the same direction as it first started to grow. It should be kept in mind that the natural direction for the crack to grow when an uniaxial load is applied, and when there is no kink, is along its own plane (i.e. along $K_{II} =$

0). The crack might kink from its plane of growth due to material inhomogeneities or due to material defects.

The biaxial stress (k = 5) state is also examined, and the results for mode I and II stress intensity factors and T–stress are plotted in Figures 21, 23 and 25 respectively. These plots present an interesting deviation from the case when k = 0. The mode I stress intensity factor (Figure 21) increases with an increasing kink length for all kink angles. The mode II stress intensity factor (Figure 23) shows a local minimum (i.e. $K_{II} = 0$) for kink angles other than zero degrees. Therefore the crack can deviate and run along directions other than $\theta = 0$. But crack growth in all directions is not stable as seen in Figure 25. Only for kink angles greater than 45 degrees does the T–stress become less than T_{crit} and hence the crack growth is stable.

The results discussed for the infinite coupon geometry can be qualitatively extended to the case of finite coupon geometry. Consider two tension specimen of varying dimension as shown in Figure 26. From Richardson [94] it can be noted that, on application of load and before the crack starts growing, a compressive T–stress exists in front of the edge crack in the 3 in. tension specimen and a tensile T–stress exist in front of the edge crack in the 2 in. compact tension specimen. The behavior of the cracks in the test coupons with compressive and tensile T–stresses can be understood by studying the branched crack in an infinite coupon under uniaxial and biaxial load respectively.

First consider the case of the 3 in. tension specimen with T/P = –0.6, where P is the applied load. Since only qualitative predictions will be made about crack turning angle this coupon geometry can be compared to a flat crack in an infinite plane where $T/\sigma = -1$, where σ is the applied load. It can be seen from Figure 24 that for $\theta = 0$, T/σ is –1. If then due to the presence of some defect or inhomogeneity in the material the crack kinks out of its plane, the T–stress in front of the kink becomes greater than T_{crit} for very short kink lengths (less than 0.5% of the main crack length) and hence the kink turns back towards the main

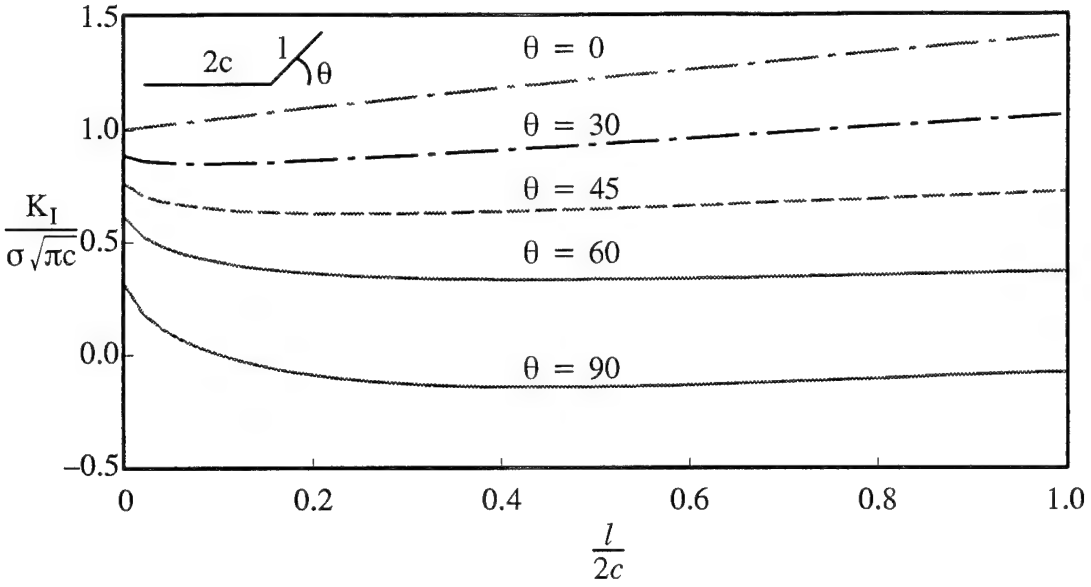

Figure 20. Variation of Normalized K_I with Normalized Kink Length l (k=0)

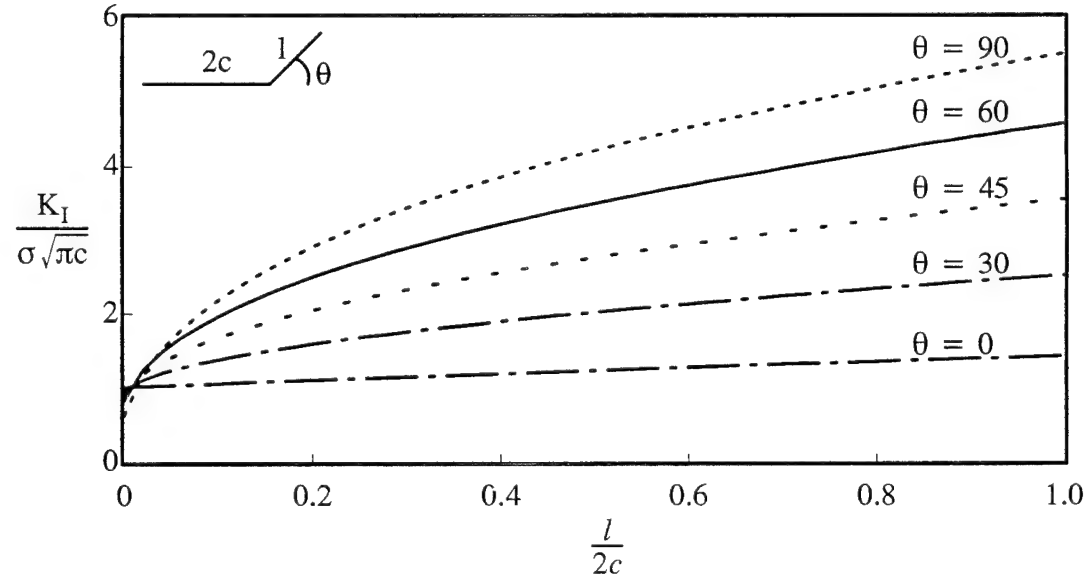

Figure 21. Variation of Normalized K_I with Normalized Kink Length l (k=5)

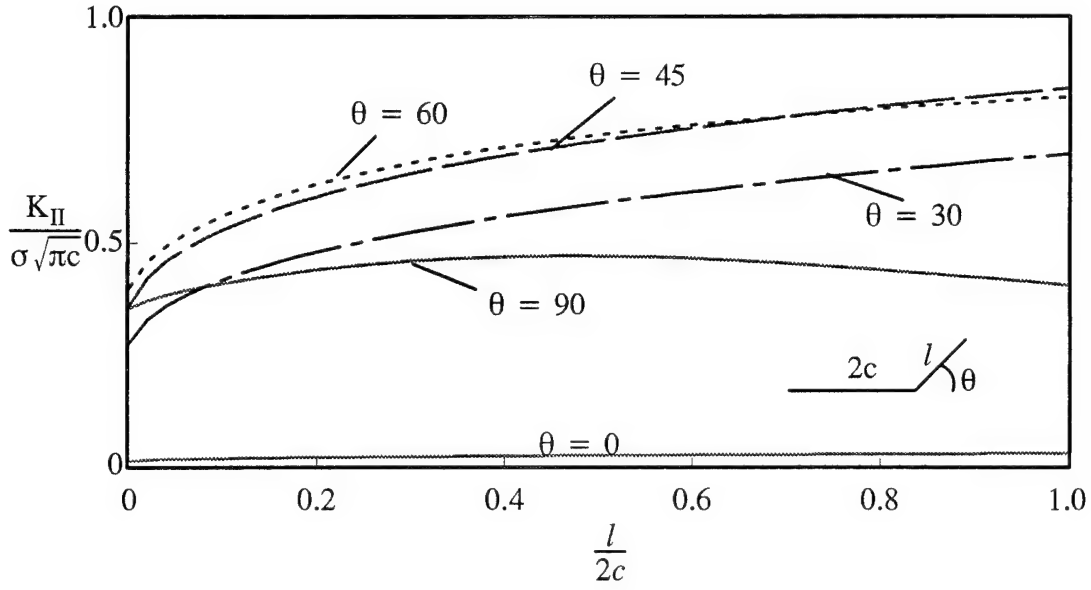

Figure 22. Variation of Normalized K_{II} with Normalized Kink Length l (k=0)

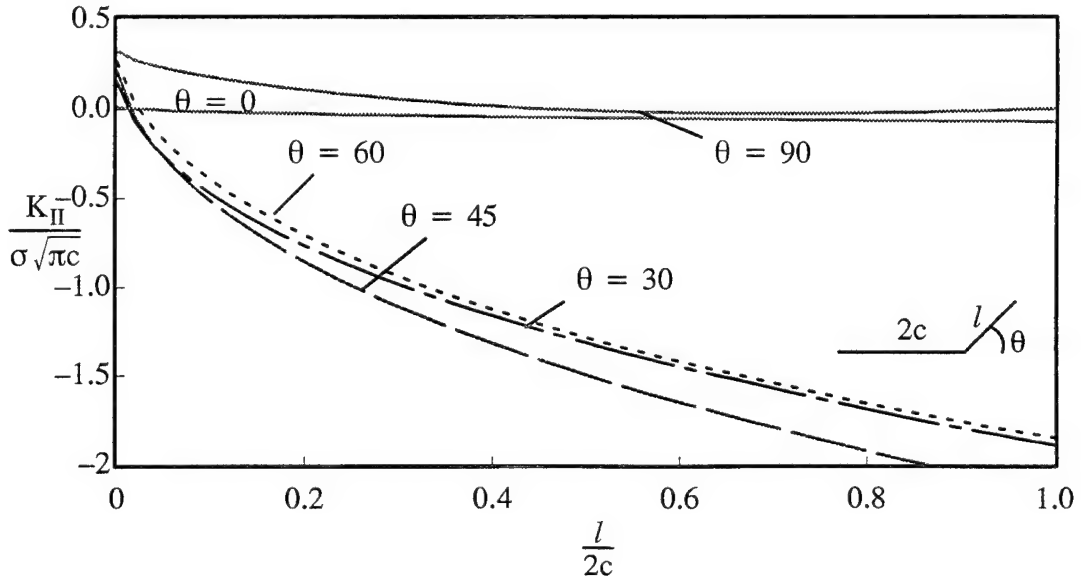

Figure 23. Variation of Normalized K_{II} with Normalized Kink Length l (k=5)

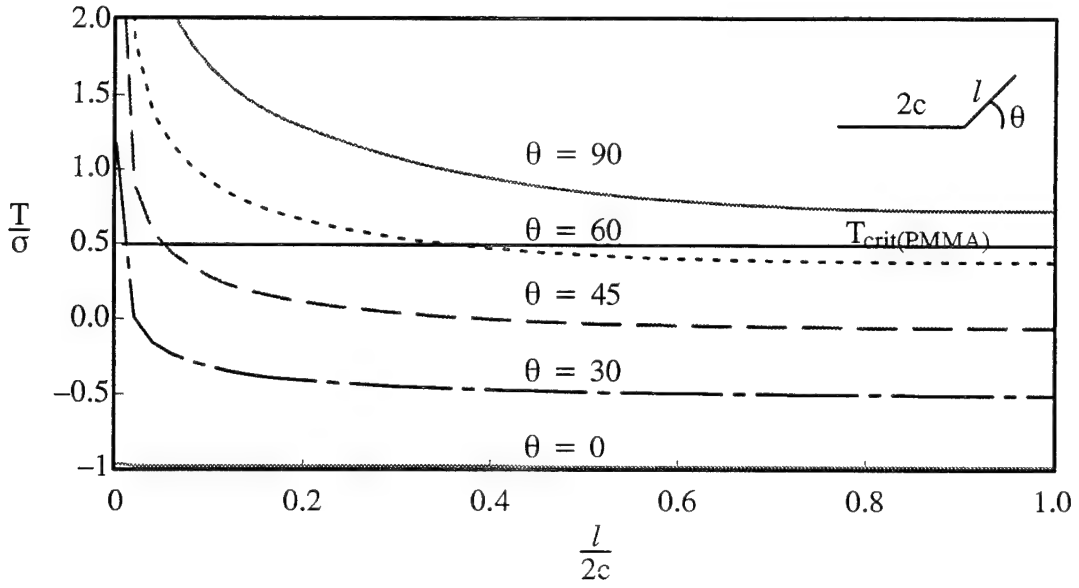

Figure 24. Variation of Normalized T–stress with Normalized Kink Length l (k = 0)

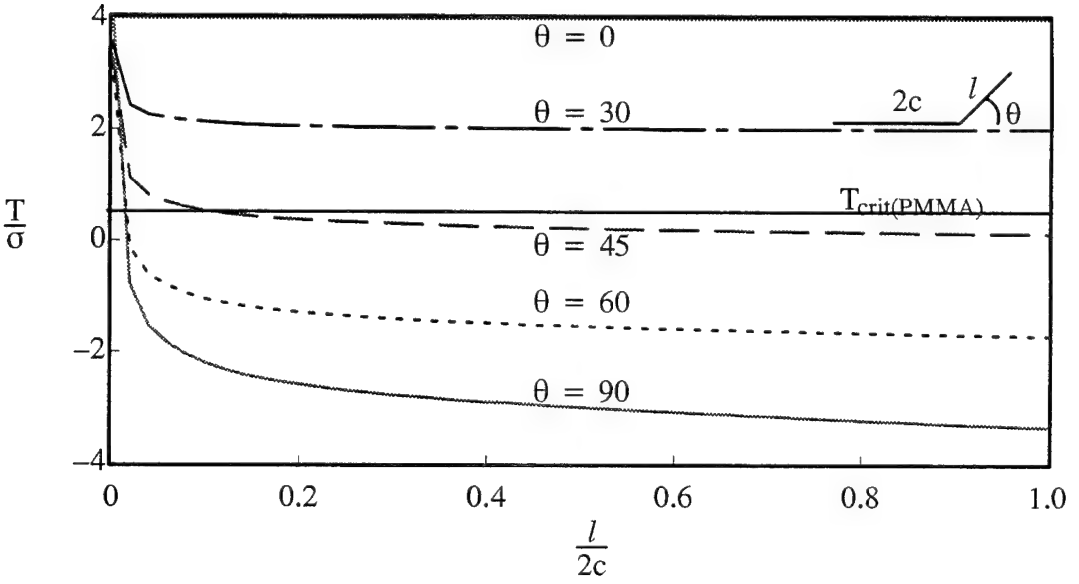

Figure 25. Variation of Normalized T–stress with Normalized Kink Length l (k = 5)

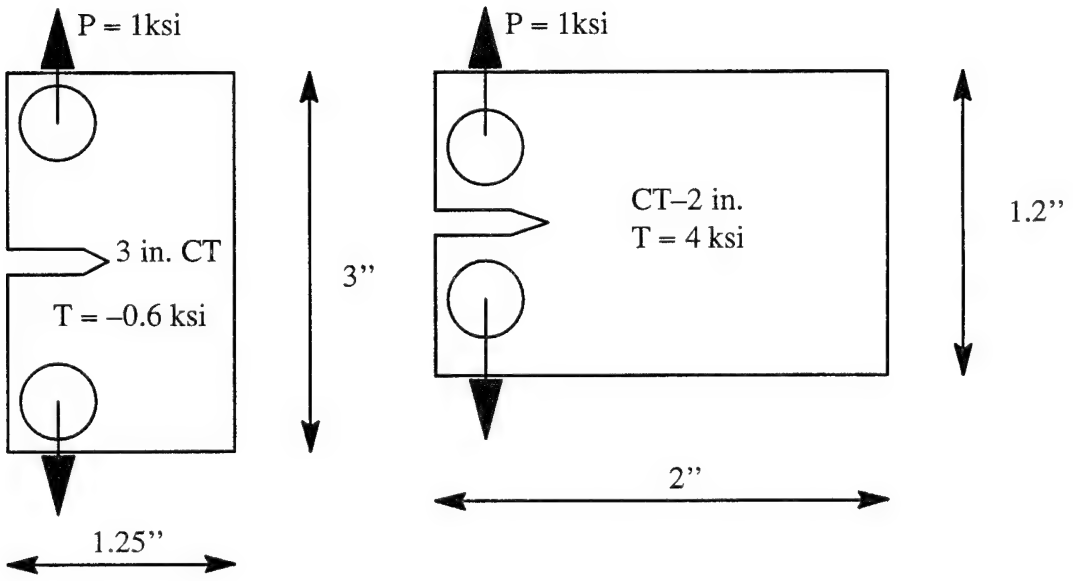

Figure 26. Geometry of PMMA Test Coupons

crack direction and continues to grow. The kink comes back to the main crack direction because along that direction $K_{II} = 0$ (Figure 22) and the T–stress is less than T_{crit} (Figure 24). If the kink length is long enough (more than 40% of the main crack length), then according to Figure 24 the T–stress becomes less than T_{crit}, and hence the kink can grow at angles less than 60 degrees. This does not happen for the 3 in. PMMA coupons because the kink, initially, does not make long enough excursions from it plane of growth to really experience a decrease in T–stress values. Therefore, in the absence of large inhomogeneities or discontinuities in the tension specimen, which might cause the kink to have long excursion from the main crack, the crack in the 3 in. tension coupon grows straight which is also observed experimentally.

In a similar manner the 2 in. tension specimen with T/P = 4 can be compared to an infinite coupon geometry with k = 5. When the kink angle is zero the T–stress is greater than T_{crit} as in the test coupon. Now if the crack deviates from its plane of growth, for short kink lengths (i.e. for kink lengths less than 0.5% of main crack), the kink can either turn back and run along the main crack direction or it can deviate further away from the main crack. It is more likely that the kink will turn away from the main crack direction and run in a direction along which the T–stress is less than T_{crit} since only along this direction stable crack growth can occur. From Figure 23 it can be observed that the kink angles for which $K_{II} = 0$ (plane of local symmetry), is smaller for smaller kink lengths. Therefore, short excursions from the main crack direction results in shallow turning angles as seen in PMMA test coupons, and longer excursions of the kink results in sharp turning of kink. Ultimately for the infinite coupon the kink is likely to turn by more than 45 degrees since only then does the T–stress become less than T_{crit}.

Kink Closing Angle

Kink closing angle (θ_c) can be defined as that kink angle at which the mode I stress intensity factor (K_I) vanishes (becomes zero). Figure 27 shows the kink closing angle as a

function of kink length for uniaxial loading. From this plot it can be inferred that kink closure occurs only for kink angles above 78 degrees and kink lengths less than 0.1 times the length of the main crack

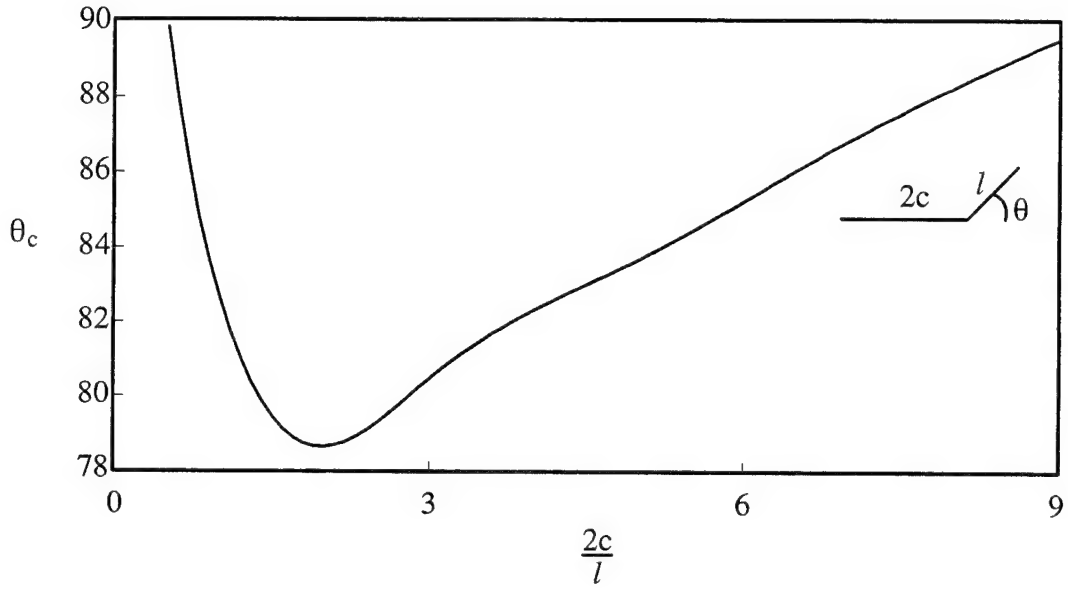

Figure 27. Kink Tip Closing Angle (θ_c) as a Function of Normalized Kink Length

CHAPTER VI

RESULTS AND DISCUSSION–II

Anisotropic Case

Before discussing the numerical results for the anisotropic case it will be useful to define some of the parameters which are used in the presentation of the results. These parameters are shown in Figure 28. X–Y are the geometric axes and 1–2 are the material axes and the angle between them, denoted by θ_m, is the material angle. The exterior angle formed between the kink and the main crack is denoted by θ_{2a} and the angle between the external bisector to the wedge angle ABC and 1–axis is denoted by θ_b. θ is the angle between the positive X axis and the kink. The 1–direction is assumed to be the direction of higher stiffness, (typically the fibre direction).

The singular integral equations (49 and 50) developed for the anisotropic case are solved using the three methods discussed in Appendix E. As discussed in Appendix E, in the first method, a stronger singularity is assumed at the kink corner where the kink and the main crack meet. In the other two methods the correct singularity, which is given by equation (99), is assumed at the kink corner. The development of this equation is given in Bogy [87] and is repeated below for completeness.

$$D = -t_5.[2\{t_4 - t_3\} + \{t_2 + t_1\}t_6] = 0 \tag{99}$$

$$t_1 = [R_1(\theta_a)^{-1}R_1(-\theta_a)R_2(\theta_a)R_2(-\theta_a)^{-1}]^{(s+1)},$$

$$t_2 = [R_1(\theta_a)R_1(-\theta_a)^{-1}R_2(\theta_a)^{-1}R_2(-\theta_a)]^{(s+1)},$$

$$t_3 = (1 - \bar{\gamma}_1\bar{\gamma}_2)^2 \cos\{(\alpha_i + 1)[\phi_1(\theta_a) - \phi_1(-\theta_a) - \phi_2(\theta_a) + \phi_2(-\theta_a)]\},$$

$$t_4 = (\bar{\gamma}_1 - \bar{\gamma}_2)^2 \cos\{(\alpha_i + 1)[\phi_1(\theta_a) - \phi_1(-\theta_a) + \phi_2(\theta_a) - \phi_2(-\theta_a)]\},$$

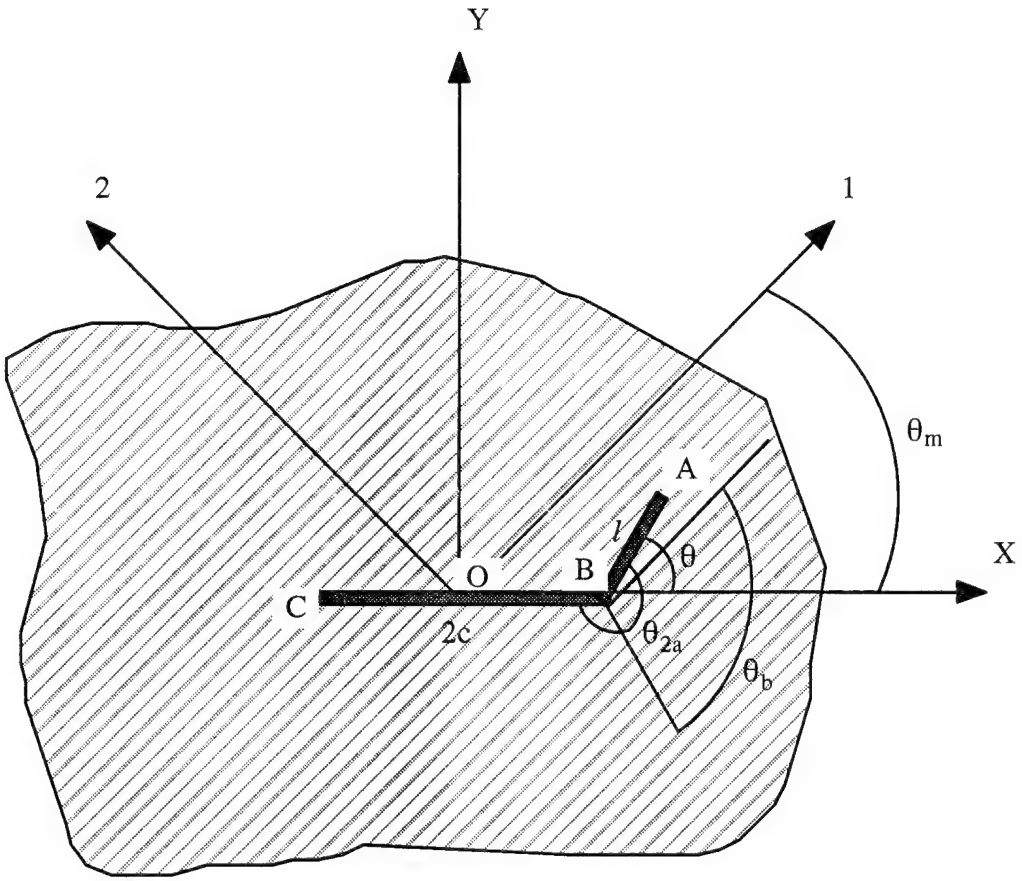

Figure 28. Geometry Showing Parameters for Anisotropic Branched Crack Problem.

$$t_5 = [R_1(\theta_a)R_1(-\theta_a)R_2(\theta_a)R_2(-\theta_a)]^{(s+1)},$$

$$t_6 = (1 - \overline{\gamma}_1^2)(1 - \overline{\gamma}_2^2),$$

where γ_i (i=1,2) are the roots of the following equation,

$$S_{11}\gamma^4 - 4S_{16}\gamma^3 + 2(S_{66} + S_{11})\gamma^2 - 4S_{16}\gamma + S_{12} = 0,$$

where,

$$S_{11} = \frac{1}{4}(c_{11} + c_{22} + c_{66} - 2c_{12}),$$

$$S_{12} = \frac{1}{4}(c_{11} + c_{22} - c_{66} - 2c_{12}),$$

$$S_{16} = \frac{1}{4}(c_{11} - c_{22}),$$

$$S_{66} = \frac{1}{4}(c_{11} + c_{22} + 2c_{12}),$$

and c_{ij}'s are the same parameters as used in equation (C.26). These c_{ij}'s can be expressed in terms of elasticity constants as shown below.

$$c_{11} = \frac{1}{E_1}.$$

$$c_{22} = \frac{1}{E_2}.$$

$$c_{12} = -\frac{\mu_{12}}{E_1}.$$

$$c_{66} = G_{12}.$$

$$R_i = (1 + \overline{\gamma}_i^2 + 2\overline{\gamma}_i \cos[2(\theta_b - \theta)])^{1/2}.$$

$$\phi_i(\theta) = \operatorname{atan}\left[\frac{\sin\theta + \overline{\gamma}_i \sin(2\theta_b - \theta^*)}{\cos\theta + \overline{\gamma}_i \cos(2\theta_b - \theta^*)}\right], i = 1,2.$$

$$\theta^* = \frac{\pi + \theta}{2}.$$

In the above equations E_1, E_2 are the stiffness along the 1 and 2 material direction, G_{12} is the shear modulus and μ_{12} is the Poison's ratio.

Table 11 shows the roots of equation (99) for different kink angles and material angles for a stiffness ratio (E_1/E_2) of 1.1. The numerical results for stress intensity factors (mode I and mode II) and the T–stress are compared using the three methods and the results are shown in Table 12. In method I, 121 quadrature points are used; in method II, 40 terms in the Jacobi polynomial series; and in Method III the first Jacobi polynomial series has 6 terms and the second Jacobi polynomial series has 4 terms. From the results shown in Table 12 it can be observed that the error in K_I, K_{II} and T–stress calculated using the three methods is always less than 1% (as seen in the isotropic case). It can also be observed that the singularity assumed at the kink corner does not affect the near–kink–tip stress state.

Table 11. Roots of Bogy's [87] Characteristic Equation (99)

θ	θ_{2a}	θ_b	α_1	α_2
10	95	85	0.0196	0.0
20	100	80	0.1855	0.0
40	110	70	0.3058	0.0
60	120	60	0.3850	0.0
80	130	50	0.4368	0.0207
90	135	45	0.4551	0.0923

Table 12. K_I, K_{II} and T–Stress Calculated Using the Three Methods ($l/2c = 0.005$, $E_1/E_2 = 1.1$)

MI (121)				MII (n=40)			MIII ($n_1+n_2 = 6+4$)		
θ	K_I	K_{II}	T	K_I	K_{II}	T	K_I	K_{II}	T
0	1.0025	0.0	–0.038	1.0024	0.0	–0.038	1.0025	0.0	–0.038
10	0.9915	0.0836	0.0826	0.9915	0.0836	0.0827	0.9915	0.0836	0.0830
20	0.9591	0.1631	0.4240	0.9591	0.1631	0.4240	0.9591	0.1631	0.4253
40	0.8382	0.2937	1.5674	0.8382	0.2938	1.5672	0.8384	0.2938	1.5718
60	0.6651	0.3664	2.9842	0.6649	0.3667	2.9824	0.6652	0.3667	2.9906
80	0.4736	0.3714	4.2815	0.4731	0.3719	4.2762	0.4732	0.3718	4.2868
90	0.3813	0.3508	4.7337	0.3807	0.3513	4.7261	0.3807	0.3513	4.7364

Figures 29, 30 and 31 show the variation of normalized mode I stress intensity factor (K_I) as a function of kink length (l) and kink angle (θ) for different stiffness ratio. From these plots the following can be observed regarding kink tip closing angle (which is defined as that kink angle at which the mode I stress intensity factor becomes zero). The kink tip closes for only a certain range of kink angle and length. The kink length and the angle at which the kink closes decreases with an increase in stiffness parallel to the direction of the main crack. For stiffness ratio between 1 and 10 crack closure is observed only for kink angles above 60 degrees. If the length and angle of the kink is large enough the kink will not close at all for uniaxial loading.

Figure 31 shows the behavior of mode I stress intensity factor K_I, when the stiffer direction is parallel to the main crack. It can be observed, that for very short kink lengths (l approaching 0), the maximum K_I does not occur at $\theta = 0$ but at kink angles other than zero. This implies that once the crack turns to form a kink it requires a relatively lower load to extend the kink further. But as the kink length increases K_I starts decreasing, which means a higher load is now required to extend the kink. Gao, et al., [56] reported that for infinitesimally small kink lengths, for stiffness ratio more than 4 (stiffer axis along the main crack direction), the maximum K_I did not necessarily occur at $\theta = 0$. The present result confirms that observation and also shows that for longer kink lengths maximum K_I always occurs at $\theta = 0$ no matter what the stiffness ratio is. Gao, et al., [56] also observed, for an infinitesimal small kink, that when the stiffer axis was along the main crack direction and the stiffness ratio was four the predicted kink growth direction based on the stress intensity factors was physically unrealistic. Due to this reason Gao, et al., [56] concluded that the stress intensity based fracture criteria may not be accurate for infinitesimally small kink lengths. For longer kink lengths, from Figures 29, 30 and 31, it can be observed that maximum K_I occurs always at $\theta = 0$ irrespective of fibre orientation and stiffness ratio. But it has been experimentally observed for polymeric composites (like graphite–epoxy) that the crack growth direction is sensitive to the fibre orientation direction since the strength of the composite also varies ac-

cording to the orientation of the fibre. Hence it can be concluded that a fracture criteria based on K_I alone might not be accurate for predicting fracture in an orthotropic body.

Figures 32, 33 and 34 shows the variation of normalized mode II stress intensity factor K_{II} as a function of kink length and angle for different stiffness ratio. Comparing these plots with Figure 22 it can be inferred that for longer kink lengths the behavior of K_{II} is similar to that observed for the isotropic case whereas for shorter kink lengths K_{II} is affected by the variation in stiffness ratio and hence behaves differently.

Figures 35, 36 and 37 shows the variation of normalized T–stress as a function of kink length and angle for different stiffness ratio. A T_{crit}/σ value of 0.5 (which is an assumption) is also shown on these figures. The T_{crit} for an orthotropic material has to be experimentally determined as in the case of an isotropic material like PMMA. Since experimental T_{crit} values, for any orthotropic material, are not available a value of 0.5 ksi is assumed for all fibre orientation with respect to the crack. It should be noted that T_{crit} varies with fibre orientation, which is not incorporated into the current assumption of T_{crit} values. However, experiments can be performed on specific orthotropic materials to determine these values which can be incorporated into the model. From these plots it can be observed that for short kink lengths the T–stress is greater than T_{crit} for all kink angles and stiffness ratios. But for longer kink lengths the T–stress can be either above or below T_{crit} depending on the kink angle, and the material stiffness ratio. Figure 35 shows the variation of T–stress for the case when the stiffer direction is perpendicular to the direction of the main crack. Using the modified T–stress based fracture criterion, if a kink is formed at a direction to the main crack and if the kink length is small then it is likely that the kink will not run in its initial direction but will turn away from that direction since the T–stress is greater than T_{crit}. If the kink length is long enough (more than 30% of the main crack length) then the kink can extend along its initial direction up to an kink angle of 80 degrees.

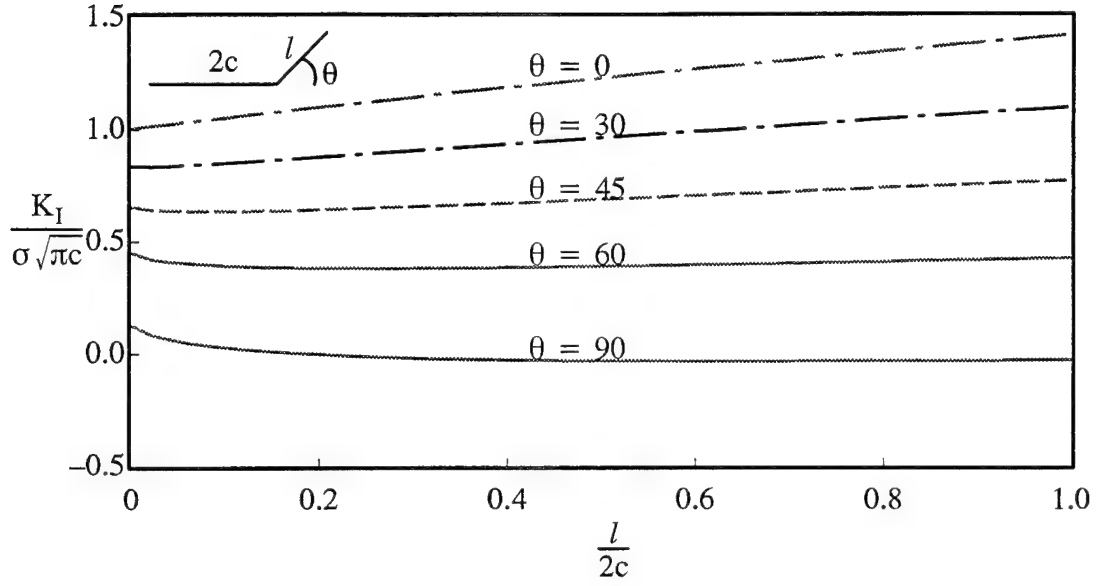

Figure 29. Variation of Normalized K_I with Normalized Kink Length l ($k = 0$, $E_1/E_2 = 10$, $\theta_m = 90$)

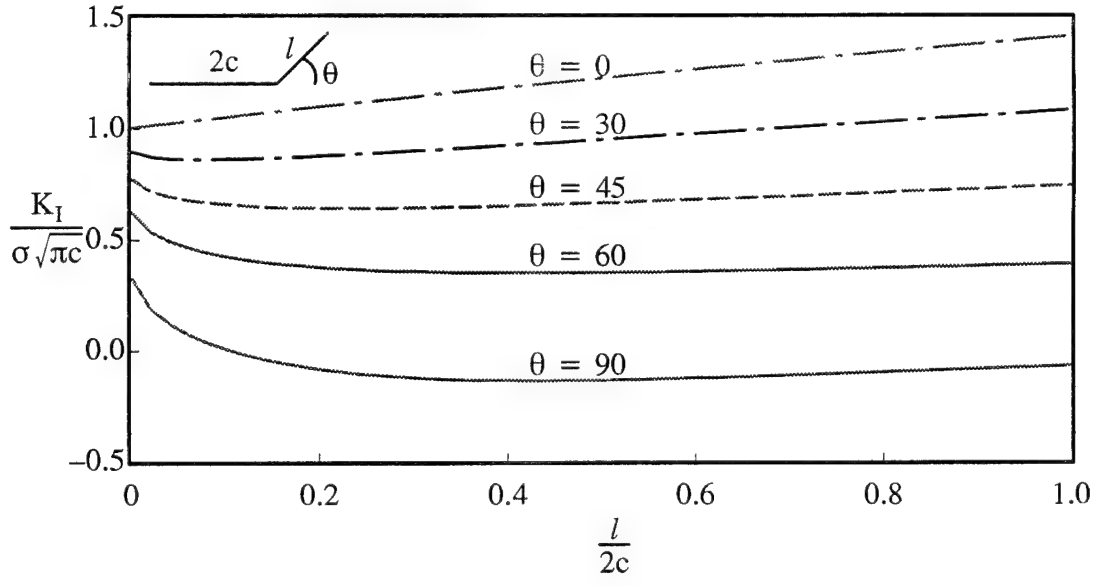

Figure 30. Variation of Normalized K_I with Normalized Kink Length l ($k = 0$, $E_1/E_2 = 1.08$, $\theta_m = 0$)

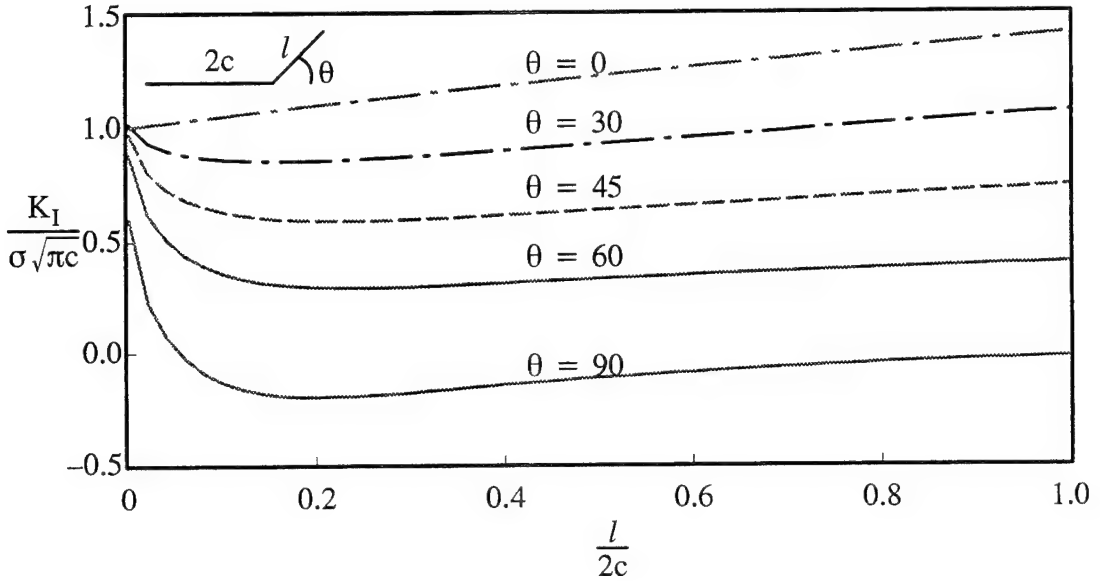

Figure 31. Variation of Normalized K_I with Normalized Kink Length l ($k = 0$, $E_1/E_2 = 10.0$, $\theta_m = 0$)

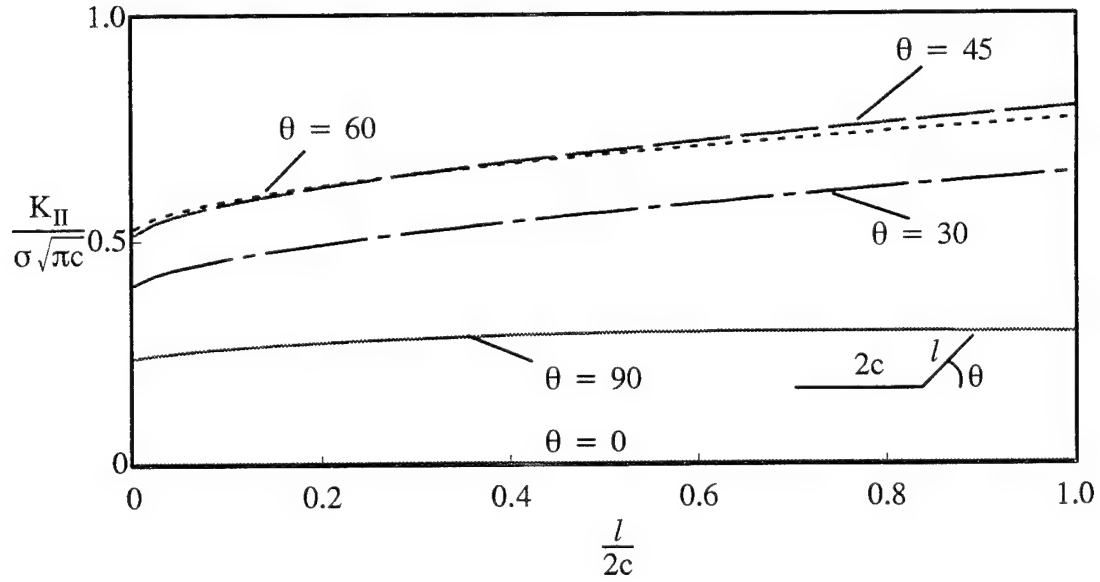

Figure 32. Variation of Normalized K_{II} with Normalized Kink Length l ($k = 0$, $E_1/E_2 = 10$, $\theta_m = 90$)

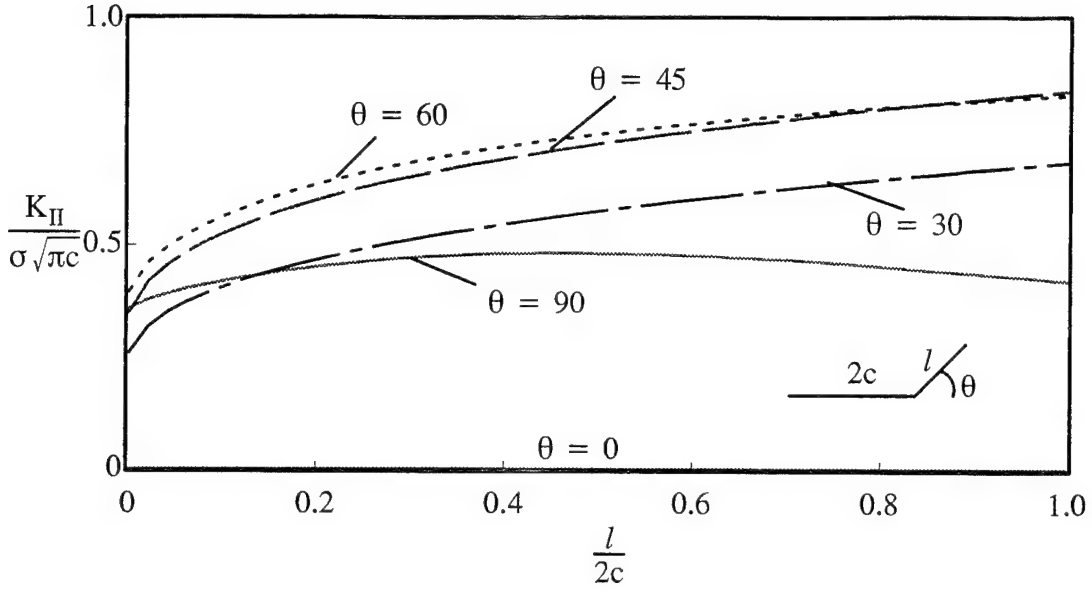

Figure 33. Variation of Normalized K_{II} with Normalized Kink Length l ($k = 0$, $E_1/E_2 = 1.08$, $\theta_m = 0$)

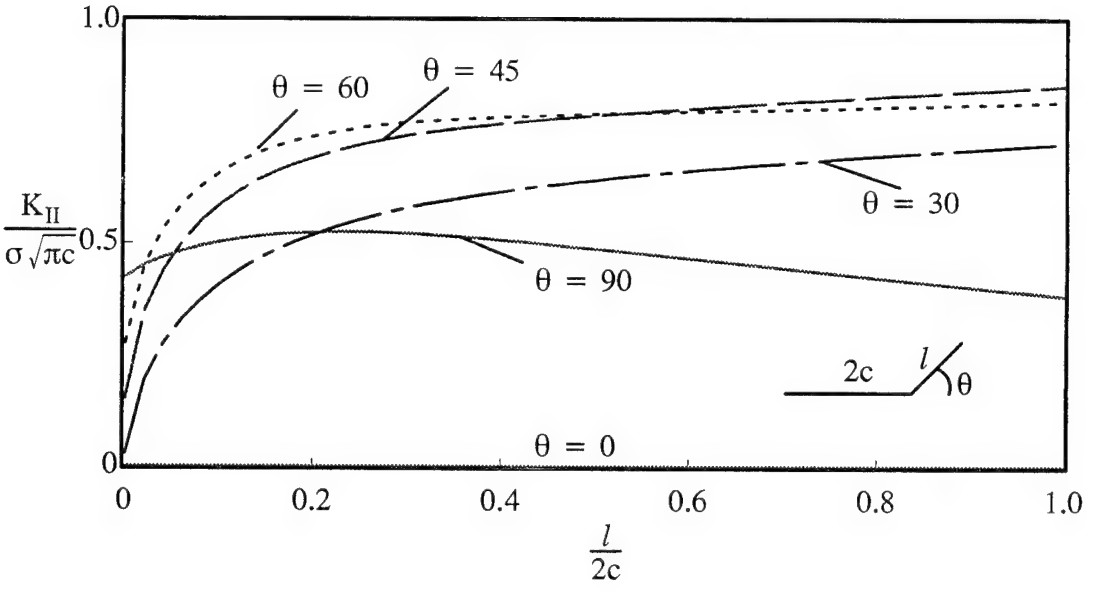

Figure 34. Variation of Normalized K_{II} with Normalized Kink Length l ($k = 0$, $E_1/E_2 = 10$, $\theta_m = 0$)

Figure 36 shows the variation of normalized T–stress for the case when the stiffness ratio is 1.1. The behavior of the T–stress is similar to that observed in the isotropic case. Figure 37 shows the variation of normalized T–stress when the stiffer axis is parallel to the main crack axis. From this plot it can be inferred that for short kink lengths, since the T–stress is greater than T_{crit}, the kink does not run along the initial kink growth direction. For longer kink lengths (more than 20% of the main crack length) and for kink angles below 30 degrees the T–stress is less than T_{crit}. This means that for sufficiently longer kink lengths the kink can run in its initial kinking direction up to an angle of 30 degrees. For angles above 30 degrees, since the T–stress is greater than T_{crit}, the kink turns from its initial direction.

Figures 38, 39 and 40 shows the variation of normalized K_I, K_{II} and T–stress respectively as a function of material angle for a kink length which is 0.2% of the main crack length and a stiffness ratio of 10. From Figures 38 and 39 it can be inferred that when the kink angle is zero, i.e. when the kink coincides with the axis of the main crack K_I and K_{II} are insensitive to the variation in material angle. For all other kink angles there is some variation in K_I and K_{II}. Figure 38 shows, as stated earlier, that it is possible for K_I to be maximum at kink angles other than zero. Figure 39 shows that K_{II} can also be zero at kink angles other than zero. Figure 40 shows some interesting variations in T–stress as compared to K_I and K_{II}. The T–stress is sensitive to variations in material angle for a kink angle of zero degrees, i.e. when the axis of the kink coincides with the axis of the main crack. For all other kink angles the T–stress shows large fluctuations as the material angle is varied. Up to a kink angle of 60 degrees the maximum T–stress below T_{crit} occurs when the kink almost parallels the stiffer axis direction. For example the maximum T–stress below T_{crit} for a kink angle of 20 degrees occurs when the material angle is close to 25 degrees. For kink angles more than 60 degrees the T–stress remains above T_{crit} for all material angles.

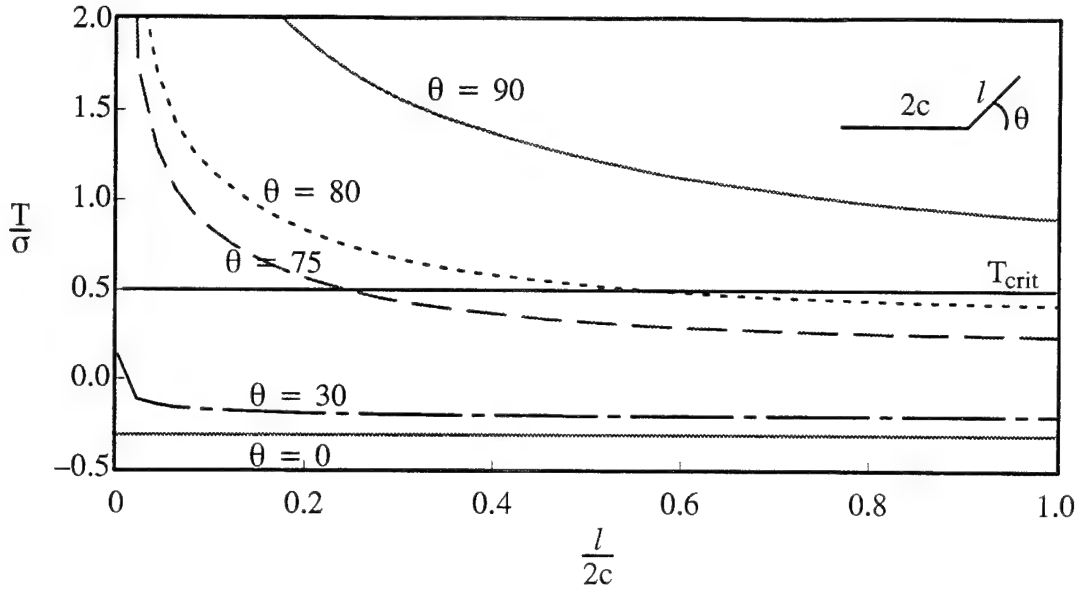

Figure 35. Variation of Normalized T–stress with Normalized Kink Length l ($k = 0$, $E_1/E_2 = 10$, $\theta_m = 90$)

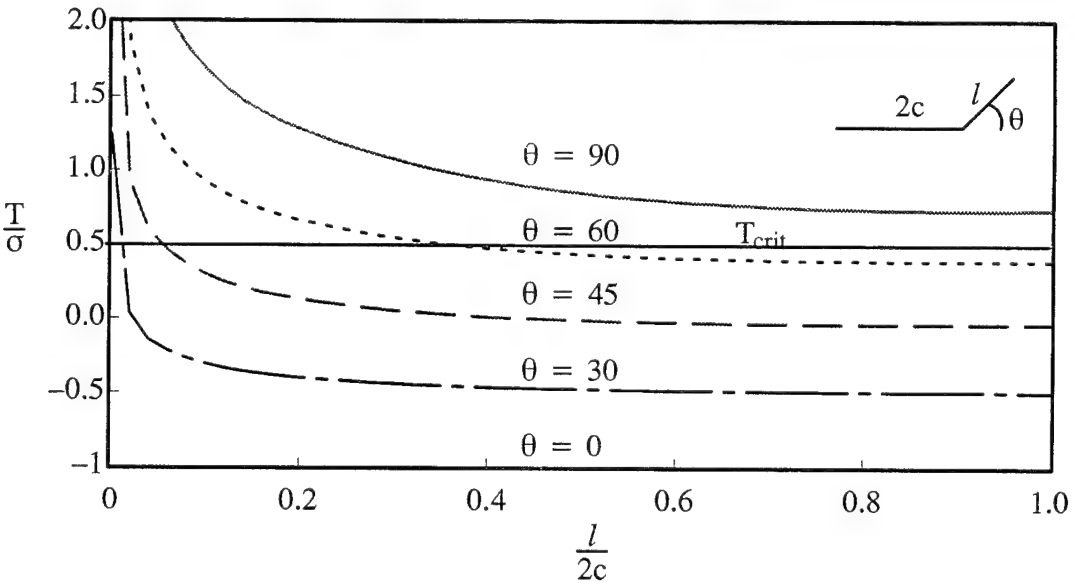

Figure 36. Variation of Normalized T–stress with Normalized Kink Length l ($k = 0$, $E_1/E_2 = 1.08$, $\theta_m = 0$)

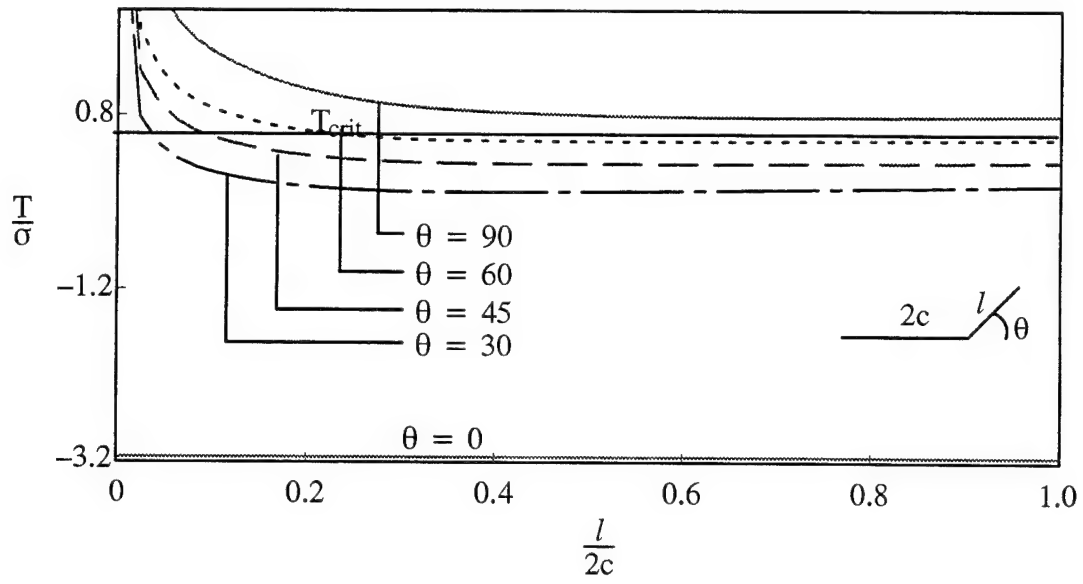

Figure 37. Variation of Normalized T–stress with Normalized Kink Length l (k = 0, E_1/E_2 = 10, θ_m = 0)

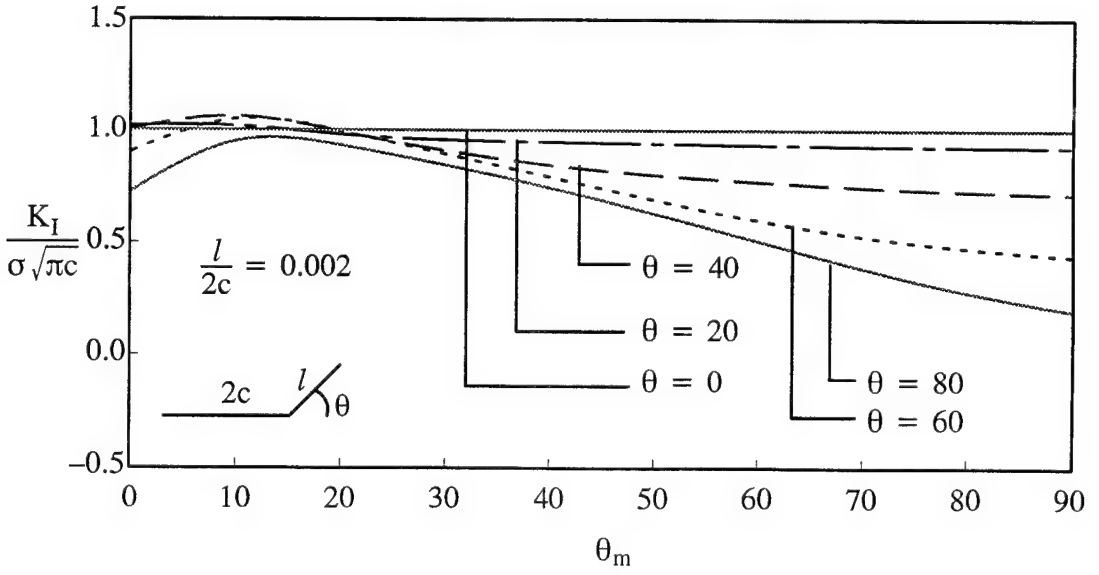

Figure 38. Variation of Normalized K_I with Material Angle θ_m (k = 0, E_1/E_2 = 10)

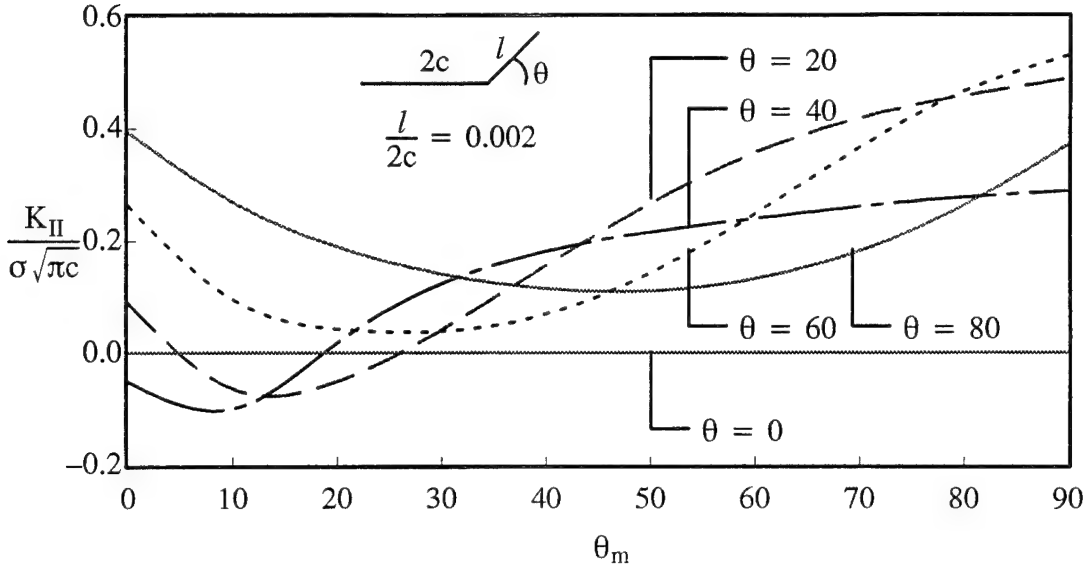

Figure 39. Variation of Normalized K_{II} with Material Angle θ_m ($k = 0$, $E_1/E_2 = 10$)

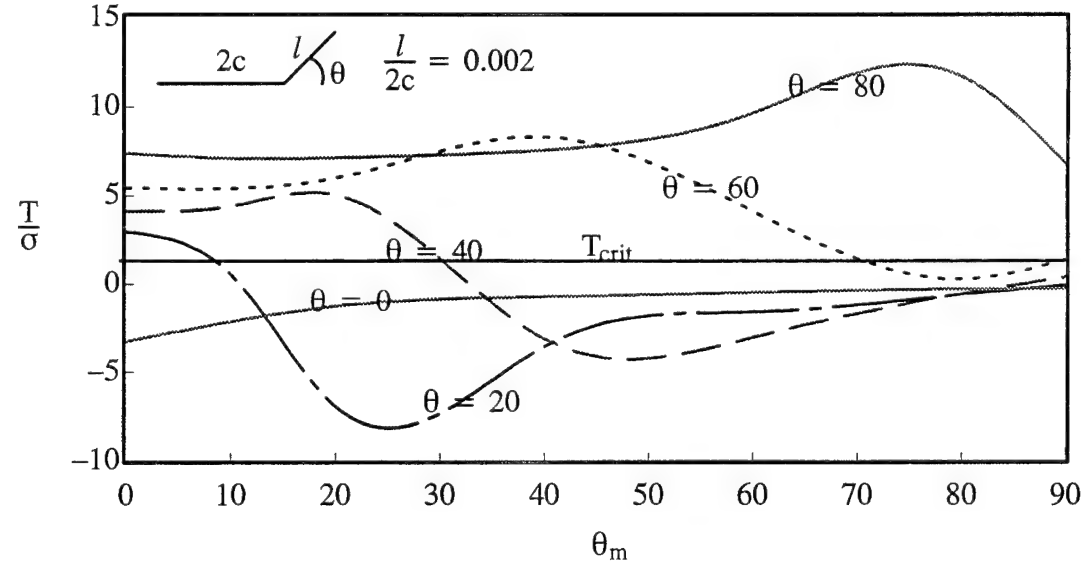

Figure 40. Variation of Normalized T–stress with Material Angle θ_m ($k = 0$, $E_1/E_2 = 10$)

Albritton and Goree [5] performed experiments on standard compact tension, single edge notched tension and center crack tension silicon carbide reinforced aluminum coupons. These test coupon had fibres running parallel to or perpendicular to the load direction. While crack turning was observed in CT test coupons where the fibres ran parallel to the load it was not observed for any of the coupons for which the fibres ran perpendicular to the load. From Figures 35 and 37 it can be seen that for a kink angle of zero degree the T–stress has a maximum value below T_{crit} when the stiffer axis is parallel to the crack (i.e. perpendicular to the load). Hence the crack in the CT test coupon, where the stiffer fibres are perpendicular to the load, runs stably when compared to the case when the fibres are parallel to the load. Albritton and Goree [5] also noted that when the fibre volume fraction increased for the case where the fibres ran parallel to the applied load, the angle at which the crack turned in the finite coupon increased. This dependence of crack turning angle on the fibre volume fraction can be attributed to the T–stress as explained in the following lines. Increasing fibre volume fraction primarily results in increase in stiffness along the fibre direction. From Figures 35 and 36 it can be seen that as the stiffness increases in a direction parallel to the load the maximum kink angle at which the T–stress is below T_{crit} increases. i.e. whereas for $E_1/E_2 = 1.1$ the T–stress is below T_{crit} up to a kink angle of 60 degrees, for $E_1/E_2 = 10$ (stiffer axis parallel to the load direction) the T–stress is greater than T_{crit} up to a kink angle of 80 degrees. Therefore, for a sufficiently long kink, the angle at which the kink can turn and run increases with the increase in the volume fraction.

It should also be noted that for an orthotropic material there exists orthotropy in strength also. Therefore the crack can turn run in a direction where the material is weak which is usually parallel to the stiffer axis. By calculating the T_{crit} value experimentally the influence of strength and stiffness of a material are also incorporated in to the fracture model through the T_{crit}. Hence by comparing the theoretically determined T–stress values with T_{crit} values the influence of strength and stiffness are also taken into account.

The current model is a macroscopic model where phenomenon such as fibre–matrix debonding, fibre or matrix cracking cannot be accounted. But these can be analyzed by using a microscopic model. Therefore this model should be used with caution when applied to such materials where the above mechanisms dominate.

CHAPTER VII

CONCLUSIONS

The branched crack problem in an isotropic and anisotropic material is solved using the method of dislocations. Stress singularities at the corner where the branched crack and the main crack meet is investigated and the singularity is shown to be given by Williams' [19] characteristic equation for the isotropic case. An accurate method is developed to evaluate the T–stress at the tip of the branched crack. It is shown that the T–stress at the branched crack tip is insensitive to the order of the singularity at the corner where the kink and main crack meet, for both isotropic and anisotropic materials. It is also verified that the mode I (K_I) and II (K_{II}) stress intensity factors at the kink tip are insensitive to the stress singularity at the reentrant wedge corner of the branched crack as well.

The values of K_I, K_{II} and the T–stress evaluated in front of the kink tip are studied as a function of kink to main crack length ratio, kink angle and the loading parameters for the isotropic case; for the anisotropic case the influence of relative stiffness property is also included. Based on the experiments performed by Richardson [94], Cotterell and Rice's [7] T–stress criteria is modified to include an experimentally determined value of T_{crit} above which a crack deviates from its plane of growth. It is proposed that a crack will continue in its plane of growth if the T–stress is less than T_{crit}, or deviate from its plane if the T–stress is more than T_{crit}. For PMMA (which is isotropic), from Richardson [94], a T_{crit} value of 0.5 ksi was experimentally determined.

The modified T–stress based fracture criteria is applied to the branched crack, in both isotropic and orthotropic material, and the behavior of the branched crack is discussed. The following conclusions are arrived at from the above study. Considering an isotropic material first, it is observed that if a crack subjected to either uniaxial or biaxial loading deviates from its path to form a kink, the length and angle of the kink with respect to the main crack deter-

mines how the kink behaves. For a short initial kink length (l tending to 0) and for all kink angles ($0<\theta<90$), under uniaxial loading, the kink aligns itself with the main crack, but under biaxial loading it deviates away from the main crack. Therefore, for a biaxial loading state, the kink direction is sensitive to the applied transverse load σ_{xx}^{∞}. For a longer kink length, the kink can continue growing in the initial direction. For example consider an isotropic material like PMMA ($T_{crit} = 0.5$ ksi) ; for a kink angle of less than 60 degrees and a kink length which is more than 40% of the main crack length the kink can extend in the initial direction it started.

Unlike the isotropic case, T_{crit} for an orthotropic material is sensitive to the material stiffness and strength of the material. i.e. the T_{crit} varies as a function of orientation of the fibre with respect to the applied load. Hence a range of T_{crit} values has to be experimentally determined in order to apply this modified fracture model to the orthotropic material. In this study, for an orthotropic material (due to the lack of experimental T_{crit} values) a T_{crit} value of 0.5 ksi is assumed for all fibre orientation. Hence the following conclusions are arrived at from the above assumptions. The behavior of short kinks (l tending to 0) is similar to the isotropic case for both uniaxial and biaxial loading conditions. Hence, it can be inferred that, the relative stiffness does not influence the kink behavior when the kink is small. On the contrary for a longer kink length, under uniaxial or biaxial loading, the behavior of the kink is influenced by the relative stiffness. For an uniaxial load, higher the stiffness, more is the tendency for the kink to run parallel to the stiffer direction.

Hence, given a material, the relative dimensions of the crack and the kink, and the T_{crit} value (which can be determined as in Richardson [94]), the present study can be used to predict how the kink will behave when subjected to different loading conditions based on the modified T–stress fracture model.

APPENDICIES

APPENDIX A

ISOTROPIC MATERIAL

Analytical Formulation for a Dislocation Function

Consider an infinite plane, as shown in Figure A.1, with a dislocation at point z_o with respect to the principal axes (X–Y). Fix another co–ordinate system (X'–Y') with z_o as origin. The most general form of the dislocation stress function, which is multi valued, can be written, following Muskhelishvili [15], as follows.

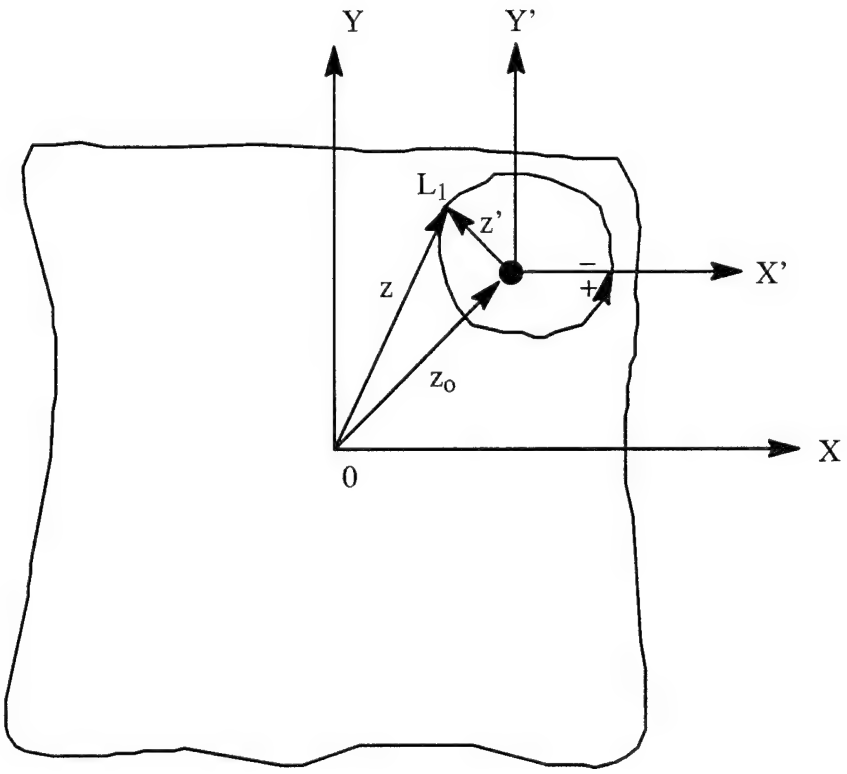

Figure A.1. Geometry of Dislocation Function

$$\phi_D(z) = \gamma_1 \ln(z')\cdot \tag{A.1}$$

$$\psi_D(z) = \gamma_2 \ln(z')\cdot \tag{A.2}$$

where, γ_1 and γ_2 are complex constants. z and z' are complex. z is written either as $te^{i\theta a}$ or $xe^{i\theta a}$. ('t' and 'x' are used interchangeably in the development of equations below). The branch cut for the multi valued function can be taken to be along the X' axis. The displacement can be be expressed in terms of the stress functions as,

$$u + iv = \frac{1}{2E}\left[\varkappa\phi_D(z') - z'\overline{\Phi_D(z')} - \overline{\psi_D(z')}\right], \tag{A.3}$$

where, E=Youngs modulus. For one circuit (L_1) around the dislocation, from the '–' side to the '+' side in anti–clockwise direction, the net change in the displacement is given as,

$$u + iv = \frac{1}{2E}\left[\varkappa\phi_D(z') - z\overline{\Phi_D(z')} - \overline{\psi_D(z')}\right]_{L_1}, \tag{A.4}$$

which, after substituting for the stress functions, can be written as,

$$[u^+ - u^-] + i[v^+ - v^-] = \frac{\pi i}{E}[\varkappa\gamma_1 + \bar{\gamma}_2]. \tag{A.5}$$

Let,

$$[b] = [u^+ - u^-] + i[v^+ - v^-], \tag{A.6}$$

where, [b] is the Burgers vector. Therefore,

$$\frac{\pi i}{E}[\varkappa\gamma_1 + \bar{\gamma}_2] = [b]. \tag{A.7}$$

The sum of external forces acting on a contour (L_1) around the dislocation should be zero. This is written in terms of the stress functions as,

$$\sum \text{Forces} = -i\left[\phi_D(z') - z'\overline{\Phi_D(z')} + \overline{\psi_D('z)}\right]_{L_1} = 0, \tag{A.8}$$

which implies that,

$$\gamma_1 = \bar{\gamma}_2. \tag{A.9}$$

Now the constants γ_1 and γ_2 are uniquely determined and the stress functions can be expressed as,

$$\phi_D(z) = \frac{[b]E}{\pi i(\varkappa + 1)}\ln(z'), \tag{A.10}$$

$$\psi_D(z) = -\frac{[\bar{b}]E}{\pi i(\varkappa + 1)}\ln(z'). \tag{A.11}$$

Changing the coordinate system from X'–Y' to X–Y coordinate system, the stress functions for the dislocation can be written as,

$$\phi_D(z) = \frac{[b]E}{\pi i(\kappa + 1)} \ln(z - z_o), \tag{A.12}$$

$$\psi_D(z) = -\frac{[\bar{b}]E}{\pi i(\kappa + 1)} \ln(z - z_o) - \bar{z}_o \frac{[b]E}{\pi i(\kappa + 1)(z - z_o)}, \tag{A.13}$$

by using the expressions given in Muskhelishvili [15]. Let,

$$\Theta(t_o) = \frac{[b]E}{\pi i(\kappa + 1)}, \tag{A.14}$$

where, t_o is some arbitrary variable. Therefore,

$$\phi_D(z) = \Theta(t_o) \ln(z - z_o), \tag{A.15}$$

$$\psi_D(z) = \overline{\Theta(t_o)} \ln(z - z_o) - \bar{z}_o \frac{\Theta(t_o)}{(z - z_o)}, \tag{A.16}$$

$$\phi'_D(z) = \Phi_D(z) = \Theta(t_o)/(z - z_o), \tag{A.17}$$

$$\psi'_D(z) = \Psi_D(z) = \overline{\Theta(t_o)}/(z - z_o) + \Theta(t_o)\bar{z}_o/(z - z_o)^2. \tag{A.18}$$

An infinitesimal burgers vector can be mathematically represented as $[b]dt_o$, where

$$[b] = \frac{\partial}{\partial t_o}[u^+ - u^-] + i[v^+ - v^-]. \tag{A.19}$$

This burgers vector can be integrated over a range to represent a crack.

Formulation of Stress Functions for the Main Crack Which Opens Up Due to the Presence of a Dislocation

The stress fields on the main crack due to a dislocation away from the crack are next evaluated by using the dislocation stress stress functions. The normal and shear stresses acting on the surface of the main crack due to a dislocation are given as,

$$\sigma_{yy}(x, 0) - i\sigma_{xy}(x, 0) = \frac{\Theta(t_o)}{x - z_o} + \frac{\Theta(t_o)}{x - \bar{z}_o} + \frac{\overline{\Theta(t_o)}(z_o - \bar{z}_o)}{(x - \bar{z}_o)^2} = -p(t_o, x), \tag{A.20}$$

where, $-2c \le x \le 0$. The stresses acting on the main crack surface is now known. Hence

the boundary value problem of a pressurized crack, shown in Figure A.2, can be solved using techniques given in Muskhelishvili [15].

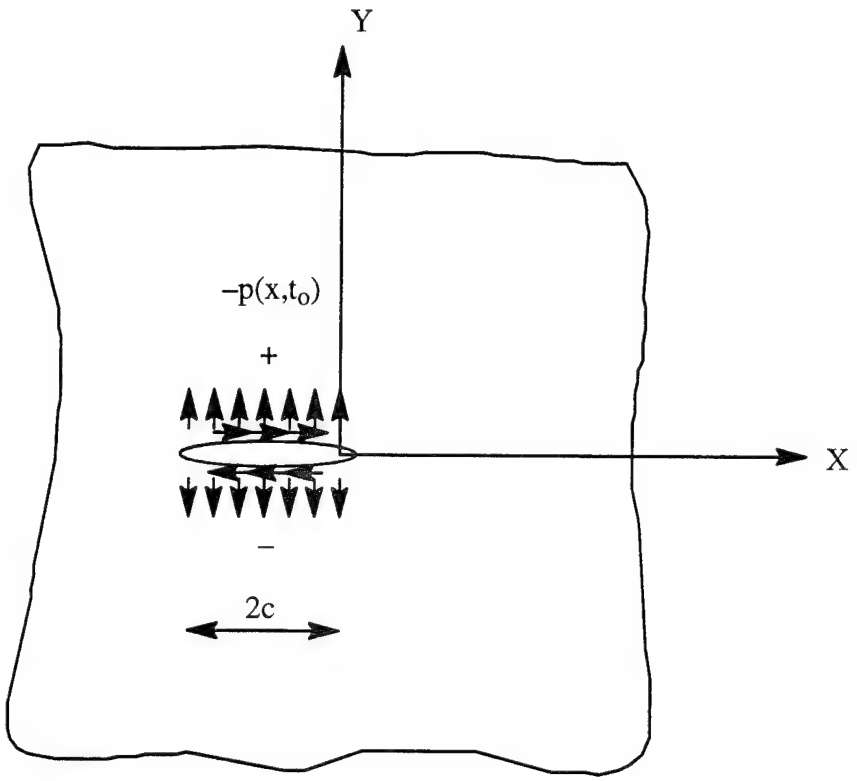

Figure A.2. Geometry of Pressurized Main Crack

Following Muskhelishvili [15] the normal and shear stresses due to the main crack alone can be written as,

$$\sigma_{yy}(z) - i\sigma_{xy}(z) = \Phi_M(z) + \overline{\Phi_M(z)} + z\overline{\Phi'_M(z)} + \overline{\Psi_M(z)}. \tag{A.21}$$

Let,

$$\Omega_M(\bar{z}) = \overline{\Phi_M(z)} + \bar{z}\overline{\Phi_M'(z)} + \overline{\Psi_M(z)}. \tag{A.22}$$

Then,

$$\sigma_{yy}(z) - i\sigma_{xy}(z) = \Phi_M(z) + \Omega_M(\bar{z}) + (z - \bar{z})\overline{\Phi_M'(z)}. \tag{A.23}$$

Let + refer to the upper side of the main crack and – refer to the lower side. Using equation A.23 the stresses on the upper and lower side of the main crack can be written as,

$$\sigma_{yy}^{+} - i\sigma_{xy}^{+} = \Phi_M^{+}(x) + \Omega_M^{-}(x), \tag{A.24}$$

$$\sigma_{yy}^{-} - i\sigma_{xy}^{-} = \Phi_M^{-}(x) + \Omega_M^{+}(x). \tag{A.25}$$

Adding equations A.24 and A.25,

$$\frac{1}{2}[\sigma_{yy}^{+} + \sigma_{yy}^{-}] - \frac{i}{2}[\sigma_{xy}^{+} + \sigma_{xy}^{-}] = [\Phi_M(x) + \Omega_M(x)]^{+} + [\Phi_M(x) + \Omega_M(x)]^{-}. \tag{A.26}$$

Similarly subtracting equation A.24 from A.25,

$$\frac{1}{2}[\sigma_{yy}^{+} - \sigma_{yy}^{-}] - \frac{i}{2}[\sigma_{xy}^{+} - \sigma_{xy}^{-}] = [\Phi_M(x) - \Omega_M(x)]^{+} - [\Phi_M(x) - \Omega_M(x)]^{-}. \tag{A.27}$$

Using theorems given in Muskhelishvili [15] A.27 can be written as,

$$[\Phi_M(z) - \Omega_M(z)] = 0. \tag{A.28}$$

Using A.26, A.20 and A.28,

$$\Phi_M(z) = \frac{1}{2\pi i X(z)} \int_L \frac{X^{+}(t)p(t, z_o)dt}{t - z} + \frac{C}{X(z)}, \tag{A.29}$$

where, $\Phi_M(z)$ is a sectionally holomorphic function which is holomorphic everywhere except on L (0 to –2c). C is a constant which has to be determined by using the condition of single valuedness of displacement. Also note that x has been replaced by t. The above function $\Phi_M(z)$ can be evaluated by using contour integrals. As an example, one term in $p(t,z_o)$ will be evaluated below.

Consider the first term in the above integral (A.29) which is repeated below with all the terms.

$$\Phi_M(z) = -\frac{1}{2\pi i X(z)} \int_L \frac{X^{+}(t)}{t - z}\left[\frac{\Theta(t_o)}{t - z_o} + \frac{\Theta(t_o)}{t - \bar{z}_o} + \frac{\overline{\Theta(t_o)}(z_o - \bar{z}_o)}{(t - \bar{z}_o)^2}\right]dt + \frac{C}{X(z)}. \tag{A.30}$$

$$F(z, z_o) = -\frac{1}{2\pi i X(z)} \int_L \frac{X^{+}(t)}{t - z}\left[\frac{\Theta(t_o)}{t - z_o}\right]dt, \tag{A.31}$$

where X(z) is a sectionally holomorphic function and its branch cut is defined as shown in Figure A.3.

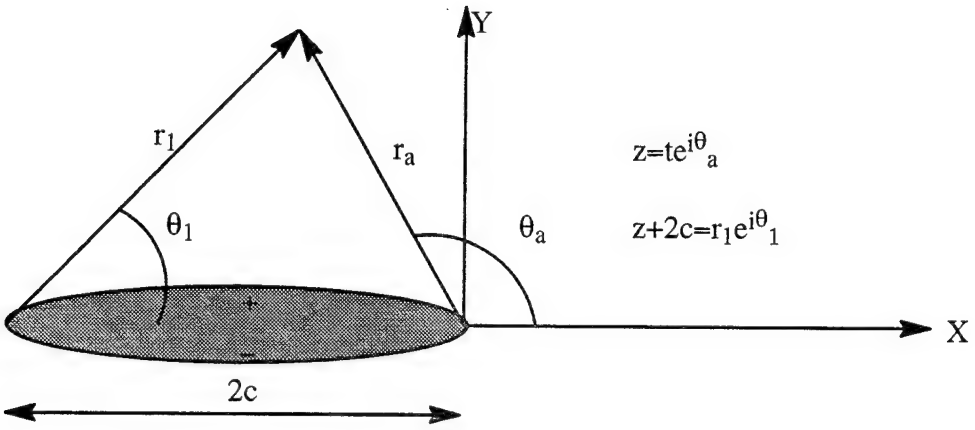

Figure A.3. Definition of the Function X(z)

$$X(z) = \sqrt{z(z + 2c)}. \tag{A.32}$$

$$X(z) = \sqrt{r_1 te^{i(\theta_a + \theta_1)}}. \tag{A.33}$$

The branch cut for $z^{1/2}$ is taken such that, $0 < \theta_a < 2\pi$ and similarly the branch cut for z+2c is taken such that $0 < \theta_1 < 2\pi$. Therefore,

$$X^+(t) = \sqrt{t(2c + t)}, \tag{A.34}$$

$$X^-(t) = -\sqrt{t(2c + t)}. \tag{A.35}$$

Consider a contour around the line of integration as shown in Figure A.4 in which the contour Γ divides the entire infinite region into two parts, S^+ and S^-.

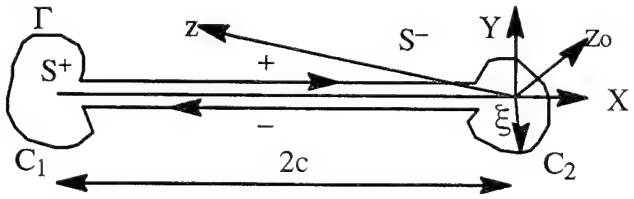

Figure A.4. Contour Γ

ξ is complex and lies on the contour Γ. The line integral, equation (A.31) can be written in terms of a contour integral as shown below.

$$\oint_{\Gamma} \frac{X(\xi)}{\xi - z}\left[\frac{\Theta(t_o)}{\xi - z_o}\right]d\xi = \oint_{C_1} \frac{X(\xi)}{\xi - z}\left[\frac{\Theta(t_o)}{\xi - z_o}\right]d\xi + \int_{L^+} \frac{X^+(t)}{t_o - z}\left[\frac{\Theta(t_o)}{t - z_o}\right]dt$$

$$+ \oint_{C_2} \frac{X(\xi)}{\xi - z}\left[\frac{\Theta(t_o)}{\xi - z_o}\right]d\xi + \int_{L^-} \frac{X^-(t)}{t_o - z}\left[\frac{\Theta(t_o)}{t - z_o}\right]dt, \qquad (A.36)$$

It can be shown that the contour integrals around C_1 and C_2 vanish as the contours are shrunk to a point. Hence this leaves the line integrals. Since $X^+(t)$ and $X^-(t)$ are related, the contour integral around Γ can be written as,

$$\oint_{\Gamma} \frac{X(\xi)}{\xi - z}\left[\frac{\Theta(t_o)}{\xi - z_o}\right]d\xi = \int_{L^+} \frac{X^+(t_o)}{t_o - z}\left[\frac{\Theta(t_o)}{t - z_o}\right]dt - \int_{L^-} \frac{X^-(t_o)}{t_o - z}\left[\frac{\Theta(t_o)}{t - z_o}\right]dt, \qquad (A.37)$$

$$\oint_{\Gamma} \frac{X(\xi)}{\xi - z}\left[\frac{\Theta(t_o)}{\xi - z_o}\right]d\xi = 2\int_{L^+} \frac{X^+(t_o)}{t_o - z}\left[\frac{\Theta(t_o)}{t - z_o}\right]dt. \qquad (A.38)$$

The contour integrals can be evaluated using the theorems given in Muskhelishvili [15], chapter 12. Let,

$$\oint_{\Gamma} \frac{X(\xi)}{\xi - z}\left[\frac{\Theta(t_o)}{\xi - z_o}\right]d\xi = \oint_{\Gamma} \frac{f(\xi)}{\xi - z}d\xi, \qquad (A.39)$$

where $f(\xi)$ is defined as,

$$f(\xi) = X(\xi)\left[\frac{\Theta(t_o)}{\xi - z_o}\right]. \qquad (A.40)$$

$f(\xi)$ is a sectionally holomorphic function in S^+, but holomorphic everywhere in S^- except at z_o where it has a simple pole. z_o is assumed to lie outside the contour. Using the theorems given for contour integrals in Muskhelishvili [15], chapter 12, the following can be written.

$$\frac{1}{2\pi i}\oint_{\Gamma}\frac{f(\xi)}{\xi - z}d\xi = f(z) - G_1(z) - G_\infty(z), \tag{A.41}$$

where, $G_1(z)$ is the principal part of the function at z_o and $G_\infty(z)$ is the principal part at infinity. Note the change in sign in equation A.41 when compared to the theorem given in Muskhelishvili [15], chapter 12, since the direction of integration considered for this study is reversed. $G_1(z)$ is evaluated as follows.

$$G_1(z) = \frac{A_1}{z - z_o}, \tag{A.42}$$

where A_1 is the residue of the function $f(\xi)$ at z_o.

$$A_1 = \lim_{\xi \to z_o}(\xi - z_o)\frac{X(\xi)\Theta(t_o)}{(\xi - z_o)}. \tag{A.43}$$

$$A_1 = X(z_o)\Theta(t_o). \tag{A.44}$$

To evaluate $G_\infty(z)$ the function $f(\xi)$ is expanded in terms of $1/\xi$ and evaluated as ξ approaches ∞.

$$G_\infty(z) = \lim_{\xi \to \infty}\left(1 + \frac{2c}{\xi}\right)^{1/2}\left(1 - \frac{z_o}{\xi}\right)^{-1}\Theta(t_o), \tag{A.45}$$

$$G_\infty(z) = \Theta(t_o). \tag{A.46}$$

Therefore,

$$\frac{1}{2\pi i}\oint_{\Gamma}\frac{f(\xi)}{\xi - z}d\xi = \frac{\Theta(t_o)X(z)}{z - z_o} - \frac{\Theta(t_o)X(z_o)}{z - z_o} - \Theta(t_o). \tag{A.47}$$

Using similar procedures, all the line integrals given in equation A.30 can be evaluated to give,

$$\Phi_M(z) = -\left\{\Theta(t_o)F^*(z, z_o) + \Theta(t_o)F^*(z, \bar{z}_o) + \overline{\Theta(t_o)}(z_o - \bar{z}_o)G^*(z, \bar{z}_o)\right\} + \frac{C}{X(z)}. \tag{A.48}$$

where,

$$F^*(z, z_o) = \frac{1}{2}\left[\frac{1}{z - z_o} - \frac{X(z_o)}{X(Z)(z - z_o)} - \frac{1}{X(Z)}\right], \tag{A.49}$$

$$G^*(z, z_o) = \frac{\partial}{\partial z_o} F^*(z, z_o), \tag{A.50}$$

and C is still unknown and can be evaluated from the condition that the displacements are single valued. The condition for single valuedness of displacement is given as,

$$\varkappa \oint_{\Gamma} [\Phi_D(z) + \Phi_M(z)]dz - \oint_{\Gamma} \left[\Omega_D(\bar{z}) + \Omega_M(\bar{z})\right]d\bar{z} = 0. \tag{A.51}$$

Contracting these contours along the line of discontinuity 0 to –2c and 0 to l (Figure A.5), the contour integrals can be written (using the relation given in A.28) as,

$$(\varkappa + 1) \int_{L_1+L_2} [\Phi_M^+(t^*) - \Phi_M^-(t^*)]dt^* + \varkappa \int_{L_1+L_2} [\Phi_D^+(t^*) - \Phi_D^-(t^*)]dt^*,$$

$$+ \int_{L_1+L_2} [\Omega_D^+(t^*) - \Omega_D^-(t^*)]dt^* = 0, \tag{A.52}$$

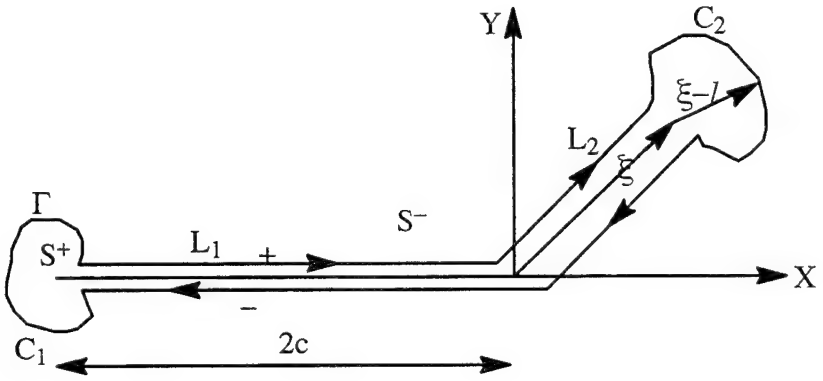

Figure A.5. Contour Γ (L_1+L_2)

where the + and – are the limiting values of the sectionally holomorphic function on the line of discontinuity. Φ_D and Ω_D are defined as,

$$\Phi_D(z) = \frac{\Theta(t_o)}{(z - z_o)}, \tag{A.53}$$

$$\Omega_D(z) = \overline{\Phi}_D(z) + z\overline{\Phi}'_D(z) + \overline{\Psi}_D(z), \tag{A.54}$$

therefore,

$$\Omega_D(z) = \frac{\Theta(t_o)}{(z - \overline{z}_o)}. \tag{A.55}$$

Using + and – limiting values of the function in the first term in equation A.52, the following is obtained.

$$(\varkappa + 1)\int_{L_1}[\Phi_M^+(t^*) - \Phi_M^-(t^*)]dt^* = (\varkappa + 1)\int_{t=-2c}^{0}\left[\frac{X(z_o)\Theta(t_o)}{X^+(t)(t - z_o)} + \frac{X(\overline{z}_o)\Theta(t_o)}{X^+(t)(t - \overline{z}_o)}\right.$$

$$\left. + \frac{2\Theta(t_o)}{X^+(t)} + \frac{\Theta(t_o)(z_o + c)(z_o - \overline{z}_o)}{X(z_o)(z - \overline{z}_o)X^+(t)} + \frac{X(\overline{z}_o)\Theta(t_o)(z_o - \overline{z}_o)}{X^+(t)(t - \overline{z}_o)^2} + \frac{2C}{X^+(t)}\right]dt \tag{A.56}$$

where, $t^* = t$. The above integrals can be evaluated using contour integrals (see Appendix D, equations D.1 – D.13) and are given as,

$$\int_{t=-2c}^{0}\frac{dt}{X^+(t)(t - z_o)} = -\frac{\pi i}{X(z_o)} \tag{A.57}$$

$$\int_{t=-2c}^{0}\frac{dt}{X^+(t)} = -\pi i \tag{A.58}$$

Substituting the above integrals in equation (A.56) the following is obtained.

$$(\varkappa + 1)\int_{L_1}[\Phi_M^+(t^*) - \Phi_M^-(t^*)]dt^* = (\varkappa + 1)(-4\pi iC - 2\pi i\Theta(t_o)). \tag{A.59}$$

The only terms from $\Phi_M(z)$ which contributes on L_2 are the following integrals,

$$-\frac{1}{2}\int_0^l\frac{\Theta(t_o)}{(t^* - z_o)}dt^* + \frac{1}{2}\int_0^l\frac{X(z_o)\Theta(t_o)}{X^+(t^*)(t^* - z_o)}dt^*$$

where $t^* \varepsilon L_2$. Their + and – limiting values, using Plemelj formula, are given below.

$$\int_0^l \frac{X(z_o)\Theta(t_o)}{X(t^*)(t^* - z_o)}dt^* = X(z_o)\Theta(t_o)\int_0^l \frac{1}{X(t^*)(t^* - z_o)}dt^*,$$

$$\left[X(z_o)\Theta(t_o)\int_0^l \frac{1}{X(t^*)(t^* - z_o)}dt^*\right]^+ = \pi i\Theta(t_o) + X(z_o)\Theta(t_o)\int_0^l \frac{1}{X(t^*)(t^* - z_o)}dt^*,$$

$$\left[X(z_o)\Theta(t_o)\int_0^l \frac{1}{X(t^*)(t^* - z_o)}dt^*\right]^- = -\pi i\Theta(t_o) + X(z_o)\Theta(t_o)\int_0^l \frac{1}{X(t^*)(t^* - z_o)}dt^*$$

and

$$\int_0^l \frac{\Theta(t_o)}{(t^* - z_o)}dt^* = \Theta(t_o)\int_{L_2} \frac{dt^*}{(t^* - z_o)},$$

$$\left[\Theta(t_o)\int_{L_2} \frac{dt^*}{(t^* - z_o)}\right]^+ = \pi i\Theta(t_o) + bf^*,$$

$$\left[\Theta(t_o)\int_{L_2} \frac{dt^*}{(t^* - z_o)}\right]^- = -\pi i\Theta(t_o) + bf^*,$$

where bf^* is a bounded function. Therefore,

$$(\varkappa + 1)\frac{1}{2}\int_{L_2}[\Phi_M^+(t^*)dz - \Phi_M^-(t^*)]dt^* = 0 \qquad (A.60)$$

Consider the next integral

$$\varkappa\int_{L_1+L_2}[\Phi_D^+(t^*) - \Phi_D^-(t^*)]dt^* + \int_{L_1+L_2}[\Omega_D^+(t^*) - \Omega_D^-(t^*)]dt^*,$$

These integrals do not have different limiting values on L_1 but only on L_2. Therefore using Plemelj formula again the limiting values of the above integrals are given below.

$$\int_{L_2} \Phi_D(z)dz = \Theta(t_o) \int_{L_2} \frac{dz}{(z - z_o)},$$

$$\left[\Theta(t_o) \int_{L_2} \frac{dz}{(z - z_o)}\right]^+ = \pi i \Theta(t_o) + bf^*,$$

$$\left[\Theta(t_o) \int_{L_2} \frac{dz}{(z - z_o)}\right]^- = -\pi i \Theta(t_o) + bf^*,$$

where bf^* is a bounded function. Therefore,

$$\varkappa \int_{L_1+L_2} [\Phi_D^+(t^*)dz - \Phi_D^-(t^*)]dt^* = \varkappa 2\pi i \Theta(t_o).$$

Similarly,

$$\int_{L_1+L_2} [\Omega_D^+(t^*) - \Omega_D^-(t^*)]dt^* = 2\pi i \Theta(t_o).$$

Therefore,

$$\varkappa \int_{L_1+L_2} [\Phi_D^+(t^*)dz - \Phi_D^-(t^*)]dt^* + \int_{L_1+L_2} [\Omega_D^+(t^*) - \Omega_D^-(t^*)]dt^*,$$

$$= (\varkappa + 1)2\pi i \Theta(t_o). \qquad (A.61)$$

Adding equations A.59, A.60 and A.61 and equating to zero,

$$(\varkappa + 1)(-2\pi i C - 4\pi i \Theta(t_o) + 2\pi i \Theta(t_o)) = 0. \qquad (A.62)$$

$$C = -\Theta(t_o). \qquad (A.63)$$

The constant C can be evaluated using a different method which is the same as that used by Lo [24]. Consider equation A.51 in which the contour is assumed to enclose the branched or kinked crack also. Therefore,

$$\varkappa \oint_{\Gamma} [\Phi_D(z) + \Phi_M(z)]dz - \oint_{\Gamma} [\Omega_D(\bar{z}) + \Omega_M(\bar{z})]d\bar{z} = 0. \tag{A.64}$$

where the contour Γ extends to ∞. Expanding the above integrals in terms of $1/z$ and $1/\bar{z}$,

$$\varkappa \oint_{\Gamma} [\Phi_M(z) + \Phi_D(z)]dz = \lim_{z\to\infty} \oint_{\Gamma} \left\{ \frac{1}{z}[C + \Theta(t_o)dt_o] + o\left(\frac{1}{z^2}\right) \right\} dz, \tag{A.65}$$

$$\oint_{\Gamma} [\Omega_D(\bar{z}) + \Omega_M(\bar{z})]d\bar{z} = = \lim_{\bar{z}\to\infty} \oint_{\Gamma} \left\{ \frac{1}{\bar{z}}[C + \Theta(t_o)dt_o] + o\left(\frac{1}{\bar{z}^2}\right) \right\} d\bar{z}. \tag{A.66}$$

If,

$$C = -\Theta(t_o), \tag{A.67}$$

then the contour integrals, in both of the above equations, vanishes as z tends to ∞. Therefore the functions $\Phi_M(z)$,$\Phi_D(z)$, $\Psi_M(z)$ and $\Psi_D(z)$ are single valued in the entire plane, including infinity, except along the main and kinked crack respectively.

Using equation (A.67) in (A.48),

$$\Phi_M(z) = -\left\{\Theta(t_o)F(z, z_o) + \Theta(t_o)F(z, \bar{z}_o) + \overline{\Theta(t_o)}(z_o - \bar{z}_o)G(z, \bar{z}_o)\right\}. \tag{A.68}$$

where,

$$F(z, z_o) = \frac{1}{2}\left[\frac{1}{z - z_o} - \frac{X(z_o)}{X(Z)(z - z_o)}\right], \tag{A.69}$$

$$G(z, z_o) = \frac{\partial}{\partial z_o} F(z, z_o), \tag{A.70}$$

and

$$\Omega_M(\bar{z}) = \overline{\Phi_M(z)} + \bar{z}\overline{\Phi_M'(z)} + \overline{\Psi_M(z)}, \tag{A.71}$$

therefore,

$$\Psi_M(z) = \overline{\Phi}_M(z) - \Phi_M(z) - z\Phi_M'(z). \tag{A.72}$$

Formulation of the Solution for a Infinite Plane with a Crack.

The next step is to derive the equations for an infinite plate with a crack which is subjected to remote infinite biaxial stresses. The steps for solving this problem follows directly from Muskhelishvili [15], chapter. 19 (pg. 506 – 508).

$$\Phi_L(z) + \Omega_L(z) = 2\frac{P_1(z)}{X(z)} \tag{A.73}$$

$$P_1(z) = C_{L0}z + C_{L1}. \tag{A.74}$$

$$C_{L0} = \frac{\sigma_{yy}^{\infty}}{2}. \tag{A.75}$$

C_{L1} is a constant which has to be determined from single valuedness of displacement condition. Single valuedness of displacement condition is expressed as,

$$\int_{-2c}^{0} \frac{P_1(t)}{X^+(t)}dt = 0. \tag{A.76}$$

$$\int_{-2c}^{0} \frac{C_{L0}t + C_{L1}}{X^+(t)}dt = 0. \tag{A.77}$$

The above integral can be evaluated using contour integrals (see Appendix D, D.1 – D.25) and the following, $C_{L1}=C_{Lo}c$ is obtained. Therefore,

$$C_{L1} = \frac{c\sigma_{yy}^{\infty}}{2} \tag{A.78}$$

$$\Phi_L(z) = \frac{\sigma_{yy(}^{\infty}(z + c)}{2X(z)} + \frac{(\sigma_{xx}^{\infty} - \sigma_{yy)}^{\infty}}{4} \tag{A.79}$$

$$\Psi_L(z) = \overline{\Omega}_L(z) - \Phi_L(z) - z\Phi_L'(z). \tag{A.80}$$

$$\overline{\Omega}_L(z) = \frac{\sigma_{yy(}^{\infty}(z + c)}{2X(z)} - \frac{(\sigma_{xx}^{\infty} - \sigma_{yy)}^{\infty}}{4}. \tag{A.81}$$

Therefore,

$$\Psi_L(z) = \frac{zc^2\sigma_{yy}^{\infty}}{2[X(z)]^{3/2}} - \frac{(\sigma_{xx}^{\infty} - \sigma_{yy)}^{\infty}}{2}. \tag{A.82}$$

Let,

$$\sigma_{xx}^{\infty} = k\sigma_{yy}^{\infty}. \tag{A.83}$$

$$\Phi_L(z) = \frac{\sigma_{yy}^{\infty}(z + c)}{2X(z)} + \frac{\sigma_{yy}^{\infty}(k - 1)}{4}. \tag{A.84}$$

$$\Psi_L(z) = \frac{zc^2\sigma_{yy}^{\infty}}{2[X(z)]^{3/2}} - \frac{\sigma_{yy}^{\infty}(k - 1)}{2} \tag{A.85}$$

Formulation of the Solution for the Kinked Crack.

The final step is to satisfy the boundary condition on the kink. For this, the Plemelj formulae are used. The dislocation stress functions are the only ones which give different limiting values on the kink surfaces. The stresses due to the dislocation are given by,

$$\sigma_{\theta\theta}^{D}(z) + i\sigma_{r\theta}^{D}(z) = \Phi_D(z) + \overline{\Phi_D(z)} + e^{2i\theta}\left[\bar{z}\Phi_D'(z) + \Psi_D(z)\right]. \tag{A.86}$$

The '+' and '–' limiting values of the stresses on the kink are given by,

$$\left[\sigma_{\theta\theta}^{D}(t) + i\sigma_{r\theta}^{D}(t)\right]^{\pm} = \mp \pi i\Theta(t) + \int_0^l \frac{\Theta(t_o)e^{-i\theta}}{(t - t_o)}dt_o \pm \pi i\overline{\Theta(t)} + \int_0^l \frac{\overline{\Theta(t_o)}e^{i\theta}}{(t - t_o)}dt_o$$

$$\pm \pi i\Theta(t) + \int_0^l \frac{\Theta(t_o)e^{-i\theta}}{(t_o - t)}dt_o \mp \pi i\overline{\Theta(t)} + \int_0^l \frac{\overline{\Theta(t_o)}e^{i\theta}}{(t - t_o)}dt_o \tag{A.87}$$

$$\left[\sigma_{\theta\theta}^{D}(t) + i\sigma_{r\theta}^{D}(t)\right]^{\pm} = 2\fint_0^l \frac{\Theta(t_o)e^{-i\theta}}{(t - t_o)}dt_o$$

The above integral is interpreted as a Principal Value integral. The other stress functions are regular on the kink. Hence the stresses on the kink can be written as,

$$\sigma_{\theta\theta}(z) + i\sigma_{r\theta}(z) = 2\fint_0^l \frac{\overline{\Theta(t_o)}e^{i\theta}dt_o}{t - t_o} + \int_0^l M(t, t_o; \alpha(t_o))dt_o + \sigma_{\theta\theta}^{\infty}(z) + i\sigma_{r\theta}^{\infty}(z) = 0. \tag{A.88}$$

Where,

$$M(t, t_o, \alpha(t_o)) = \Phi_M(z) + \overline{\Phi_M(z)} + e^{2i\theta}[(\bar{z} - z)\Phi_M'(z) - \Phi_M(z) + \overline{\Phi_M}(z)], \quad (A.89)$$

$$\sigma_{\theta\theta}^{\infty}(z) + i\sigma_{r\theta}^{\infty}(z) = \Phi_L(z) + \overline{\Phi_L(z)} + e^{2i\theta}\left[\bar{z}\Phi_L'(z) + \Psi_L(z)\right]. \quad (A.90)$$

APPENDIX B

EVALUATION OF THE SINGULAR INTEGRALS

First the formula used for evaluating the singular integral is given. The derivation can be found either in Muskhelishvili [83], chapter 4 or Kaya [87]. Then the application of the formula to some typical singular integrals is shown.

Formula

Let,

$$I(z) = \int_0^l \left[\frac{\Theta(t_o)}{t_o - z} \right] dt_o, \tag{B.1}$$

where,

$$\Theta(t_o) = \frac{\beta^*(t_o)}{(t_o)^\alpha (l - t_o)^\beta}, \tag{B.2}$$

$$z = te^{i\theta_a}, \; z_o = t_o e^{i\theta}, \tag{B.3}$$

and $\beta^*(t_o)$ is a bounded function in the interval $0 - l$ and is not zero at the end points (0 and l), and $\alpha, \beta < 1$. z is any point in the infinite complex plane but not on $0 - l$ (Figure 1, page 2). The singular behavior of the above integral after normalizing the integral with respect to the kink length l as z approaches 0 is given as,

$$\lim_{t \to 0} \int_0^l \left[\frac{\Theta(t_o)}{t_o - z} \right] dt_o = - \frac{\pi \beta(0) e^{-i[\alpha(\theta_a - \pi)]} e^{-i[\theta(1-\alpha)]}}{2 \sin(\pi\alpha)} \lim_{t \to 0} \frac{1}{t^\alpha} + \Theta^*(t), \tag{B.4}$$

where, $\Theta^*(t)$ tends to a definite limit as t tends to zero and $\beta(0) = \beta^*(0)/l^{\alpha+\beta}$. The other integrals can be evaluated in a similar manner.

Some Typical Singular Integrals

For all the integrals given below the length parameter is normalized with respect to the kink length l and $\beta(0) = \beta^*(0)/l^{\alpha+\beta}$.

$$I_1 = \lim_{t\to 0}\frac{1}{2}\int_0^l \left[\frac{\Theta(t_o)}{(z - z_o)}\right] dt_o,$$

$$= \lim_{t\to 0}\frac{1}{2}\int_0^1 \left[\frac{\beta(t_o)}{t_o^{\alpha}(1 - t_o)^{\beta}}\right] \frac{dt_o}{(z - z_o)},$$

$$= \lim_{t\to 0}\frac{1}{2}\int_0^1 \left[\frac{\beta(t_o)}{t_o^{\alpha}(1 - t_o)^{\beta}}\right] \frac{dt_o}{(te^{i\theta_a} - t_o e^{i\theta})},$$

$$= \lim_{t\to 0}\frac{1}{2}\int_0^1 \left[\frac{\beta(t_o)e^{-i\theta}}{t_o^{\alpha}(1 - t_o)^{\beta}}\right] \frac{dt_o}{(te^{i(\theta_a - \theta)} - t_o)},$$

which can be written as,

$$= \lim_{t\to 0}\frac{1}{2}\int_0^1 \left[\frac{\nu(t_o)}{t_o^{\alpha}(1 - t_o)^{\beta}}\right] \frac{dt_o}{(t_o - z_1)},$$

where, $z_1 = te^{i(\theta a-\theta)}$ and $\gamma(t_o) = -\beta(t_o)e^{-i\theta}$. Using the formula given above (B.4) for singular integrals,

$$= \frac{-\pi\nu(0)e^{i\pi\alpha}}{-2\sin(\pi\alpha)} \lim_{t\to 0}\frac{1}{z_1^{\alpha}} + bf_1,$$

where bf_1 is bounded function. Substituting for $\gamma(0)$ and simplifying,

$$= -\frac{\pi\beta(0)e^{-i[\alpha(\theta_a - \pi)]}e^{-i[\theta(1-\alpha)]}}{2\sin(\pi\alpha)} \lim_{t\to 0}\frac{1}{t^{\alpha}} + bf_1.$$

Consider integral I_3.

$$I_3 = \lim_{t\to 0}\frac{1}{2}\int_0^l \left[\frac{X(z_o)\Theta(t_o)}{X(z)(z - z_o)}\right] dt_o \qquad (B.5)$$

$$= \lim_{t\to 0} \frac{1}{2} \int_0^1 \left[\frac{\beta(t_o)\sqrt{t_o e^{i\theta}(t_o e^{i\theta} + 2c)}}{(t_o)^{\alpha}(1 - t_o)^{\beta}\sqrt{te^{i\theta_a}(te^{i\theta_a} + 2c)}\,(te^{i\theta_a} - t_o e^{i\theta})} \right] dt_o$$

which can be written as,

$$= \lim_{t\to 0} \frac{e^{i\frac{\theta-\theta_a}{2}}}{2\sqrt{2ct}} \int_0^1 \left[\frac{\beta(t_o)\sqrt{(t_o e^{i\theta} + 2c)}}{(t_o)^{\alpha-\frac{1}{2}}(1 - t_o)^{\beta}(te^{i\theta_a} - t_o e^{i\theta})} \right] dt_o$$

$$= \lim_{t\to 0} \frac{e^{i\frac{\theta-\theta_a}{2}}}{2\sqrt{2ct}} \int_0^1 \left[\frac{\beta(t_o)\sqrt{(t_o e^{i\theta} + 2c)}}{(t_o)^{\alpha-\frac{1}{2}}(1 - t_o)^{\beta}(te^{i\theta_a} - t_o e^{i\theta})} \right] dt_o$$

which can be written as,

$$= \lim_{t\to 0} \frac{1}{2\sqrt{2ct}} \int_0^1 \left[\frac{\nu(t_o)}{t_o^{\alpha-\frac{1}{2}}(1 - t_o)^{\beta}} \right] \frac{dt_o}{(t_o - z_1)}.$$

where, $z_1 = te^{i(\theta_a - \theta)}$ and

$$\nu(t_o) = -\beta(t_o)\sqrt{(t_o e^{i\theta} + 2c)}\, e^{-i(\frac{\theta+\theta_a}{2})}.$$

Again, using the formulae given above (B.4) for singular integrals and by simplifying the resulting expressions, the following is obtained.

$$= -\frac{\pi\beta(0)ie^{-i[\alpha(\theta_a-\pi)]}e^{-i[\theta(1-\alpha)]}}{2\cos(\pi\alpha)} \lim_{t\to 0}\frac{1}{t^{\alpha}} + \frac{bf_4}{\sqrt{t}}. \qquad \text{(B.6)}$$

where bf_4 is a bounded function. Integrals with $1/(z - z_o)^2$ terms can be treated as follows.

$$\lim_{t\to 0} I_5(z) = \lim_{t\to 0} \frac{1}{2} \int_0^l \frac{\overline{\Theta(t_o)}(z_o - \overline{z}_o)}{(z - \overline{z}_o)^2} dt_o,$$

$$\lim_{t\to 0} I_5(z) = -\lim_{t\to 0} \frac{d}{dz} \frac{1}{2} \int_0^l \frac{\overline{\Theta(t_o)}(z_o - \overline{z}_o)}{(z - \overline{z}_o)} dt_o.$$

The singular part of the integral can now be evaluated using the formula for singular integrals and is given below.

$$= \frac{\pi\overline{\beta(0)}i(1-\alpha)e^{-i[\alpha(\theta_a-\pi)]}e^{-i[\theta(\alpha-2)]}}{\sin(\pi\alpha)} \lim_{t\to 0}\frac{1}{t^{\alpha}} + bf_5,$$

where bf_5 is a bounded function. All the other integrals can be evaluated in a similar manner as given above.

APPENDIX C

ANISOTROPIC MATERIAL

Formulation of Governing Equations for an Anisotropic Elastic Body

The Hooke's law for an anisotropic material possessing one plane of elastic symmetry which is perpendicular to the z axis is given as,

$$\varepsilon_{xx} = c_{11}\sigma_{xx} + c_{12}\sigma_{yy} + c_{16}\tau_{xy} + c_{13}\sigma_{zz}, \tag{C.1}$$

$$\varepsilon_{yy} = c_{21}\sigma_{xx} + c_{22}\sigma_{yy} + c_{26}\tau_{xy} + c_{23}\sigma_{zz}, \tag{C.2}$$

$$\varepsilon_{zz} = c_{13}\sigma_{xx} + c_{23}\sigma_{yy} + c_{36}\tau_{xy} + c_{33}\sigma_{zz}, \tag{C.3}$$

$$2\varepsilon_{xy} = c_{16}\sigma_{xx} + c_{26}\sigma_{yy} + c_{36}\sigma_{zz} + c_{66}\tau_{xy}, \tag{C.4}$$

where, c_{ij}'s are the material constants. If plane stress conditions are assumed, where $\sigma_{zz} = 0$, the following equations are obtained.

$$\varepsilon_{xx} = c_{11}\sigma_x + c_{12}\sigma_y + c_{16}\tau_{xy}, \tag{C.5}$$

$$\varepsilon_{yy} = c_{12}\sigma_x + c_{22}\sigma_y + c_{26}\tau_{xy}, \tag{C.6}$$

$$\varepsilon_{zz} = c_{13}\sigma_{xx} + c_{23}\sigma_{yy} + c_{36}\tau_{xy}, \tag{C.7}$$

$$2\varepsilon_{xy} = c_{16}\sigma_x + c_{26}\sigma_y + c_{66}\tau_{xy}. \tag{C.8}$$

If plane strain conditions are assumed then $\varepsilon_{zz}=0$. Solving for σ_{zz} using equation C.3 the following relationships are obtained.

$$\varepsilon_{xx} = a_{11}\sigma_{xx} + a_{12}\sigma_{yy} + a_{16}\tau_{xy}, \tag{C.9}$$

$$\varepsilon_{yy} = a_{12}\sigma_{xx} + a_{22}\sigma_{yy} + a_{26}\tau_{xy}, \tag{C.10}$$

$$2\varepsilon_{xy} = a_{16}\sigma_{xx} + a_{26}\sigma_{yy} + a_{66}\tau_{xy}. \tag{C.11}$$

The c_{ij}'s are related to the a_{ij}'s by the following relationships.

$$a_{11} = \frac{c_{11}c_{33} - c_{13}^2}{c_{33}}, \tag{C.12}$$

$$a_{22} = \frac{c_{22}c_{33} - c_{23}^2}{c_{33}}, \tag{C.13}$$

$$a_{12} = \frac{c_{12}c_{33} - c_{13}c_{23}}{c_{33}}, \tag{C.14}$$

$$a_{26} = \frac{c_{26}c_{33} - c_{23}c_{36}}{c_{33}}, \tag{C.15}$$

$$a_{16} = \frac{c_{16}c_{33} - c_{13}c_{36}}{c_{33}}, \tag{C.16}$$

$$a_{66} = \frac{c_{66}c_{33} - c_{36}^2}{c_{33}} \tag{C.17}$$

The equilibrium equations for a 2–D plane problem where the body forces are neglected are given by,

$$\frac{\partial \sigma_{xx}}{\partial x} + \frac{\partial \tau_{xy}}{\partial y} = 0, \tag{C.18}$$

$$\frac{\partial \sigma_{yy}}{\partial y} + \frac{\partial \tau_{xy}}{\partial x} = 0. \tag{C.19}$$

The compatibility equation is given by,

$$\frac{\partial^2 \varepsilon_{xx}}{\partial y^2} + \frac{\partial^2 \varepsilon_{yy}}{\partial x^2} = \frac{2\partial^2 \varepsilon_{xy}}{\partial x \partial y}. \tag{C.20}$$

Let,

$$\sigma_{xx} = \frac{\partial^2 U(x, y)}{\partial y^2}, \tag{C.21}$$

$$\sigma_{yy} = \frac{\partial^2 U(x, y)}{\partial x^2}, \tag{C.22}$$

$$\tau_{xy} = -\frac{\partial^2 U(x, y)}{\partial x \partial y}. \tag{C.23}$$

These equations satisfy the equilibrium equations. Substituting these in equations C.5, C.6 and C.8 and then substituting them back in the compatibility equation C.20 the following homogeneous partial differential equation is obtained.

$$c_{22}\frac{\partial^4 U}{\partial x^4} - 2c_{26}\frac{\partial^4 U}{\partial x^3 \partial y} + (2c_{12} + c_{66})\frac{\partial^4 U}{\partial x^2 \partial y^2} - 2c_{16}\frac{\partial^4 U}{\partial x \partial y^3} + c_{11}\frac{\partial^4 U}{\partial y^4} = 0 \tag{C.24}$$

The solution for the above partial differential equation can be written as,

$$U = F(x + sy) \tag{C.25}$$

Substituting the above solution in equation (C.24) the following equation is obtained.

$$c_{11}s^4 - 2c_{16}s^3 + (2c_{12} + c_{66})s^2 - 2c_{26}s + c_{22} = 0. \quad \text{(C.26)}$$

Based on energy principle Lekhnitskii has shown that the roots of the above equation are always complex. Let s_1, s_2, s_3 and s_4 be the four complex roots ($s_3 = \bar{s}_1$, $s_4 = \bar{s}_2$) of the above equation. Then the complete solution of partial differential equation can be written as,

$$U = F_1(x + s_1y) + F_2(x + s_2y) + F_3(x + s_3y) + F_4(x + s_4y) \quad \text{(C.27)}$$

The following conditions hold for the complex roots s_i, i=1..4. Let,

$$s_1 = \alpha_1 + i\beta_1 \quad \text{(C.28)}$$

$$s_2 = \alpha_2 + i\beta_2 \quad \text{(C.29)}$$

where, α_1, α_2, β_1, β_2 are all real.

$$\beta_1 > 0,\ \beta_2 > 0 \text{ and } \beta_1 \neq \beta_2 \quad \text{(C.30)}$$

Let,

$$z_1 = x + s_1y,\ z_2 = x + s_2y \quad \text{(C.31)}$$

then,

$$U = F_1(z_1) + F_2(z_2) + \overline{F_1(z_1)} + \overline{F_2(z_2)}. \quad \text{(C.32)}$$

Let,

$$\frac{dF_1}{dz_1} = \phi(z_1). \quad \text{(C.33)}$$

$$\frac{dF_2}{dz_2} = \psi(z_2). \quad \text{(C.34)}$$

Using C.32 to C.34 in C.21 to C.23 the stresses can be written as,

$$\sigma_{xx} = 2\mathrm{Re}[s_1^2\,\phi'(z_1) + s_2^2\,\psi'(z_2)]. \quad \text{(C.35)}$$

$$\sigma_{yy} = 2\mathrm{Re}[\phi'(z_1) + \psi'(z_2)]. \quad \text{(C.36)}$$

$$\tau_{xy} = -2\mathrm{Re}[s_1\,\phi'(z_1) + s_2\,\psi'(z_2)]. \quad \text{(C.37)}$$

Substituting the above relations in the Hooke's law (C.9–C.11) and after integration and neglecting the rigid body displacements and rotations the following displacement equations are obtained.

$$u(x,y) = 2Re[p_1\phi(z_1) + p_2\psi(z_2)]. \tag{C.38}$$

$$v(x,y) = 2Re[q_1\phi(z_1) + q_2\psi(z_2)]. \tag{C.39}$$

where,

$$p_1 = c_{11}s_1^2 + c_{12} - c_{16}s_1 .$$

$$p_2 = c_{11}s_2^2 + c_{12} - c_{16}s_2 .$$

$$q_1 = \frac{c_{12}s_1^2 + c_{22} - c_{26}s_1}{s_1} .$$

$$q_2 = \frac{c_{12}s_2^2 + c_{22} - c_{26}s_2}{s_2} .$$

Analytical Formulation For Dislocation Function

The analytical formulation for the dislocation function is given below. Consider an infinite plane, as shown in Figure C.1, with a dislocation at point z_{o1} ($z_{oi} = x_{oi} + s_i y_{oi}$, i = 1..4) with respect to the principal axis (X–Y). The most general form of the dislocation stress function, which is multi valued, can be written as follows.

$$\phi_D(z_1) = A\ln(z_1 - z_{o1}), \tag{C.40}$$

$$\psi_D(z_2) = B\ln(z_2 - z_{o2}). \tag{C.41}$$

In the above equations (C.40, C.41) z_1, z_2, z_{o1}, z_{o2}, A and B are complex. The constants A and B can be determined by using the conditions that there is a discontinuity in displacements for one revolution around a contour L_1 which goes around the dislocation and by satisfying the condition that the resultant force vector around a contour is zero. Let the jump in discontinuity in displacement be represented by B_x and B_y which are the X and Y components of the Burgers vector. The '+' and '–' superscript represents the upper and lower

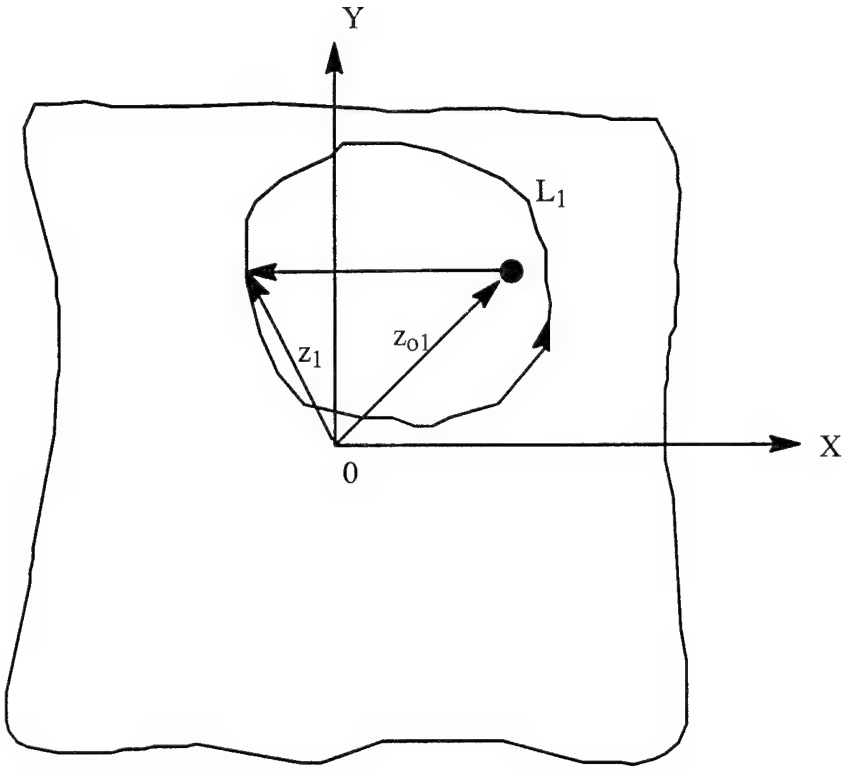

Figure C.1. Geometry of Dislocation Function

side of the dislocation or the discontinuity in displacement. The resultant force vector is given by,

$$X + iY = -i\left[(1 - is_1)\phi_D(z_1) + (1 - i\bar{s}_1)\overline{\phi_D(z_1)} + (1 + is_2)\psi_D(z_2) + (1 + i\bar{s}_2)\overline{\psi_D(z_2)}\right]_{L_1}$$

. (C.42)

Using equations C.40, C.41 in C.42 the following equations are obtained.

$$(1 + is_1)A - (1 + i\bar{s}_1)\overline{A} + (1 + is_2)B + (1 + i\bar{s}_2)\overline{B} = 0. \quad \text{(C.43)}$$

$$(1 - i\bar{s}_1)\overline{A} - (1 - is_1)A + (1 - i\bar{s}_2)\overline{B} - (1 - is_2)B = 0. \quad \text{(C.44)}$$

$$(\bar{p}_1 - i\bar{q}_1)\overline{A} - (p_1 - iq_1)A + (\bar{p}_2 - i\bar{q}_2)\overline{B} - (p_2 - iq_2)B = \frac{B_x - iB_y}{-2\pi i}. \quad \text{(C.45)}$$

$$-(\bar{p}_1 + i\bar{q}_1)\overline{A} + (p_1 + iq_1)A - (\bar{p}_2 + i\bar{q}_2)\overline{B} + (p_2 + iq_2)B = \frac{B_x + iB_y}{2\pi i}. \quad \text{(C.46)}$$

The above four equations are solved using Maple [88] and the following expressions are obtained for A and B.

$$A = \frac{s_1(B_x c_{22} - s_2 s_3 s_4 c_{11} B_y)}{(s_1 - s_2)(s_1 - s_3)(s_1 - s_4)c_{22}c_{11}}. \quad \text{(C.47)}$$

$$B = \frac{s_2(B_x c_{22} - s_1 s_3 s_4 c_{11} B_y)}{(s_2 - s_1)(s_2 - s_3)(s_2 - s_4)c_{22}c_{11}}. \quad \text{(C.48)}$$

If $c_{16} = c_{26} = 0$ then,

$$s_1 s_2 = \overline{s_1 s_2} = \sqrt{\frac{c_{22}}{c_{11}}}. \quad \text{(C.49)}$$

Using the above equation in the expressions for A and B, the dislocation density function is given as,

$$\phi_D(z_1) = \frac{s_1 B_x - B_y}{(s_1 - s_2)(s_1 - s_3)(s_1 - s_4)c_{11}} \ln(z_1 - z_{01}). \quad \text{(C.50)}$$

$$\psi_D(z_2) = \frac{s_2 B_x - B_y}{(s_2 - s_1)(s_2 - s_3)(s_2 - s_4)c_{11}} \ln(z_2 - z_{02}). \quad \text{(C.51)}$$

Therefore,

$$\Phi_D(z_1) = \phi'_D(z_1) = \frac{s_1 B_x - B_y}{(s_1 - s_2)(s_1 - s_3)(s_1 - s_4)c_{11}} \frac{1}{(z_1 - z_{01})}. \quad (C.52)$$

$$\Psi_D(z_2) = \psi'_D(z_2) = \frac{s_2 B_x - B_y}{(s_2 - s_1)(s_2 - s_3)(s_2 - s_4)c_{11}} \frac{1}{(z_2 - z_{02})}. \quad (C.53)$$

An infinitesimal Burgers vector can be mathematically represented as $[B_x]dt_o$ and $[B_y]dt_o$, where

$$[B_x] = \frac{\partial}{\partial t_o}[u^+ - u^-]. \quad (C.54)$$

$$[B_y] = \frac{\partial}{\partial t_o}[v^+ - v^-]. \quad (C.55)$$

This Burgers vector can be integrated over a range to represent a crack in that range.

Formulation of Stress Functions for the Main Crack Which Opens Up Due to the Presence of a Dislocation

The stress fields on the main crack due to this dislocation are next evaluated by using the dislocation stress functions (C.52, C.53). The negative of this stress field is applied on the main crack and the stress field due to the interaction between the main crack and the dislocation is derived. The development of these stress functions follows the method formulated by Krenk [52]. Following the formulation of Krenk [52] four new complex stress functions are defined in terms of the known stress functions as follows.

$$2\Theta_1(z_1) = \Phi(z_1) + \overline{\Phi}(z_1). \quad (C.56)$$

$$2\Theta_2(z_2) = \Psi(z_2) + \overline{\Psi}(z_2). \quad (C.57)$$

$$2\Omega_1(z_1) = \Psi(z_1) - \overline{\Psi}(z_1). \quad (C.58)$$

$$2\Omega_2(z_2) = \Psi(z_2) - \overline{\Psi}(z_2). \quad (C.59)$$

The normal and shear stresses can be defined using the newly introduced stress functions as,

$$\sigma_{yy} = \{\Theta_1(z_1) + \Omega_1(z_1) + \Theta_2(z_2) + \Omega_2(z_2) + \Theta_1(\overline{z}_1) - \Omega_1(\overline{z}_1) + \Theta_2(\overline{z}_2) - \Omega_2(\overline{z}_2)\} \quad (C.60)$$

$$\sigma_{xy} = -\{s_1\Theta_1(z_1) + s_1\Omega_1(z_1) + s_2\Theta_2(z_2) + s_2\Omega_2(z_2)$$

$$+ s_3\Theta_1(\bar{z}_1) - s_3\Omega_1(\bar{z}_1) + s_4\Theta_2(\bar{z}_2) - s_4\Omega_2(\bar{z}_2)\} \quad \text{(C.61)}$$

Let the stresses on the crack surface be represented by the following functions,

$$f(t) = \frac{(\sigma_{yy}^{+} + \sigma_{yy}^{-})}{2} \quad \text{(C.62)}$$

$$h(t) = \frac{(\sigma_{xy}^{+} + \sigma_{xy}^{-})}{2}. \quad \text{(C.63)}$$

$$g(t) = \frac{(\sigma_{yy}^{+} - \sigma_{yy}^{-})}{2}. \quad \text{(C.64)}$$

$$k(t) = \frac{(\sigma_{xy}^{+} - \sigma_{xy}^{-})}{2}. \quad \text{(C.65)}$$

The '+' and '–' values represent the value of the sectionally holomorphic function as it approaches the upper and lower surface of the main crack surface (Figure C.2).

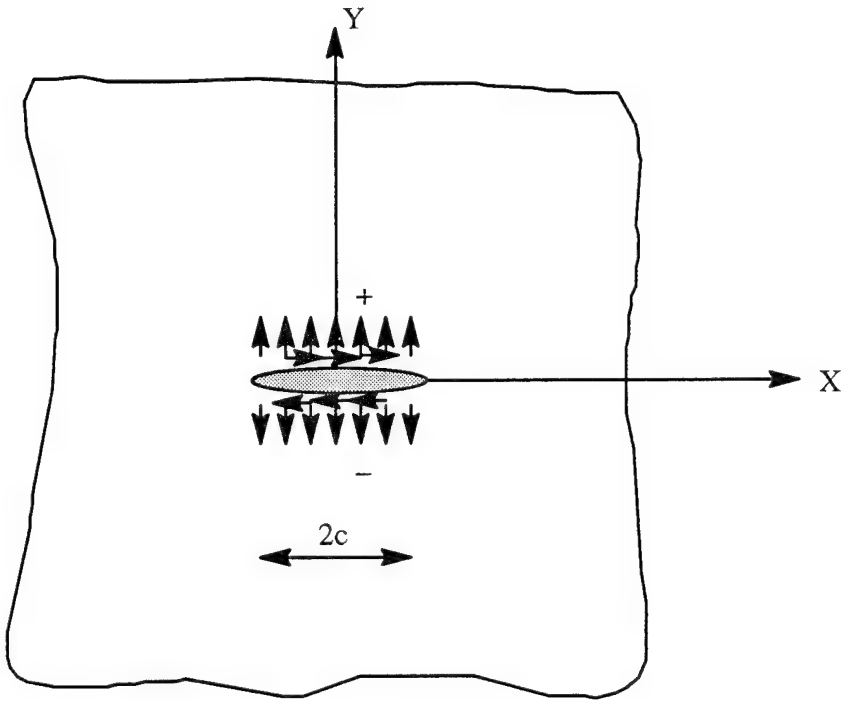

Figure C.2. Geometry of Pressurized Main Crack

Let the main crack extend from –c to +c along Y=0 axis. Then,

$$\sigma_{yy}^{+} = \{[\Theta_1 + \Omega_1 + \Theta_2 + \Omega_2]^{+} + [\Theta_1 - \Omega_1 + \Theta_2 - \Omega_2]^{-}. \quad (C.66)$$

$$\sigma_{yy}^{-} = \{[\Theta_1 + \Omega_1 + \Theta_2 + \Omega_2]^{-} + [\Theta_1 - \Omega_1 + \Theta_2 - \Omega_2]^{+}. \quad (C.67)$$

$$\sigma_{xy}^{+} = -\{[s_1\Theta_1 + s_1\Omega_1 + s_2\Theta_2 + s_2\Omega_2]^{+}$$

$$- [s_3\Theta_1 - s_3\Omega_1 + s_4\Theta_2 - s_4\Omega_2]^{-}\} \quad (C.68)$$

$$\sigma_{xy}^{-} = -\{[s_1\Theta_1 + s_1\Omega_1 + s_2\Theta_2 + s_2\Omega_2]^{-}$$

$$- [s_3\Theta_1 - s_3\Omega_1 + s_4\Theta_2 - s_4\Omega_2]^{+}\} \quad (C.69)$$

Therefore,

$$f(t) = \{[\Theta_1 + \Theta_2]^{+} + [\Theta_1 + \Theta_2]^{-}\}. \quad (C.70)$$

$$-h(t) = \{[\Theta_1\alpha_1 + \Omega_1 i\beta_1 + \Theta_2\alpha_2 + \Omega_2 i\beta_2]^{-}$$

$$+ [\Theta_1\alpha_1 + \Omega_1 i\beta_1 + \Theta_2\alpha_2 + \Omega_2 i\beta_2]^{+} \quad (C.71)$$

$$g(t) = -\{[\Omega_1 + \Omega_2]^{+} - [\Omega_1 + \Omega_2]^{-}\}. \quad (C.72)$$

$$-k(t) = \{[\Omega_1\alpha_1 + \Theta_1 i\beta_1 + \Omega_2\alpha_2 + \Theta_2 i\beta_2]^{-}$$

$$+ [\Omega_1\alpha_1 + \Theta_1 i\beta_1 + \Omega_2\alpha_2 + \Theta_2 i\beta_2]^{+}\} \quad (C.73)$$

where, $-c < t < c$.

Using Muskhelishvili [15], the most general solution for above problem can be written as,

$$\Theta_1(z) + \Theta_2(z) = \frac{1}{2\pi i X(z)} \int_L \frac{f(t)}{X^{+}(t)(t - z)} dt + \frac{P(z)}{X(z)}, \quad (C.74)$$

$$\alpha_1\Theta_1(z) + \alpha_2\Theta_2(z) + i\beta_1\Omega_1(z) + i\beta_2\Omega_2(z) = -\frac{1}{2\pi i X(z)} \int_L \frac{h(t)}{X^{+}(t)(t - z)} dt + \frac{Q(z)}{X(z)}. \quad (C.75)$$

$$\Omega_1(z) + \Omega_2(z) = \frac{1}{2\pi i X(z)} \int_L \frac{g(t)}{(t - z)} dt, \quad (C.76)$$

$$\alpha_1\Omega_1(z) + \alpha_2\Omega_2(z) + i\beta_1\Theta_1(z) + i\beta_2\Theta_2(z) = \frac{1}{2\pi i X(z)}\int_L \frac{k(t)}{X^+(t)(t - z)}dt. \tag{C.77}$$

where,

$$P(z) = \sum_{n=0}^{n} A_n z^n. \tag{C.78}$$

$$Q(z) = \sum_{n=0}^{n} B_n z^n. \tag{C.79}$$

where n is the number of cuts (i.e. cracks). Now from equation C.56,

$$2\Theta_1(z_1) = \Phi(z_1) + \overline{\Phi}(z_1). \tag{C.80}$$

$$2\overline{\Theta}_1(z_1) = \Phi(z_1) + \overline{\Phi}(z_1). \tag{C.81}$$

Therefore,

$$\Theta_1(z_1) = \overline{\Theta}_1(z_1). \tag{C.82}$$

Similarly,

$$\Theta_2(z_1) = \overline{\Theta}_2(z_1). \tag{C.83}$$

$$\Omega_1(z_1) = -\overline{\Omega}_1(z_1). \tag{C.84}$$

$$\Omega_2(z_1) = -\overline{\Omega}_2(z_1). \tag{C.85}$$

Hence,

$$\Theta_1(z_1) + \Theta_2(z_1) = \overline{\Theta}_1(z_1) + \overline{\Theta}_2(z_1). \tag{C.86}$$

$$\Omega_1(z_1) + \Omega_2(z_2) = -\overline{\Omega}_1(z_1) - \overline{\Omega}_2(z_2). \tag{C.87}$$

From equations C.74 and C.75,

$$P(z) = \overline{P}(z). \tag{C.88}$$

$$Q(z) = \overline{Q}(z). \tag{C.89}$$

Therefore the constants in P(z) and Q(z) are all real.

In the present case n (the number of cracks) is 1 therefore, from equations C.78 and C.79 there are 4 undetermined constants. By enforcing the condition that the stresses at infin-

ity vanish, A_1 and B_1 vanishes. A_0 and B_0 have to be determined from the single valuedness of displacement conditions. Since $\sigma^+_{yy}=\sigma^-_{yy}$ and $\sigma^+_{xy}=\sigma^-_{xy}$, therefore $g(t) = k(t) = 0$. The stress functions can now be written as,

$$(s_2 - s_1)\Phi_M(z_1) = \frac{1}{2\pi i X(z_1)} \int_L \frac{X^+(t)(s_2 f(t) + h(t))}{(t - z_1)} dt + \frac{s_2 A_0 + B_0}{X(z_1)} \tag{C.90}$$

$$(s_1 - s_2)\Psi_M(z_2) = \frac{1}{2\pi i X(z_2)} \int_L \frac{X^+(t)(s_1 f(t) + h(t))}{(t - z_2)} dt + \frac{s_1 A_0 + B_0}{X(z_2)}, \tag{C.91}$$

where $-c \le L \le c$ and

$$f(t)s_2 + h(t) = \frac{(s_1 - s_2)f_1}{t - z_{01}} + \frac{(s_3 - s_2)\bar{f}_1}{t - z_{03}} + \frac{(s_4 - s_2)\bar{f}_2}{t - z_{04}}. \tag{C.92}$$

$$f(t)s_1 + h(t) = \frac{(s_2 - s_1)f_2}{t - z_{02}} + \frac{(s_3 - s_1)\bar{f}_1}{t - z_{03}} + \frac{(s_4 - s_1)\bar{f}_2}{t - z_{04}}, \tag{C.93}$$

where,

$$f_1 = \frac{1}{2\pi i} \frac{s_1 B_x - B_y}{(s_1 - s_2)(s_1 - s_3)(s_1 - s_4)c_{11}}, \tag{C.94}$$

$$f_2 = \frac{1}{2\pi i} \frac{s_2 B_x - B_y}{(s_2 - s_1)(s_2 - s_3)(s_2 - s_4)c_{11}}. \tag{C.95}$$

X(z) is a sectionally holomorphic function and its branch cut is defined as shown in Figure C.3.

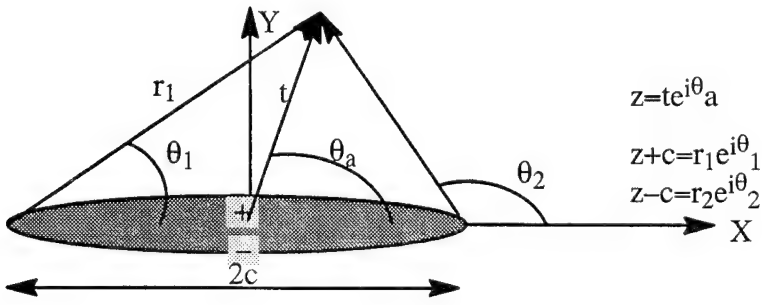

Figure C.3. Geometry for the Function X(z)

From Figure C.3,

$$X(z) = \sqrt{z^2 - c^2}, \tag{C.96}$$

$$X(z) = \sqrt{r_1 r_2 e^{i(\theta_2 + \theta_1)}}. \tag{C.97}$$

The branch cut for z+c is taken such that, $0 < \theta_1 < 2\pi$ and similarly the branch cut for z–c is taken such that $0 < \theta_2 < 2\pi$. Therefore,

$$X^+(t) = i\sqrt{c^2 - t^2}, \tag{C.98}$$

$$X^-(t) = -i\sqrt{c^2 - t^2}. \tag{C.99}$$

Using the methods described in Appendix A (A.29 – A.50) equations C.90 and C.91 can be evaluated and are given below.

$$(s_2 - s_1)\Phi_M(z) = \frac{1}{2}\left\{\frac{(s_1 - s_2)f_1}{z - z_{01}} - \frac{X(z_{01})(s_1 - s_2)f_1}{X(z)(z - z_{01})} - \frac{(s_1 - s_2)f_1}{X(z)}\right\}$$

$$+ \frac{1}{2}\left\{\frac{(s_3 - s_2)\bar{f}_1}{z - z_{03}} - \frac{X(z_{03})(s_3 - s_2)\bar{f}_1}{X(z)(z - z_{03})} - \frac{(s_3 - s_2)\bar{f}_1}{X(z)}\right\}$$

$$+ \frac{1}{2}\left\{\frac{(s_4 - s_2)\bar{f}_2}{z - z_{04}} - \frac{X(z_{04})(s_4 - s_2)\bar{f}_2}{X(z)(z - z_{04})} - \frac{(s_4 - s_2)\bar{f}_2}{X(z)}\right\}$$

$$+ \frac{s_2 A_o + B_o}{X(z)}. \tag{C.100}$$

Similarly,

$$(s_1 - s_2)\Psi_M(z) = \frac{1}{2}\left\{\frac{(s_2 - s_1)f_2}{z - z_{02}} - \frac{X(z_{02})(s_2 - s_1)f_2}{X(z)(z - z_{02})} - \frac{(s_2 - s_1)f_2}{X(z)}\right\}$$

$$+ \frac{1}{2}\left\{\frac{(s_3 - s_1)\bar{f}_1}{z - z_{03}} - \frac{X(z_{03})(s_3 - s_1)\bar{f}_1}{X(z)(z - z_{03})} - \frac{(s_3 - s_1)\bar{f}_1}{X(z)}\right\}$$

$$+ \frac{1}{2}\left\{\frac{(s_4 - s_1)\bar{f}_2}{z - z_{04}} - \frac{X(z_{04})(s_4 - s_1)\bar{f}_2}{X(z)(z - z_{04})} - \frac{(s_4 - s_1)\bar{f}_2}{X(z)}\right\}$$

$$+ \frac{s_1 A_o + B_o}{X(z)} \tag{C.101}$$

The constants A_o and B_o are determined from the condition that the displacements are single valued. This condition can be expressed as,

$$\oint 2\mathrm{Re}[(p_1\Phi_D(z_1) + p_1\Phi_M(z_1))dz_1 + (p_2\Psi_D(z_2) + p_2\Psi_M(z_2))dz_2] = 0. \qquad (C.102)$$

$$\oint 2\mathrm{Re}[(q_1\Phi_D(z_1) + q_1\Phi_M(z_1))dz_1 + (q_2\Psi_D(z_2) + q_2\Psi_M(z_2))dz_2] = 0. \qquad (C.103)$$

where the contour is drawn around the two cuts as shown in Appendix A (Figure A.5, page 95). Shrinking the contours around the cuts, the following integrals are obtained.

$$\int_{L_1+L_2} 2\mathrm{Re}[\left((p_1\Phi_D^+(t) + p_1\Phi_M^+(t) - p_1\Phi_D^-(t) - p_1\Phi_M^-(t)\right)$$

$$+ (p_2\Psi_D^+(t) + p_2\Psi_M^+(t) - p_2\Psi_D^-(t) - p_2\Psi_M^-(t))]dt = 0. \qquad (C.104)$$

$$\int_{L_1+L_2} 2\mathrm{Re}[\left((q_1\Phi_D^+(t) + q_1\Phi_M^+(t) - q_1\Phi_D^-(t) - q_1\Phi_M^-(t)\right)$$

$$+ (q_2\Psi_D^+(t) + q_2\Psi_M^+(t) - q_2\Psi_D^-(t) - q_2\Psi_M^-(t))]dt = 0. \qquad (C.105)$$

Now consider equation C.104. Like the isotropic case, Φ_M, Ψ_M gives different limiting values on L_1 only and Φ_D,Ψ_D gives different limiting values on L_2 only. Therefore, using the Plemelj formulae,

$$\int_{L_2} [p_1\Phi_D^+(t) - p_1\Phi_D^-(t)]dt = p_1 2\pi i f_1. \qquad (C.106)$$

$$\int_{L_1} [p_1\Phi_M^+(t) - p_1\Phi_M^-(t)]dt = \int_{L_1} \left\{ - \frac{X(z_{o1})(s_1 - s_2)f_1}{X^+(t)(z - z_{01})} - \frac{(s_1 - s_2)f_1}{X^+(t)} \right.$$

$$- \frac{X(z_{o3})(s_3 - s_2)\bar{f}_1}{X^+(t)(z - z_{03})} - \frac{(s_3 - s_2)\bar{f}_1}{X^+(t)} - \frac{X(z_{o4})(s_3 - s_2)\bar{f}_2}{X^+(t)(z - z_{04})} - \frac{(s_3 - s_2)\bar{f}_2}{X^+(t)}$$

$$\left. + 2\frac{s_2A_0 + B_0}{X^+(t)} \right\} \frac{p_1 dt}{(s_2 - s_1)} \qquad (C.107)$$

The above integrals can be evaluated using contour integrals which results in the following expression.

$$\int_{L_1} \left[p_1 \Phi_M^+(t) - p_1 \Phi_{\bar{M}}(t)\right] dt$$

$$= \left\{f_1(s_1 - s_2) + \bar{f}_1(s_3 - s_2) + \bar{f}_2(s_4 - s_2) - (s_2 A_o + B_o)\right\} \frac{2\pi i p_1}{(s_2 - s_1)} \qquad \text{(C.108)}$$

Similarly,

$$\int_{L_2} [p_2 \Psi_D^+(t) - p_2 \Psi_{\bar{D}}(t)] dt = p_2 2\pi i f_2. \qquad \text{(C.109)}$$

$$\int_{L_2} [p_2 \Psi_M^+(t) - p_2 \Psi_{\bar{M}}(t)] dt = \left\{f_2(s_2 - s_1) + \bar{f}_1(s_3 - s_1)\right.$$

$$\left. + \bar{f}_2(s_4 - s_1) - (s_1 A_o + B_o)\right\} \frac{2\pi i p_2}{(s_1 - s_2)} \qquad \text{(C.110)}$$

Using the above integrals in equation C.104 the following equation is obtained.

$$2\,\mathrm{Re}\left\{\bar{f}_1(s_3 - s_2)p_1 + \bar{f}_2(s_4 - s_2)p_1 - \bar{f}_1(s_3 - s_1)p_2\right.$$

$$\left. - \bar{f}_2(s_4 - s_1)p_2 - (s_2 A_o + B_o)p_1 + (s_1 A_o + B_o)p_2\right\} = 0 \qquad \text{(C.111)}$$

This can be written as,

$$2\,\mathrm{Re}\left\{(\bar{f}_1 + \bar{f}_2)(p_2 s_1 - p_1 s_2) + (\bar{f}_1 s_3 + \bar{f}_2 s_4)(p_1 - p_2)\right.$$

$$\left. + A_o(p_2 s_1 - p_1 s_2) + B_o(p_2 - p_1)\right\} = 0$$

By observation,

$$A_o = -(\bar{f}_1 + \bar{f}_2)$$

$$B_o = (s_3 \bar{f}_1 + s_4 \bar{f}_2)$$

Since A_o and B_o are real,

$$A_o = -\frac{1}{2}(\bar{f}_1 + \bar{f}_2 + f_1 + f_2) \qquad \text{(C.112)}$$

$$B_o = \frac{1}{2}(f_1 s_1 + f_2 s_2 + s_3 \bar{f}_1 + s_4 \bar{f}_2) \qquad \text{(C.113)}$$

Using these in C.100 and C.101 the following are obtained.

$$(s_2 - s_1)\Phi_M(z) = \frac{1}{2}\left\{\frac{(s_1 - s_2)f_1}{z - z_{01}} - \frac{X(z_{o1})(s_1 - s_2)f_1}{X(z)(z - z_{01})} - \frac{(s_1 - s_2)f_1}{X(z)}\right\}$$

$$+ \frac{1}{2}\left\{\frac{(s_3 - s_2)\bar{f}_1}{z - z_{03}} - \frac{X(z_{o3})(s_3 - s_2)\bar{f}_1}{X(z)(z - z_{03})} - \frac{(s_3 - s_2)\bar{f}_1}{X(z)}\right\}$$

$$+ \frac{1}{2}\left\{\frac{(s_4 - s_2)\bar{f}_2}{z - z_{04}} - \frac{X(z_{o4})(s_4 - s_2)\bar{f}_2}{X(z)(z - z_{04})} - \frac{(s_4 - s_2)\bar{f}_2}{X(z)}\right\}$$

$$+ \frac{f_1(s_1 - s_2) + \bar{f}_1(s_3 - s_2) + \bar{f}_2(s_4 - s_2)}{2X(z)} \qquad \text{(C.114)}$$

Similarly,

$$(s_1 - s_2)\Psi_M(z) = \frac{1}{2}\left\{\frac{(s_2 - s_1)f_2}{z - z_{02}} - \frac{X(z_{o2})(s_2 - s_1)f_2}{X(z)(z - z_{02})} - \frac{(s_2 - s_1)f_2}{X(z)}\right\}$$

$$+ \frac{1}{2}\left\{\frac{(s_3 - s_1)\bar{f}_1}{z - z_{03}} - \frac{X(z_{o3})(s_3 - s_1)\bar{f}_1}{X(z)(z - z_{03})} - \frac{(s_3 - s_1)\bar{f}_1}{X(z)}\right\}$$

$$+ \frac{1}{2}\left\{\frac{(s_4 - s_1)\bar{f}_2}{z - z_{04}} - \frac{X(z_{o4})(s_4 - s_1)\bar{f}_2}{X(z)(z - z_{04})} - \frac{(s_4 - s_1)\bar{f}_2}{X(z)}\right\}$$

$$+ \frac{f_2(s_2 - s_1) + \bar{f}_1(s_3 - s_1) + \bar{f}_2(s_4 - s_1)}{2X(z)} \qquad \text{(C.115)}$$

Simplifying the above expressions the following are obtained.

$$\Phi_M(z) = \frac{1}{c_{11}}\frac{1}{4\pi i}\frac{1}{(s_2 - s_1)}\left\{\frac{s_1B_x - B_y}{(s_1 - s_3)(s_1 - s_4)}\frac{1}{z - z_{01}}\left(1 - \frac{X(z_{o1})}{X(z)}\right)\right.$$

$$- \frac{s_3B_x - B_y}{(s_3 - s_4)(s_3 - s_1)}\frac{1}{z - z_{03}}\left(1 - \frac{X(z_{o3})}{X(z)}\right)$$

$$\left. - \frac{s_4B_x - B_y}{(s_4 - s_3)(s_4 - s_1)}\frac{1}{z - z_{04}}\left(1 - \frac{X(z_{o4})}{X(z)}\right)\right\} \qquad \text{(C.116)}$$

$$\Psi_M(z) = \frac{1}{c_{11}}\frac{1}{4\pi i}\frac{1}{(s_1 - s_2)}\left\{\frac{s_2B_x - B_y}{(s_2 - s_3)(s_2 - s_4)}\frac{1}{z - z_{02}}\left(1 - \frac{X(z_{o2})}{X(z)}\right)\right.$$

$$- \frac{s_3 B_x - B_y}{(s_3 - s_4)(s_3 - s_2)} \frac{1}{z - z_{03}} \left(1 - \frac{X(z_{03})}{X(z)}\right)$$

$$- \frac{s_4 B_x - B_y}{(s_4 - s_3)(s_4 - s_2)} \frac{1}{z - z_{04}} \left(1 - \frac{X(z_{04})}{X(z)}\right) \Bigg\} \qquad \text{(C.117)}$$

The equations given above are the same as that obtained by Obata et.al [54] using a different procedure.

Formulation of Stress Functions for the Main Crack Which Opens Up Due to Loads at Infinity

The stress functions for the problem of the main crack with remote loadings (Φ_L, Ψ_L) can be obtained using the same approach as discussed in the previous section (see also Krenk [52]) and are given below.

$$\Phi_L(z) = \frac{Q(z) + s_2 P(z)}{(s_2 - s_1)X(z)} - \frac{s_2 \overline{\Gamma}' + \overline{\Lambda}}{(s_2 - s_1)}. \qquad \text{(C.118)}$$

$$\Psi_L(z) = \frac{Q(z) + s_1 P(z)}{(s_1 - s_2)X(z)} - \frac{s_1 \overline{\Gamma}' + \overline{\Lambda}}{(s_1 - s_2)}, \qquad \text{(C.119)}$$

where, Γ and Λ are pure imaginary constants which have to be determined from remote boundary conditions and

$$P(z) = \sum_{n=0}^{n} A_n z^n, \qquad \text{(C.120)}$$

$$Q(z) = \sum_{n=0}^{n} B_n z^n, \qquad \text{(C.121)}$$

where n is the number of cuts or crack and A_n and B_n are real. In the above case n = 1 therefore,

$$P(z) = A_o + A_1 z, \qquad \text{(C.122)}$$

$$Q(z) = B_o + B_1 z. \qquad \text{(C.123)}$$

Using equation C.118 and C.119 in the expression for stresses (C.35 to C.37) at infinity (i.e. z tends to ∞) the following relations can be obtained.

$$A_1 = \frac{\sigma_{yy}^{\infty}}{2}, \tag{C.124}$$

$$B_1 = \frac{\sigma_{xy}^{\infty}}{2}, \tag{C.125}$$

$$2\mathrm{Re}\left\{(s_1 + s_2)(\overline{\Lambda} - B_1) + s_1 s_2(\overline{\Gamma}' - A_1)\right\} = \sigma_{xx}^{\infty}. \tag{C.126}$$

Let,

$$\Gamma' = iC, \tag{C.127}$$

$$\Lambda = iD. \tag{C.128}$$

Therefore,

$$C[\alpha_1\beta_2 + \beta_1\alpha_2] + D[\beta_1 + \beta_2] = \frac{\sigma_{xx}^{\infty}}{2} + \frac{\sigma_{xy}^{\infty}}{2}(\alpha_1 + \alpha_2) + \frac{\sigma_{yy}^{\infty}}{2}(\alpha_1\alpha_2 - \beta_1\beta_2), \tag{C.129}$$

where C or D have to be chosen arbitrarily from which the other constant is determined. Now A_o and B_o have to determined from the single valuedness of displacement condition which can be expressed as,

$$\int_{L_1} 2\mathrm{Re}\left(\left(p_1\Phi_L^{+}(t) - p_1\Phi_L^{-}(t)\right) + \left(p_2\Psi_L^{+}(t) - p_2\Psi_L^{-}(t)\right)\right)dt$$

where $L_1 \in \{-a, a\}$. After substituting the limiting values of the stress functions and using the following integral formulas (See Appendix D, D.26 – D.38),

$$\int_{L_1} \frac{dt}{X^{+}(t)} = -\pi i$$

$$\int_{L_1} \frac{tdt}{X^{+}(t)} = 0$$

$A_o = 0$ and $B_o = 0$ is obtained. Assuming C =0, the stress functions for remote loading can be expressed as,

$$\Phi_L(z) = 2\,\mathrm{Re}\left(\frac{\sigma_{xy}^{\infty} + s_2\sigma_{yy}^{\infty}}{2(s_2 - s_1)}\frac{z}{X(z)} + i\frac{\sigma_{xx}^{\infty} + (\alpha_1\alpha_2 - \beta_1\beta_2)\sigma_{yy}^{\infty} + (\alpha_1 + \alpha_2)\sigma_{xy}^{\infty}}{2(s_2 - s_1)(\beta_1 + \beta_2)}\right) \tag{C.130}$$

$$\Psi_L(z) = 2\,\mathrm{Re}\left(\frac{\sigma^{\infty}_{xy} + s_1\sigma^{\infty}_{yy}}{2(s_1 - s_2)}\frac{z}{X(z)} + i\frac{\sigma^{\infty}_{xx} + (\alpha_1\alpha_2 - \beta_1\beta_2)\sigma^{\infty}_{yy} + (\alpha_1 + \alpha_2)\sigma^{\infty}_{xy}}{2(s_1 - s_2)(\beta_1 + \beta_2)}\right) \tag{C.131}$$

Since in the present study $\sigma^{\infty}{}_{xy} = 0$,

$$\Phi_L(z) = 2\,\mathrm{Re}\left(\frac{s_2\sigma^{\infty}_{yy}}{2(s_2 - s_1)}\frac{z}{X(z)} + i\frac{\sigma^{\infty}_{xx} + (\alpha_1\alpha_2 - \beta_1\beta_2)\sigma^{\infty}_{yy}}{2(s_2 - s_1)(\beta_1 + \beta_2)}\right) \tag{C.132}$$

$$\Psi_L(z) = 2\,\mathrm{Re}\left(\frac{s_1\sigma^{\infty}_{yy}}{2(s_1 - s_2)}\frac{z}{X(z)} + i\frac{\sigma^{\infty}_{xx} + (\alpha_1\alpha_2 - \beta_1\beta_2)\sigma^{\infty}_{yy}}{2(s_1 - s_2)(\beta_1 + \beta_2)}\right). \tag{C.133}$$

Formulation of the Singular Integral Equation

$B_x(t_o)$ and $B_y(t_o)$ can be treated as Green's function for a point dislocation and can be integrated over a given range to represent a crack. Then the only boundary condition that remains to be satisfied is the stress free condition on the branched crack. This is expressed as,

$$\sigma_{\theta\theta}(r, \theta) = 0,$$

$$\sigma_{r\theta}(r, \theta) = 0.$$

where, $0 < r < l$ and θ is the kink angle and l is the kink length. Using the stress transformation relations given below,

$$\sigma_{\theta\theta} = \sigma_{xx}\cos^2\theta + \sigma_{yy}\sin^2\theta + 2\sigma_{xy}\cos\theta\sin\theta,$$

$$\sigma_{r\theta} = (\sigma_{yy} - \sigma_{xx})\sin\theta\cos\theta + 2\sigma_{xy}(\cos^2\theta - \sin^2\theta),$$

and substituting for σ_{xx}, σ_{yy} and σ_{xy} the following relations are obtained.

$$\sigma^{i}_{\theta\theta} = 2\,\mathrm{Re}\left[\Phi_i(z_1)(s_1\sin\theta + \cos\theta)^2 + \Psi_i(z_2)(s_2\sin\theta + \cos\theta)^2\right]$$

$$\sigma^{i}_{r\theta} = 2\,\mathrm{Re}\left[\Phi_i(z_1)\left(\left(1 - s_1^2\right)\sin\theta\cos\theta - s_1\cos 2\theta\right)\right.$$

$$\left. + \Psi_i(z_2)\left(\left(1 - s_2^2\right)\sin\theta\cos\theta - s_2\cos 2\theta\right)\right]$$

$$\sigma_{\theta\theta} = \sigma^{D}_{\theta\theta} + \sigma^{M}_{\theta\theta} + \sigma^{L}_{\theta\theta}$$

$$\sigma_{r\theta} = \sigma_{r\theta}^{D} + \sigma_{r\theta}^{M} + \sigma_{r\theta}^{L}$$

where i = D, M and L. Substituting for the stress functions and simplifying, the following pair of singular integral equations are obtained.

$$\sigma_{\theta\theta} = \int_0^l \frac{M_{11}B_x(t_o) + M_{12}B_y(t_o)}{t - t_o} dt_o$$

$$+ \int_0^l 2\,\mathrm{Re}\left[\left(s_1 \sin\theta + \cos\theta\right)^2 \Phi_M(z_1) + \left(s_2 \sin\theta + \cos\theta\right)^2 \Psi_M(z_2)\right] dt_o$$

$$+ 2\,\mathrm{Re}\left[\left(s_1 \sin\theta + \cos\theta\right)^2 \Phi_L(z_1) + \left(s_2 \sin\theta + \cos\theta\right)^2 \Psi_L(z_2)\right] = 0$$

$$\sigma_{r\theta} = \int_0^l \frac{M_{21}B_x(t_o) + M_{22}B_y(t_o)}{t - t_o} dt_o$$

$$+ \int_0^l 2\,\mathrm{Re}\left[\left(\left(1 - s_1^2\right)\sin\theta\cos\theta - s_1\cos 2\theta\right)\Phi_M(z_1)\right.$$

$$\left. + \left(\left(1 - s_2^2\right)\sin\theta\cos\theta - s_2\cos 2\theta\right)\Psi_M(z_2)\right] dt_o$$

$$+ 2\,\mathrm{Re}\left[\left(\left(1 - s_1^2\right)\sin\theta\cos\theta - s_1\cos 2\theta\right)\Phi_L(z_1)\right.$$

$$\left. + \left(\left(1 - s_2^2\right)\sin\theta\cos\theta - s_2\cos 2\theta\right)\Psi_L(z_2)\right] = 0$$

where,

$$z_i = a + t(\cos\theta + s_i \sin\theta), \tag{C.134}$$

$$z_{oi} = a + t_o(\cos\theta + s_i \sin\theta), \tag{C.135}$$

and i = 1, 2. Also

$$M_{11} = 2\,\mathrm{Re}\left[\frac{1}{2\pi i}\frac{1}{c_{11}}\left\{\frac{s_1}{(s_1 - s_2)(s_1 - s_3)(s_1 - s_4)}(\cos\theta + s_1 \sin\theta)\right.\right.$$

$$\frac{s_2}{(s_2 - s_1)(s_2 - s_3)(s_2 - s_4)}(\cos\theta + s_2 \sin\theta)\Bigg\}\Bigg], \tag{C.136}$$

$$M_{12} = -2\,\mathrm{Re}\Bigg[\frac{1}{2\pi i}\frac{1}{c_{11}}\Bigg\{\frac{1}{(s_1 - s_2)(s_1 - s_3)(s_1 - s_4)}(\cos\theta + s_1 \sin\theta)$$

$$\frac{1}{(s_2 - s_1)(s_2 - s_3)(s_2 - s_4)}(\cos\theta + s_2 \sin\theta)\Bigg\}\Bigg], \tag{C.137}$$

$$M_{21} = 2\,\mathrm{Re}\Bigg[\frac{1}{2\pi i}\frac{1}{c_{11}}\Bigg\{\frac{s_1}{(s_1 - s_2)(s_1 - s_3)(s_1 - s_4)}\frac{\left(\left(1 - s_1^2\right)\sin\theta\cos\theta - s_1\cos 2\theta\right)}{(\cos\theta + s_1 \sin\theta)}$$

$$\frac{s_2}{(s_2 - s_1)(s_2 - s_3)(s_2 - s_4)}\frac{\left(\left(1 - s_2^2\right)\sin\theta\cos\theta - s_2\cos 2\theta\right)}{(\cos\theta + s_2 \sin\theta)}\Bigg\}\Bigg], \tag{C.138}$$

$$M_{22} = -2\,\mathrm{Re}\Bigg[\frac{1}{2\pi i}\frac{1}{c_{11}}\Bigg\{\frac{1}{(s_1 - s_2)(s_1 - s_3)(s_1 - s_4)}\frac{\left(\left(1 - s_1^2\right)\sin\theta\cos\theta - s_1\cos 2\theta\right)}{(\cos\theta + s_1 \sin\theta)}$$

$$\frac{1}{(s_2 - s_1)(s_2 - s_3)(s_2 - s_4)}\frac{\left(\left(1 - s_2^2\right)\sin\theta\cos\theta - s_2\cos 2\theta\right)}{(\cos\theta + s_2 \sin\theta)}\Bigg\}\Bigg]. \tag{C.139}$$

APPENDIX D

EVALUATION OF SOME CONTOUR INTEGRALS

Given below are some of the contour integrals which occur during the development of the elasticity solution discussed in chapter II and III. Consider the integral,

$$A_1 = \int_L \frac{dt}{X^+(t)} \tag{D.1}$$

where, by superscript + is meant the limiting value of function X(t) on L where L ($-2c \leq t \leq 0$) is defined in Figure D.1 and

$$X^+(t) = \sqrt{t(t + 2c)}. \tag{D.2}$$

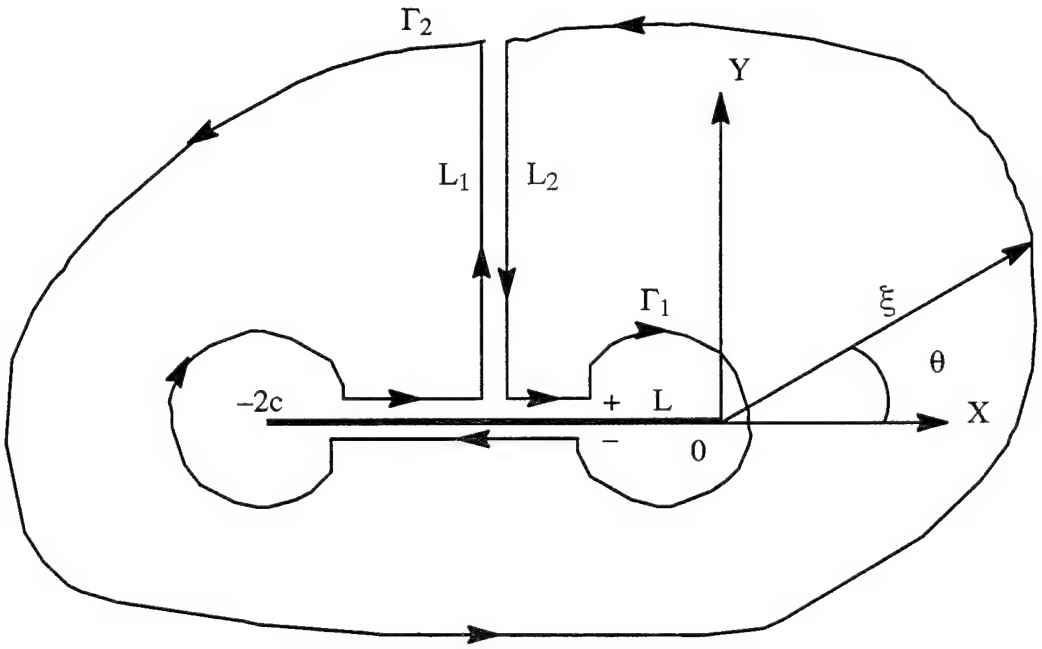

Figure D.1. Contour Assumed for Evaluating Integral D.1

Using Cauchy's integral theorem [89],

$$\oint_{\Gamma_1} \frac{d\xi}{X(\xi)} + \oint_{\Gamma_2} \frac{d\xi}{X(\xi)} = 0. \tag{D.3}$$

Where the contour is shown in Figure D.1. Note that the contours Γ_1 and Γ_2 are of opposite directions. The direction assumed for Γ_2 is taken to be positive. The outer contour Γ_2 can be extended to infinity and evaluated and similarly the inner contour Γ_1 can be shrunk on–to the line L across which $X(\xi)$ is discontinuous. The contours on L_1 and L_2 cancel each other in the limit. Consider the integral on Γ_2 which can be written as

$$\oint_{\Gamma_2} \left[\frac{1}{\xi} + O\left(\frac{1}{\xi^2}\right) \right] d\xi. \tag{D.4}$$

as ξ tends to ∞. Let,

$$\xi = Re^{i\theta}, \; d\xi = iRe^{i\theta}d\theta. \tag{D.5}$$

The $O(1/\xi^2)$ term vanishes as ξ tends to ∞. Therefore,

$$\oint_{\Gamma_2} \left[\frac{1}{\xi} \right] d\xi = i \int_0^{2\pi} d\theta, \tag{D.6}$$

$$= 2\pi i. \tag{D.7}$$

Consider the integral on Γ_1, which can be written as,

$$\oint_{\Gamma_1} \frac{d\xi}{X(\xi)} = 2 \int_{-2c}^{0} \frac{dt}{X^+(t)} + \oint_{C_1} \frac{d\xi}{X(\xi)} + \oint_{C_2} \frac{d\xi}{X(\xi)}. \tag{D.8}$$

Let,

$$\xi = R_{C_1} e^{i\theta_{C_1}} + 2c, \; d\xi = R_{C_1} e^{i\theta_{C_1}} i d\theta_{C_1}, \tag{D.9}$$

where R_{C1} is the radius of the contour C_1 and θ_{C1} is the angle from the positive direction for the radius R_{C1}. Then as the radius R_{C1} tends to zero,

$$\oint_{C_1}\left[\frac{R_{C_1}e^{i\theta_{c_1}}id\theta_{C_1}}{\sqrt{\left(R_{C_1}e^{i\theta}+2c\right)\left(R_{C_1}e^{i\theta}+4c\right)}}\right]=O\left(R_{C_1}\right), \tag{D.10}$$

Similarly,

$$\oint_{C_2}\left[\frac{R_{C_2}e^{i\theta_{C_2}}id\theta_{C_2}}{\sqrt{\left(R_{C_2}e^{i\theta_{C_2}}\right)\left(R_{C_2}e^{i\theta_{C_2}}+2c\right)}}\right]=O\left(\sqrt{R_{C_2}}\right). \tag{D.11}$$

where R_{C2} and θ_{C2} have the same meaning as described above. Therefore the integrals on contour C_1 and C_2 vanish as their radius vanishes. Hence

$$\oint_{\Gamma_1}\frac{d\xi}{X(\xi)}=2\int_{-2c}^{0}\frac{dt}{X^{+}(t)}=-2\pi i, \tag{D.12}$$

$$\int_{-2c}^{0}\frac{dt}{X^{+}(t)}=-\pi i. \tag{D.13}$$

Consider the integral

$$\int_{-2c}^{0}\frac{tdt}{X^{+}(t)}, \tag{D.14}$$

where X(t) is defined as before. Let the contour be assumed as shown in Figure D.1. Therefore as before,

$$\oint_{\Gamma_1}\frac{\xi d\xi}{X(\xi)}+\oint_{\Gamma_2}\frac{\xi d\xi}{X(\xi)}=0, \tag{D.15}$$

$$\lim_{\xi\to\infty}\oint_{\Gamma_2}\frac{\xi d\xi}{X(\xi)}=\oint_{\Gamma_2}\left(1-\frac{c}{\xi}+O(\frac{1}{\xi^2})\right)d\xi, \tag{D.16}$$

$$=(0-2\pi ic). \tag{D.17}$$

The integral on Γ_1 is given as,

$$\oint_{\Gamma_1} \frac{\xi d\xi}{X(\xi)} = 2\int_{-2c}^{0} \frac{tdt}{X^+(t)} + \oint_{C_1} \frac{\xi d\xi}{X(\xi)} + \oint_{C_2} \frac{\xi d\xi}{X(\xi)}. \tag{D.18}$$

As before the integral on C_1 and C_2 vanishes. Therefore

$$\int_{-2c}^{0} \frac{tdt}{X^+(t)} = \pi ic. \tag{D.19}$$

Consider the integral

$$\int_{-2c}^{0} \frac{dt}{(t - z_o)X^+(t)}, \tag{D.20}$$

where X(t) is defined as before. Let the contour be assumed as shown in Figure D.2. Therefore as before,

$$\oint_{\Gamma_1} \frac{d\xi}{(\xi - z_o)X(\xi)} + \oint_{\Gamma_2} \frac{d\xi}{(\xi - z_o)X(\xi)} = -\frac{2\pi i}{X(z_o)}, \tag{D.21}$$

The right hand side is obtained from the fact that there exists a pole at z_{o1} and it is negative because the contour enclosing it is in the negative direction. Considering the contour on Γ_2,

$$\lim_{\xi \to \infty} \oint_{\Gamma_2} \frac{d\xi}{(\xi - z_o)X(\xi)} = \oint_{\Gamma_2} \left(O(\frac{1}{\xi^2}) \right) d\xi, \tag{D.22}$$

$$= 0. \tag{D.23}$$

The integral on Γ_1 is given as,

$$\oint_{\Gamma_1} \frac{d\xi}{(\xi - z_o)X(\xi)} = 2\int_{-2c}^{0} \frac{dt}{(t - z_o)X^+(t)}$$

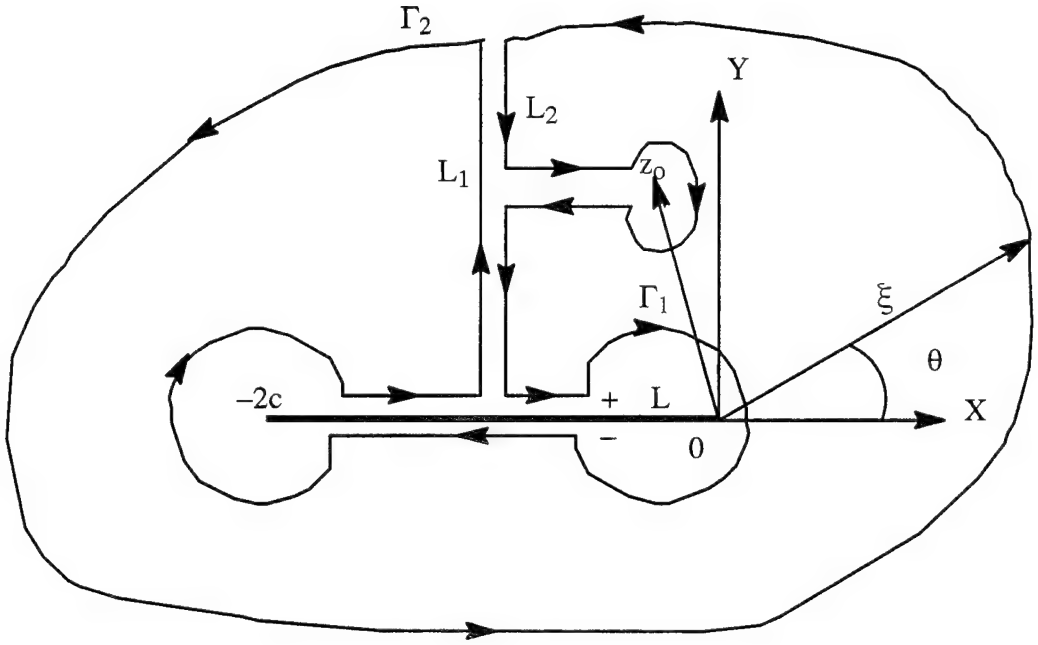

Figure D.2. Contour Assumed for Evaluating Integral D.20

$$+ \oint_{C_1} \frac{d\xi}{(t - z_o)X(\xi)} + \oint_{C_2} \frac{d\xi}{(t - z_o)X(\xi)}. \tag{D.24}$$

As before the integral on C_1 and C_2 vanishes. Therefore

$$\int_{-2c}^{0} \frac{dt}{(t - z_o)X^+(t)} = -\frac{\pi i}{X(z_o)}. \tag{D.25}$$

Consider the integral

$$\int_{-c}^{c} \frac{dt}{X^+(t)}. \tag{D.26}$$

where,

$$X^+(t) = i\sqrt{(c^2 - t^2)}. \tag{D.27}$$

Define another contour as shown in Figure D.3.

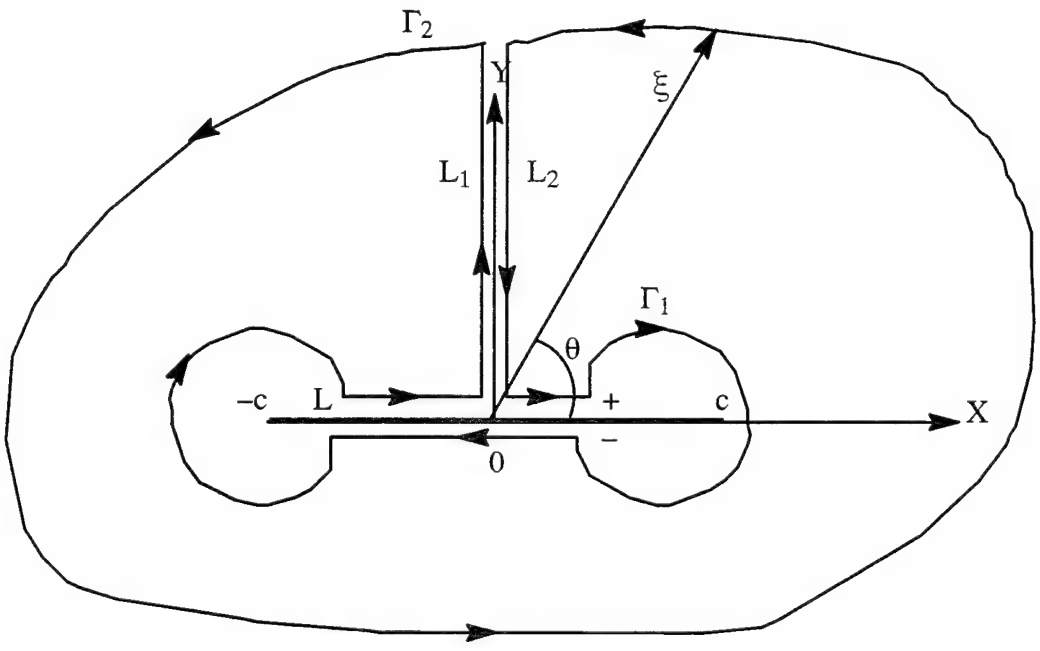

Figure D.3. Contour Assumed for Evaluating Integral D.26, D.33

As before,

$$\oint_{\Gamma_1} \frac{d\xi}{X(\xi)} + \oint_{\Gamma_2} \frac{d\xi}{X(\xi)} = 0. \tag{D.28}$$

Consider the integral on Γ_2 which can be written as,

$$\lim_{\xi \to \infty} \oint_{\Gamma_2} \frac{d\xi}{X(\xi)} = \oint_{\Gamma_2} \left(\frac{1}{\xi} + O(\frac{1}{\xi^3}) \right) d\xi, \tag{D.29}$$

$$= 2\pi i, \tag{D.30}$$

The integral on Γ_1 is given as,

$$\oint_{\Gamma_1} \frac{\xi d\xi}{X(\xi)} = 2 \int_{-2c}^{0} \frac{tdt}{X^+(t)} + \oint_{C_1} \frac{\xi d\xi}{X(\xi)} + \oint_{C_2} \frac{\xi d\xi}{X(\xi)}. \tag{D.31}$$

As before the integral on C_1 and C_2 vanishes. Therefore

$$\int_{-c}^{c} \frac{dt}{X^+(t)} = -\pi i. \tag{D.32}$$

Consider the integral

$$\int_{-c}^{c} \frac{tdt}{X^+(t)}, \tag{D.33}$$

where X(t) is defined as before. Let the contour be assumed as shown in Figure D.3. Therefore,

$$\oint_{\Gamma_1} \frac{\xi d\xi}{X(\xi)} + \oint_{\Gamma_2} \frac{\xi d\xi}{X(\xi)} = 0, \tag{D.34}$$

$$\lim_{\xi \to \infty} \oint_{\Gamma_2} \frac{\xi d\xi}{X(\xi)} = \oint_{\Gamma_2} \left(1 + O(\frac{1}{\xi^2}) \right) d\xi, \tag{D.35}$$

$$= 0. \tag{D.36}$$

The integral on Γ_1 is given as,

$$\oint_{\Gamma_1} \frac{\xi d\xi}{X(\xi)} = 2 \int_{-2c}^{0} \frac{tdt}{X^+(t)} + \oint_{C_1} \frac{\xi d\xi}{X(\xi)} + \oint_{C_2} \frac{\xi d\xi}{X(\xi)}. \tag{D.37}$$

As before the integral on C_1 and C_2 vanishes. Therefore

$$\int_{-c}^{c} \frac{tdt}{X^+(t)} = 0. \tag{D.38}$$

APPENDIX E

NUMERICAL TECHNIQUES.

The numerical techniques used for the branched crack problem is similar for both the isotropic and anisotropic case. Therefore, the solution will be shown for a general case and it can be applied for either the isotropic or the anisotropic case. Consider the integral,

$$\int_0^l \frac{\alpha(t_o)}{t_o - t} dt_o + \int_0^l M[\alpha(t_o), t, t_o] dt_o = f(t), \tag{E.1}$$

where,

$$\alpha(t_o) = \frac{\beta(t_o)}{t_o^{\alpha}(l - t_o)^{\beta}}. \tag{E.2}$$

and the first integral is interpreted in a Cauchy's principal value sense. The function $\alpha(t_o)$ (dislocation density function) is a flux type function which can be expressed in terms of a bounded function $\beta(t_o)$ as shown in equation (E.2). The denominator of equation E.2 is also known as the fundamental function (or the weight function), and α and β are the stress singularities at the kink corner and tip respectively. $M[\alpha(t_o), t, t_o]$ contains the terms which arise due to the interactions between the main crack and the dislocation and f(t)is due to the remotely applied load.

The above singular integral equation is solved using three different numerical techniques as given in: 1, Erdogan, et al., [90]; 2, He and Hutchinson [91]; and 3, Kaya and Erdogan [85]. In the above three methods the limits of the integral equations are changed so that the limits are from –1 to 1 by using the transformations given below.

$$t_o = \frac{l}{2}(\xi_o + 1), \quad t = \frac{l}{2}(\xi + 1), \quad dt_o = \frac{l}{2} d\xi_o. \tag{E.3}$$

Method I: Solution by Gauss–Chebychev Integration Formula [90]

Following [90] the singular integral equation is reduced to a system of linear equations as shown below.

$$\sum_{j=1}^{n} W_j \beta(t_{oj}) \left[\frac{1}{t_{oj} - t_i} + M\left[\alpha(t_{oj}), t_i, t_{oj}\right] \right] = f(t_i), \quad (i = 1, ..n - 1). \tag{E.4}$$

where,

$$T_n(t_{oj}) = 0, t_{oj} = \cos\left(\pi \frac{2j - 1}{2n}\right), \quad (j = 1, ..n), \tag{E.5}$$

$$U_{n-1}(t_i) = 0, \; t_i = \cos\left(\frac{\pi i}{n}\right), \quad (i = 1, ..n - 1), \tag{E.6}$$

$$W_j = \frac{\pi}{n}, \; (j = 1, ..n). \tag{E.7}$$

$T_n(t)$ and $U_{n-1}(t)$ are the Chebychev polynomial of the first and second kind respectively and W_j are the weights. This results in (n–1) equations in n unknowns. For the complete solution one more additional condition is required which is obtained as follows.

In method I, the singularity at both ends of the branched crack or kink is assumed to be 1/2. Since the singularity at the kink corner, where the kink joins with the main crack, is actually less than 1/2, the value of the bounded function $\beta(t_o)$ at the kink corner is assumed to be 0. i.e. $\beta(-1) = 0$. With this condition the above system of linear equations can be completely solved. This method was used by Lo [24].

Method II: Solution by Jacobi Polynomials

In this method the correct singularity is assumed at the kink corner. The correct singularity is given by the Williams, characteristic equations [19] for the isotropic case and by Bogy's [92] equation for the anisotropic case. This method is similar to the manner in which the singular integral equation was solved by He et.al. [91] though in their approach a simple algebraic polynomial was used instead of Jacobi polynomials. The advantage of using Jacobi polynomials over algebraic polynomials is that the inherent properties of Jacobi polyno-

mials can be used to obtain a simplified numerical scheme. The unknown function $\beta(t_o)$ is expanded in terms of Jacobi polynomials as shown below.

$$\beta(t_o) = \sum_{i=0}^{n} C_i P_i^{(\alpha,\beta)}(t_o). \tag{E.8}$$

α and β are the stress singularities and C_i is a complex constant. Substituting the above equation in equation (E.1) the following system of linear algebraic equation is obtained.

$$\sum_{i=0}^{n} C_i \sum_{j=1}^{m} \left[\frac{P_i^{(\alpha,\beta)}(t_{oj})W_j}{t_{oj} - t_i}\right] + M\left(\sum_{i=0}^{n} C_i \sum_{j=1}^{m} P_i^{(\alpha,\beta)}(t_{oj})W_j, t_i, t_{oj}\right) = f(t_i). \tag{E.9}$$

where t_{oj} is the root of Jacobi polynomial given by equation (E.10) and t_i are given by the roots of the Chebychev polynomials (equation E.11).

$$P_m^{(\alpha,\beta)}(t_{oj}) = 0, \quad j = 1, ..., m. \tag{E.10}$$

$$t_i = \cos\left(\frac{2k + 1}{n + 1}\frac{\pi}{2}\right), \quad k = 0, ..., n. \tag{E.11}$$

Method III: Solution by Double Series Jacobi Polynomials

The bounded function $\beta(t_o)$ can be written as, (following Kaya et.al [85])

$$\beta(t_o) = \sum_{i=1}^{n}\sum_{j=1}^{m} \frac{\beta_{ij}}{(1 - t)^{\beta_j - \beta_1}(1 + t)^{\alpha_i - \alpha_1}}, \quad \alpha_1 > \alpha_i, \ \beta_1 > \beta_j. \tag{E.12}$$

If $(-1-\alpha_i+\alpha_1)$ or $(-1-\beta_j+\beta_1) < 0$ then the derivative of $\beta(t_o)$ is not bounded at the ends of the integration limits. If that is the case then expanding $\alpha(t_o)$ as shown below will improve the rate of convergence for the numerical scheme.

$$\alpha(t_o) = \frac{\beta_1(t_o)}{(1 - t_o)^{1/2}(1 + t_o)^{\alpha_1}} + \frac{\beta_2(t_o)}{(1 - t_o)^{1/2}(1 + t_o)^{\alpha_2}}, \alpha_1 \neq \alpha_2. \tag{E.13}$$

α_1 and α_2 are the roots of the Williams characteristic equation [19] for the isotropic case and the roots of equation given by Bogy [92] for the anisotropic case. $\beta_1(t_o)$ and $\beta_2(t_o)$ are expanded in terms of Jacobi polynomials as in Method II and the unknown dislocation density

function is evaluated. The collocation points for this method are again given by the roots of the Chebychev polynomials as shown below.

$$t_i = \cos\left(\frac{2k+1}{n_1+n_2+2}\frac{\pi}{2}\right), \quad k = 0, \ldots, n_1 + n_2 + 1. \tag{E.14}$$

n_1 and n_2 represent the number of terms in the Jacobi polynomial series used to represent $\beta_1(t_o)$ and $\beta_2(t_o)$ respectively.

It should be noted that where as Kaya, et al., [85] used the above method for a potential type function (i.e. crack opening displacement) this current method is used for flux type function where the unknown is the slope of the crack opening displacement. The above three methods are also referred to in short form as MI, MII and MIII for method I, method II and method III respectively.

LITERATURE CITED

1. J.J. Kibler and R. Roberts, "The Effect of Biaxial Stresses on Fatigue and Fracture," Journal of Engineering for Industry, pp. 727, 1970.

2. J.C. Radon, P.S. Leevers and L.E. Culver, "Fracture Toughness of PMMA Under Biaxial Stress," Fracture, Vol. 3, 1977.

3. E.D. Reedy, "On the Specimen Dependence of Unidirectional Boron/Aluminum Fracture Toughness," Journal of Composite Materials Supplement, Vol. 14, pp. 118, 1980.

4. S. Mostovy, P.B. Crosley and E.J. Ripling, "Use of Crack–Line–Loaded Specimens for Measuring Plane Strain Fracture Toughness," Journal of Materials, Vol. 2, pp. 661, 1967.

5. J.R. Albritton and J.G. Goree, "Fracture of Silicon Carbide Whisker Reinforced Aluminum," Proceedings of the 7th International Conference on Fracture (ICF7), pp. 749–760, 1989.

6. D.E. Richardson and J.G. Goree, "Experimental Verification of a New Two Parameter Fracture Model," Fracture Mechanics: Twenty–Third Symposium. ASTM STP 1189, pp. 738–750, 1993.

7. B. Cotterell and J.R. Rice, "Slightly Curved or Kinked Cracks," International Journal of Fracture, Vol. 16, No. 2, pp. 526–528, 1980.

8. E. H. Yoffe, "The Moving Griffith Crack," Philosophical Magazine, pp. 739–750, 1951.

9. H. Schardin, "Velocity Effects in Fracturem," Fracture, Ed. B.L. Auerbach, D.K. Felbeck, G.I. Hahn and D.A. Thomas, pp. 297–329, 1959.

10. A.B. Clark and G.R. Irwin, "Crack–Propagation Behaviors," Experimental Mechanics, Vol. 6, pp. 321–330, 1966.

11. J. Congleton and N.J. Petch, "Crack–Branching," Philosophical Magazine, 1967, pp. 749–760.

12. C.S. Carter, "Stress Corrosion Crack Branching in High–Strength Steels," Engineering Fracture Mechanics, 1971, Vol. 3, pp. 1–13.

13. H. Andersson, "Stress–Intensity Factors at the Tips of a Star–Shaped Contour in an Infinite Tensile Sheet," J. Mech. Phys. Solids, 1969, Vol. 17, pp. 405–417.

14. H. Andersson, Erratum in [9], J. Mech. Phys. Solids, 1970, Vol. 18, pp. 437.

15. N. Muskhelishvili, Some Basic Problems of the Mathematical Theory of Elasticity, Groningen, Noordhoff, 1963.

16. V.V. Dudukalenko and N.B. Romalis, "Direction of Crack Growth Under Plane–Stress–State Conditions," Izv. An SSR, MTT, Vol. 8, No. 2, pp. 129–136, 1973.

17. K. Palaniswamy and W.G. Knauss, "On the Problem of Crack Extension in Brittle Solids Under General Loading," Mechanics Today, Vol. 4, Edited by S. Nemat–Nasser, pp. 87–148, 1978.

18. S.N. Chatterjee, "The Stress Fields in the Neighborhood of a Branched Crack in an Infinite Elastic Sheet," International Journal of Solids and Structures, Vol. 11, pp. 521–538, 1975.

19. M.L. Williams, "Stress Singularities Resulting from Various Boundary conditions in Angular Corners of Plates in Extension," Journal of Applied Mechanics, Vol. 19, pp. 526–528, 1952.

20. M.A. Hussain, S.L. Pu and J.Underwood, "Strain Energy Release Rate for a Crack Under Combined Mode I and Mode II Loading," Presented at 7th National Fracture Mechanics Symposium, University of Maryland, August 1972, Benet Weapons Laboratory, Watervliet Arsenal, N.Y.

21. H. Kitagawa, R. Yuuki and T. Ohira, "Crack–Morphological Aspects in Fracture Mechanics," Engineering Fracture Mechanics, Vol. 7, pp. 515–529, 1975.

22. H. Kitagawa and R. Yuuki, "Analysis of Branched Cracks Under Biaxial Stresses," Fracture, Vol. 3, ICF4, Waterloo, Canada, pp. 201–211, 1975.

23. F. Erdogan and G.E. Sih, "On the Crack Extension in Plates Under Plane Loading and Transverse Shear," Journal of Basic Engineering, Vol. 85, pp. 519–527, 1963.

24. K.K. Lo, "Analysis of Branched Cracks," Journal of Applied Mechanics, Vol. 45, pp. 797–803, 1978.

25. B.L. Karihaloo, L.M. Keer and S. Nemat–Nasser, "Crack Kinking Under Nonsymmetric Loading," Engineering Fracture Mechanics, Vol. 13, pp. 879–888, 1980.

26. K. Hayashi and S. Nemat–Nasser, "Energy–Release Rate and Crack Kinking Under Combined Loading," Journal of Applied Mechanics, Vol. 48, pp. 520–524, 1981.

27. A.P. Datsyshin and M.P. Savruk, "A System of Arbitrarily Oriented Cracks in Elastic Solids," Journal of Applied Mathematics and Mechanics(PMM), Vol. 37, pp. 306–313, 1973.

28. P.S. Theocaris and N. Ioakimidis, "The Symmetrically Branched Crack in an Infinite Elastic Medium," Journal of Applied Mathematics and Physics, Vol. 27, pp. 801–814, 1976.

29. P.S. Theocaris and C.H. Blonzou, "Symmetric Branching of Cracks in PMMA (Plexiglass)," Materialprufung, Vol. 15, pp. 123–130, 1973.

30. P.S. Theocaris, "Asymmetric Branching of Cracks," Journal of Applied Mechanics, Vol. 44, pp. 611–618, 1977.

31. A.A. Khrapkov, "The First Basic Problem for a Notch at the Apex of an Infinite Wedge," International Journal of Fracture Mechanics, Vol. 7, No. 4, pp. 373–382, 1971.

32. B.A. Bilby and G.E. Cardew, "The Crack with a Kinked Tip," International Journal of Fracture, Vol. 11, pp. 708–712, 1975.

33. B.A. Bilby, G.E. Cardew and I.C. Howard, "Stress Intensity factors at the Tips of Kinked and Forked Cracks," Fracture, ICF4, Waterloo, Canada, pp. 197–200, 1977.

34. S. Mellin, "Accurate Data for Stress Intensity Factors at Infinitesimal Kinks," Journal of Applied Mechanics, Vol. 61, pp. 467–470, 1994.

35. N.V. Banichuk, "Using the Small–Parameter Method to Determine the Form of a Curved Crack," Izv. An SSR, MTT, Vol. 5, No. 2, pp. 130–137, 1970.

36. R.V. Gol'dstein and R.L. Salganik, "Brittle Fracture of Solids with Arbitrary Cracks," International Journal of Fracture Mechanics, Vol. 10, No. 4, pp. 507–523, 1974.

37. Y. Sumi, S. Nemat–Nasser and L.M. Keer, "On Crack Branching and Curving in a Finite Body," International Journal of Fracture, Vol. 21, pp. 67–79, 1983.

38. B.L. Karihaloo, L.M. Keer, S. Nemat–Nasser and A. Oranratnachai, "Approximate Description of Crack Kinking and Curving," Journal of Applied Mechanics, Vol. 48, pp. 515–519, 1981.

39. J.B. Leblond, "Crack Paths in Plane Situations–I. General Form of the Expansion of the Stress Intensity Factors," International Journal of Solids and Structures, Vol. 25, pp. 1311–1325, 1989.

40. M. Amestoy and J.B. Leblond, "Crack Paths in Plane Situations–II. Detailed Form of the Expansion of the Stress Intensity Factors," International Journal of Solids and Structures, Vol. 29, pp. 465–501, 1992.

41. J.D. Eshelby, "Edge Dislocation in Anisotropic Materials," Philosophical Magazine, Vol. 40, pp. 903–912, 1949.

42. F.C. Frank, "Crystal Dislocation–Elementary Concepts and Definitions," Philosophical Magazine, Vol. 42, pp. 809–819, 1951.

43. J.D. Eshelby, W.T. Read and W. Shockley, "Anisotropic Elasticity with Applications to Dislocation Theory," Acta Metallurgica, Vol. 1, pp. 251–259, 1953.

44. A.N. Stroh, "Dislocation and Cracks in Anisotropic Elasticity," Philosophical Magazine, Vol. 3, pp. 625–646, 1958.

45. C. Atkinson, "The Propagation of Fracture in Aelotropic Materials," International Journal of Fracture Mechanics, Vol. 1, pp. 47–55, 1965

46. C. Atkinson, "The Interaction Between a Dislocation and a Crack," International Journal of Fracture Mechanics, Vol. 2, pp. 567–574, 1966.

47. S.G. Lekhnitskii, Theory of Elasticity of an Anisotropic Body, Mir Publishers, Moscow, 1981.

48. A.E. Green and W. Zerna, Theoretical Elasticity, Clarendon Press, Oxford, 1954.

49. G.N. Savin, Stress Concentration Around Holes, Pergamon Press, Oxford, 1961.

50. G.C. Sih, P.C. Paris and G.R. Irwin, "On Cracks in Rectilinearly Anisotropic Bodies," International Journal of Fracture, Vol. 1, pp. 189–203, 1965.

51. E. M. Wu, "Fracture Mechanics of Anisotropic Plates," Composite Mechanics Workshop, Technomic Publishing Co., Inc., Lancaster, PA, pp. 20–43, 1965.

52. S. Krenk, "The Stress Distribution in an Infinite Anisotropic Plate with Co–linear Cracks," International Journal of Solids and Structures, Vol. 11, pp. 449–460, 1975.

53. P.W. Tan and C.A. Bigelow, "An Improved Boundary Force Method for Analyzing Cracked Anisotropic Materials," Engineering Fracture Mechanics, Vol. 34, pp. 347–357, 1989.

54. M. Obata, S. Nemat–Nasser and Y. Goto, "Branched Crack in Anisotropic Solids," Journal of Applied Mechanics, Vol. 56, pp. 858–864, 1989.

55. C.R. Chiang, "Kinked Cracks in an Anisotropic Material," Engineering Fracture Mechanics, Vol. 39, pp. 927–930, 1991.

56. H. Gao and V. Chiu, "Slightly Curved or Kinked Cracks in Anisotropic Elastic Solids," International Journal of Solids and Structures, Vol. 29, pp. 947–972, 1992.

57. Y. Xu and L.M. Keer, "Crack Curving in Anisotropic Elastic Solids," Engineering Fracture Mechanics, Vol. 44, pp. 63–73, 1993.

58. M.B. Buczek and C.T. Herakovich, "Direction of Crack Growth in Fibrous Composites," Mechanics of Composite Materials, Edited by G.J. Dvorak, ASME AMD, Vol. 58, , pp. 75–82, 1983.

59. M.A. Gregory and C.T. Herakovich, "Predicting Crack Growth in Unidirectional Composites," J. Compos Mater, Vol. 20, pp. 67–85, 1986.

60. A.A. Griffith, "The Phenomena of Rupture and Flow in Solids," Phil. Trans. Roy. Soc. (Lond), Vol. 221, pp. 163–198, 1920.

61. A.A. Griffith, "The Theory of Rupture," Proc. of the 1st International Congress for Appl. Mech, Delft, pp. 55–63, 1924.

62. G.R. Irwin, "Analysis of Stress and Strain Near the End of a Crack Transversing a Plate," Journal of Applied Mechanics, Vol. 24, pp. 361–364, 1957.

63. V.V. Panasyuk, L.T. Berezhnitskiy and S.Ye. Kovchik, "Propagation of an Arbitrarily Oriented Rectilinear Crack During Extension of a Plate," NASA Technical Translation F–402, 1965.

64. J.G. Williams and P.D. Ewing, "Fracture Under Complex Stress–The Angled Crack Problem," International Journal of Fracture Mechanics, Vol. 8, pp. 441–446, 1972.

65. I. Finnie and A. Saith, "A Note on the Angled Crack Problem and the Directional Stability of Cracks," International Journal of Fracture, Vol. 9, pp. 484–486, 1973.

66. G.C. Sih, "Some Basic Problems in Fracture Mechanics and New Concepts," Engineering Fracture Mechanics, Vol. 3, pp. 365–377, 1973.

67. G.C. Sih, "Strain–Energy–Density–Factor Applied to Mixed Mode Crack Problems," International Journal of Fracture, Vol. 10, pp. 305–321, 1974.

68. C.H. Wu, "Fracture Under Combined Loads by Maximum–Energy–Release–Rate Criterion," Journal of Applied Mechanics, Vol. 45, pp. 553–558, 1978.

69. C.H. Wu, "Explicit Asymptotic Solution for the Maximum–Energy–release–Rate Problem," International Journal of Solids and Structure, Vol. 15, pp. 561–566, 1979.

70. S.K. Maiti and R.A. Smith, "Criteria for Brittle Fracture in Biaxial Tension," Engineering Fracture Mechanics, Vol. 19, pp. 793–804, 1984.

71. A.C. Chrysakis, "A New Criterion of Mixed–Mode Crack Propagation Based on the Maximization of Principal Stress σ_1," Engineering Fracture Mechanics, Vol. 24, pp. 361–369, 1986.

72. A.C. Chrysakis, "Improvement o the maxσ_r, max $|\tau_{r\theta}|$ and max σ_1 Criteria for Mixed Mode Fracture," Engineering Fracture Mechanics, Vol. 24, pp. 651–656, 1986.

73. S.K. Maiti, "An Approximate Method for Calculation of Strain Energy Release Rate Associated with Kinking of a Mode I crack Located Initially in an Orthotropic Direction," International Journal of Fracture, Vol. 32, pp. R33–R36, 1986.

74. V.E. Saouma, M.L. Ayari and D.A. Leavell, "Mixed Mode Crack Propagation in Homogeneous Anisotropic Solids," Engineering Fracture Mechanics, Vol. 27, pp. 171–184, 1987.

75. S.Y. Zhang, "A Note on fracture Toughness of Unidirectional Composites," International Journal of Fracture, Vol. 35, pp. R57–R60, 1987.

76. P.K. Sarkar and S.K. Maiti, "Prediction of Mode I Fracture Toughness of Unidirectional Fibre Composites with Arbitrary Crack–Fibre Orientation from its Lowest or Matrix–Fracture Toughness," International Journal of Fracture, Vol. 40, pp. R91–R96, 1989.

77. S.Q. Zhang, B.Z. Jang, B.T. Valaire and J.C. Suhling, "A New Criterion for Composite Material Mixed Mode Fracture Analysis," Engineering Fracture Mechanics, Vol. 34, pp. 749–769, 1989.

78. S.Y. Zhang, "Extending Tsai–Hill and Norris Criteria to Predict Cracking Direction in Orthotropic Materials," International Journal of Fracture, Vol. 40, pp. R101–R104, 1989.

79. F. Ellyin and H.E. Kadi, "Predicting Crack Growth Direction in Unidirectional Composite Laminae," Engineering Fracture Mechanics, Vol. 36, pp. 27–37, 1990.

80. A.P. Datsyshin and M.P. Savruk, "Integral Equations of the Plane Problem of Crack Theory," Journal of Applied Mathematics and Mechanics (PMM), Vol. 38, pp. 728–737, 1974.

81. K. Hayashi and S. Nemat–Nasser, "On Branched Interface Cracks," Journal of Applied Mechanics, Vol. 48, pp. 529–533, 1981.

82. K. Hayashi and S. Nemat–Nasser, "Energy Release Rate and Crack Kinking," International Journal of Solids and Structures, Vol. 17, pp. 107–114, 1981.

83. N. Muskhelishvili, Singular Integral Equations, Dover Publications, Inc., N.Y, 1992.

84. S.P. Timoshenko and J.N. Goodier, Theory of Elasticity, McGraw Hill, 1982.

85. A.C. Kaya and F. Erdogan, "On the Solution of Integral Equations with a Generalized Cauchy Kernel," Quarterly Applied Mathematics, Vol. 45, No. 3, pp. 455–469, 1987.

86. M. Isida and T. Nishino, "Formulae of Stress Intensity Factors at Tips of Kinked Cracks Under Various Loadings," Engineering Fracture Mechanics, Vol. 36, No. 5, pp. 697–711, 1990.

87. A.C. Kaya, Application of Integral Equations with Strong Singularities in Fracture Mechanics, Ph.D Thesis, Lehigh University, 1984.

88. Maple V Release 3, Waterloo Maple Software, 1994.

89. P.V. O'Neil, Advanced Engineering Mathematics, Wadsworth Publishing Inc., California, 1991.

90. F. Erdogan and G.D. Gupta, "On the Numerical Solution of Singular Integral Equations," Quarterly Applied Mathematics, Vol. 29, No. 3, pp. 525–534, 1972.

91. M. He and J.W. Hutchinson, "Kinking of a Crack Out of an Interface," Journal of Applied Mechanics, Vol. 56, pp. 270–278, 1989.

92. M.C. Kuo and D.B. Bogy, "Plane Solutions for Traction Problems on Orthotropic Unsymmetrical Wedges and Symmetrically Twinned Wedges," Journal of Applied Mechanics, Vol. 41, pp. 203–208, 1974.

93. Cotterell, B., "Notes on the Paths and Stability of Cracks," International Journal of Fracture Mechanics, Vol. 13, pp. 526–533, 1980.

94. Richardson, D.E., A New Biaxial Stress Fracture Criterion, Ph.D Thesis, Clemson University, August 1991.